NASA TECHNICAL NOTE

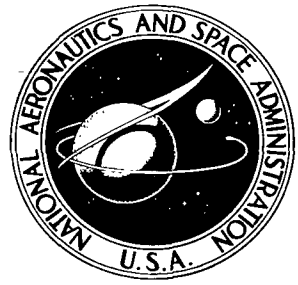




# LOW-SPEED WIND-TUNNEL INVESTIGATION OF A FOUR-ENGINE UPPER SURFACE BLOWN MODEL HAVING A SWEPT WING AND RECTANGULAR AND D-SHAPED EXHAUST NOZZLES

*William C. Sleeman, Jr., and William C. Hohlweg*

*Langley Research Center*
*Hampton, Va. 23665*

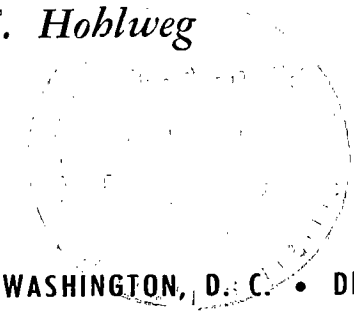


NATIONAL AERONAUTICS AND SPACE ADMINISTRATION • WASHINGTON, D. C. • DECEMBER 1975

| 1 Report No | 2. Government Accession No. | 3. Recipient's Catalog No. |
|---|---|---|
| NASA TN D-8061 | | |

| 4. Title and Subtitle | 5. Report Date |
|---|---|
| LOW-SPEED WIND-TUNNEL INVESTIGATION OF A FOUR-ENGINE UPPER SURFACE BLOWN MODEL HAVING A SWEPT WING AND RECTANGULAR AND D-SHAPED EXHAUST NOZZLES | December 1975 |
| | 6. Performing Organization Code |
| 7. Author(s) | 8. Performing Organization Report No. |
| William C. Sleeman, Jr., and William C. Hohlweg | L-10173 |
| | 10. Work Unit No. |
| 9. Performing Organization Name and Address | 505-10-41-03 |
| NASA Langley Research Center<br>Hampton, Va. 23665 | 11. Contract or Grant No. |
| | 13. Type of Report and Period Covered |
| 12. Sponsoring Agency Name and Address | Technical Note |
| National Aeronautics and Space Administration<br>Washington, D.C. 20546 | 14. Sponsoring Agency Code |

15. Supplementary Notes

William C. Hohlweg: Graduate research scholar assistant from George Washington University.

16 Abstract

A low-speed investigation was conducted in the Langley V/STOL tunnel to determine the power-on static-turning and powered-lift aerodynamic performance of a four-engine upper surface blown transport configuration. Initial tests with a D-shaped exhaust nozzle showed relatively poor flow-turning capability, and the D-nozzles were replaced by rectangular nozzles with a width-height ratio of 6.0. The high-lift system consisted of a leading-edge slat and two different trailing-edge-flap configurations. A double-slotted flap with the gaps sealed was investigated and a simple radius flap was also tested. A maximum lift coefficient of approximately 9.3 was obtained for the model with the rectangular exhaust nozzles with both the double-slotted flap deflected $50^{\circ}$ and the radius flap deflected $90^{\circ}$.

| 17. Key Words (Suggested by Author(s)) | 18. Distribution Statement |
|---|---|
| STOL transport<br>Upper surface blowing<br>Rectangular exhaust nozzles<br>Powered-lift aerodynamics | Unclassified – Unlimited<br><br>Subject Category 02 |

| 19. Security Classif. (of this report) | 20. Security Classif. (of this page) | 21. No. of Pages | 22. Price* |
|---|---|---|---|
| Unclassified | Unclassified | 116 | $5.25 |

*For sale by the National Technical Information Service, Springfield, Virginia 22161

# LOW-SPEED WIND-TUNNEL INVESTIGATION OF A FOUR-ENGINE UPPER SURFACE BLOWN MODEL HAVING A SWEPT WING AND RECTANGULAR AND D-SHAPED EXHAUST NOZZLES

William C. Sleeman, Jr., and William C. Hohlweg*
Langley Research Center

## SUMMARY

A low-speed investigation was conducted in the Langley V/STOL tunnel to determine the power-on static turning characteristics of the simulated engine flow and the powered-lift aerodynamic performance of a four-engine upper surface blown transport configuration having a 30° swept wing. D-shaped exhaust nozzles and rectangular nozzles having a width-height ratio of 6.0 were investigated. A partial-span 35-percent-chord double-slotted flap with the gaps sealed was investigated with both exhaust nozzle configurations and a partial-span radius flap was tested on the model with the rectangular nozzles.

The test results indicated that the static-turning and static-thrust recovery efficiencies obtained generally were indicative of the powered-lift aerodynamic performance to be expected. The overall results obtained on the model with the D-nozzles indicated that the turning radius associated with the higher flap deflections was too abrupt to maintain attached flow of the relatively thick jet efflux from the D-nozzles. Thinning and spreading of the jet exhaust by the use of high-aspect-ratio rectangular nozzles provided significant improvements in powered-lift performance.

Maximum lift coefficients of about 6.3 were obtained with the rectangular nozzles for both the 50° basic flap deflection and the 90° radius flap deflection at a thrust coefficient of 2.0, positive drag being indicated for lift coefficients greater than 5.5. The highest lift coefficients obtained with these flap deflections were about 9.3 at a thrust coefficient of 4.0.

## INTRODUCTION

Various propulsive-lift concepts have been investigated in studies of means for directing the efflux from turbofan engines to interact with the wing and high-lift system to provide very large increases in the lift-producing potential of airplanes for take-off and landing. Recent investigations of the upper surface blown powered-lift concept have shown potential

*Graduate Research Assistant, George Washington University.

for attaining good powered-lift performance (refs. 1 to 3) and also for inherently lower ground-noise levels because the engine exhaust nozzles are above the wing and are thereby shielded by the wing in the radiation of noise to the ground.

A low-speed research program has been undertaken in the Langley V/STOL tunnel to investigate the high-lift performance of several upper surface blown model configurations. The present investigation explored the aerodynamic characteristics of a four-engine, swept-wing powered model with two different upper surface blown exhaust-nozzle configurations. The first nozzle arrangement investigated was D-shaped and had an aspect ratio (nozzle width-height ratio) of about 2.63. The high-lift performance of the model with the D-nozzles and basic flap system was not as high as expected, and these nozzles were replaced with aspect-ratio-6.0, spread, rectangular nozzles.

The basic model used in the present investigation was the same model used in tests of externally blown flaps (see refs. 4 and 5), but the engine positions and nacelle afterbody shapes were modified for blowing and spreading the exhaust over the upper surface of the wing. The high-lift system had double-slotted flaps and leading-edge slats, but the gaps between the trailing-edge flap elements were filled in over the flap span impinged by the exhaust flow in order to aid flow attachment of the jet sheet to the flap upper surface.

Test results obtained early in the present program indicated difficulties in attaining attachment of the exhaust flow to the upper surface of the trailing-edge flap at high flap deflections. A simple 0.3-chord radius trailing-edge flap was also tested as a means of providing more gradual turning of the flow than could be obtained with the basic multiple-element flap. Most of the tests were conducted with the horizontal tail removed; however, some complete model tests were made to obtain some indication of longitudinal stability and trim characteristics. Some tests were also conducted through an angle-of-attack range with the model at $\pm 5^{\circ}$ sideslip in order to determine lateral-stability derivatives.

## SYMBOLS

The static longitudinal- and lateral-stability data are presented about the stability-axis system. The positive direction of forces, moments, and angles is indicated in figure 1. The model moment-reference point was located at the 40.6-percent mean aerodynamic chord on the fuselage reference line.

The measurements of this investigation are presented in the International System of Units (SI). Details concerning the use of SI Units, together with physical constants and conversion factors are presented in reference 6.

$b$ wing span, m

$C_D$ drag coefficient, $\frac{\text{Drag}}{qS}$

$C_L$ lift coefficient, $\frac{\text{Lift}}{qS}$

$C_l$ rolling-moment coefficient, $\frac{\text{Rolling moment}}{qSb}$

$C_m$ pitching-moment coefficient, $\frac{\text{Pitching moment}}{qS\bar{c}}$

$C_n$ yawing-moment coefficient, $\frac{\text{Yawing moment}}{qSb}$

$C_Y$ side-force coefficient, $\frac{\text{Side force}}{qS}$

$C_\mu$ total thrust coefficient of all engines, $\frac{\text{Total thrust}}{qS}$

$C_{l_\beta}$ effective-dihedral parameter, $\frac{\Delta C_l}{\Delta \beta}$ $\left(\text{for } \beta = \pm 5^\circ\right)$, per deg

$C_{n_\beta}$ directional-stability parameter, $\frac{\Delta C_n}{\Delta \beta}$ $\left(\text{for } \beta = \pm 5^\circ\right)$, per deg

$C_{Y_\beta}$ side-force parameter, $\frac{\Delta C_Y}{\Delta \beta}$ $\left(\text{for } \beta = \pm 5^\circ\right)$, per deg

$c$ local wing chord, m

$\bar{c}$ mean aerodynamic chord of wing, cm

$\bar{c}_h$ mean aerodynamic chord of horizontal tail, cm

$\bar{c}_v$ mean aerodynamic chord of vertical tail, cm

$F_A$ axial force, N

$F_N$ normal force, N

$i_t$ incidence angle of horizontal stabilizer (positive, trailing edge down), deg

$q$ free-stream dynamic pressure, $N/m^2$

$R$ radius of flap (see fig. 2(f)) or radius on D-nozzle (see fig. 2(b)), cm

$S$ wing area, $m^2$

$T$ static-thrust force based on engine calibrations with flaps removed $\left(T = \sqrt{F_N{}^2 + F_A{}^2}\right)$, N

$\alpha$ angle of attack of fuselage reference line, deg

$\beta$ angle of sideslip, deg

$\delta_f$ flap defection measured streamwise, deg

$\delta_j$ static-thrust turning angle, $\tan^{-1}\frac{F_N}{F_A}$, deg

$\delta_{j,o}$ static-thrust turning angle for flap deflection of $0^o$, deg

$\delta_s$ deflection of leading-edge slat (see fig. 2(d)), deg

$\eta$ static-thrust–recovery efficiency, $\frac{\sqrt{F_N{}^2 + F_A{}^2}}{T}$

## MODEL DESCRIPTION

The model used in the present investigation was the same general research model that was tested with externally blown flaps (refs. 4 and 5) with the nacelles and engine mounting modified for upper surface blowing. A drawing of the general arrangement of the model is given in figure 2(a), and details of the nacelles and high-lift system are given in figures 2(b) to 2(f). Photographs of the model in the Langley V/STOL tunnel are presented in figure 3.

### Wing

The wing had supercritical airfoil sections with a maximum thickness of 9.3-percent chord, a nominal quarter-chord sweep angle of $30^o$, an aspect ratio of 7.48, and a taper ratio of 0.247. The wing was mounted in a high position on the fuselage and had $0^o$ dihedral. Transition strips 0.25 cm wide of No. 80 carborundum were applied to the upper and lower surfaces of the wing 4.29 cm behind the leading edge.

The basic high-lift system on the wing consisted of a partial-span, 35-percent chord, double-slotted flap which extended from the wing-fuselage juncture to the 70.4-percent wing-semispan station, and a full-span, 15-percent-chord leading-edge slat. Flap deflection angles of $35^o$, $50^o$, and $65^o$ measured in the streamwise direction (see fig. 2(e)) were investigated.

The leading-edge slat was deflected 40° when the trailing-edge flaps were deflected, and the slat was removed ($\delta_s = 0°$) for tests with the flaps undeflected.

A simple radius flap was investigated on the model with the rectangular nozzles as well as the basic two-element high-lift flaps. The radius flap was formed with a radius of 0.3 chord and was tangent to the wing upper surface at the 75.5-percent chord line. (See fig. 2(f).) Deflections of the radius flap were defined as the included angle of the sector between the tangent point on the wing and the trailing edge; the 90° radius flap deflection was a quarter circle.

## Fuselage

The fuselage of the model had circular cross sections except at the afterbody where the circular shape was modified on the bottom to accommodate the support sting. (See fig. 2(a).) Overall dimensions of the fuselage are given in figure 2(a). A fiberglass-resin shell, 0.32 cm thick, formed the outer shape of the fuselage and was attached to a metal strongback which housed the engine air plenum and the six-component strain-gage balance. An electronic angle-of-attack sensor was mounted to the internal strongback to provide the measured geometric angle of attack of the model during the tests.

## Tail Surfaces

The location and principal dimensions of the horizontal and vertical tails are given in figure 2(a). The leading edge of the vertical tail was swept 25° and the vertical tail had 11-percent-thick symmetrical supercritical airfoil sections. The horizontal tail had a leading-edge sweep of 25° and 11-percent-thick symmetrical supercritical airfoil sections. The horizontal tail was mounted at the tip of the vertical tail and had the capability of varying its incidence at fixed stabilizer settings for a range of incidence angles from −5° to 5°. A 15-percent-chord inverted leading-edge slat and constant-chord (4.45-cm) simulated split-flap elevators were attached to the horizontal tail for tests of the model with the wing high-lift system deflected in order to provide more nose-up trimming moments than could be obtained with the plain horizontal tail. The split-flap deflection was 25° for all tests with this flap deflected.

## Engine Nacelles

Four engine nacelles were mounted to the wing upper surface in a manner to provide attached engine-exhaust flow over the midchord sections of the wing ahead of the trailing-edge flaps. (See fig. 2.) Four air ejectors provided the engine simulation with a high-pressure air supply. The engines were located at 25.4 and 41.7 percent of the wing semispan. Each engine simulator was a two-part ejector with individual air supply lines from the fuselage plenum and control valves to permit simulation of the exhaust-flow characteristics of turbofan

engines. Only the outer flow from the fan section was used in the present tests; there was no primary flow through the gas-generator section of the engine simulator.

Initial tests of the model were made with D-nozzles which had an aspect ratio (width/height) of 2.63 and an exit area of 46.07 $cm^2$. (See fig. 2(b).) The D-nozzles provided good impingement on the upper surface and fairly good spreading of the exhaust flow across the wing and flap; however, static turning with flap deflections greater than $35^o$ was poor. The nacelle afterbody of the D-nozzle configuration was, therefore, modified to provide a thinner and much more spread jet exhaust through aspect-ratio-6 rectangular nozzles. (See fig. 2(c).) The aft parts of the nacelles with the aspect-ratio-6 nozzles were unsymmetrical, with opposite side flare for the inboard and outboard nacelles. The inboard nacelles had their side flare principally on the inboard side; the flare on the outboard nacelles was principally on the outboard side in order to obtain as much jet spreading over the surface of the wing and flap as feasible on the present model. A converging internal cross-sectional area distribution from the circular internal shape to the rectangular nozzle exit was selected to match the internal area characteristics of the D-nozzle and to reduce the tendency for the internal flow to separate from the fairly large side flare angle of $29^o$.

## Modifications to the Basic Model

The basic model configuration is defined as the wing-body–vertical-tail configuration shown in figure 2(a), with the high-lift system shown in figure 2(e), and with either the D-nozzles or the aspect-ratio-6 rectangular nozzles. Modifications to the model with the D-nozzles included an upper surface bump and an external airfoil vane. Internal wedge modifications to the model with rectangular nozzles were tested with both the basic flap and the radius flap.

Upper surface bump.- Static tests of the model with the D-nozzles and flap deflections of $50^o$ and $65^o$ indicated very poor static-flow turning and means were sought to improve the turning. Past experience on another model showed turning improvement with a smooth bump located on the wing upper surface immediately ahead of the knee of the flap. As a matter of expediency during testing, sections of a 20-percent-chord leading-edge slat for the outboard section of the wing were installed as a bump on the wing upper surface, as shown in figure 2(d), with the slat leading edge lying along the 75.5-percent wing chord line and its trailing edge forward.

External vane.- Static-turning capability of the model with the D-nozzles and the upper surface bump was found to be adequate and additional means for improving the static turning were sought. An external airfoil vane mounted above the wing surface in approximately the same chordwise and spanwise location as the bump was investigated (fig. 2(d)). The vane was a part of the leading-edge slat from a large general research model, and its trailing edge

was located about 0.85 cm above the wing surface with the external airfoil trailing edge over the wing 75.5-percent chord line and inclined about 23° nose-up with respect to the wing chord plane.

Internal wedges in rectangular nozzles.- Tuft surveys for the static-thrust condition with the rectangular nozzles showed appreciable flow separation that originated from spreading of the jet flow from the outboard lip of the inboard nozzle which impinged on the inboard side of the outboard nacelle afterbody. A small internal wedge, which effectively removed the side flare of the outboard lip of the inboard nozzle, was installed. (See fig. 2(c).) Static-force tests with and without this wedge installed indicated that the internal wedge improved the static turning; the wedge was in the inboard nozzle for all subsequent calibrations and tests of the model. The exit area of each inboard nozzle was reduced to 43.44 $cm^2$ with the small wedges, and the aspect ratio of the inboard nozzles was reduced to 5.66.

Tuft surveys made over the inboard part of the wing upper surface indicated that the large inboard flare of the inboard nacelle was spreading the flow over the fuselage in static-thrust tests. Large internal wedges were installed in the inboard nacelles for a few exploratory tests to reduce the inward spreading of the jet. Static-force tests, with and without these large wedges, failed to show significant improvements in static turning; thus, the large wedges were not used in tests of the model.

## TESTS AND CORRECTIONS

The investigation was conducted in the Langley V/STOL tunnel; aerodynamic tests were conducted at dynamic pressures of 814 $N/m^2$ and 766 $N/m^2$ for the model with the D-nozzles and the aspect-ratio-6 nozzles, respectively. The corresponding test Reynolds numbers were $7.23 \times 10^5$ and $7.02 \times 10^5$, based on the wing mean aerodynamic chord of 0.2899 m.

### Thrust Calibrations

Engine static-thrust calibrations were made prior to testing in order to determine the static thrust for each individual engine as a function of an engine reference pressure. All static calibrations were made with the engines installed on the model and with the wing flaps and wing trailing edge aft of the 75.5-percent chord line removed. Static-thrust calibrations for all four engines together were made after the thrusts of the individual engines were balanced, based on their individual calibrations and the net yawing moment of the model with all engines operating. The static thrust from the calibrations was computed as the resultant of the normal and axial forces $T = \sqrt{F_N^2 + F_A^2}$. The stated thrust coefficients for the wind-on aerodynamic tests were determined from summation of the static thrust for the individual engines, which was based on the engine reference pressure recorded at each wind-on data point.

## Static Tests

Static tests of the model with the horizontal tail removed and the model at an angle of attack of $0^\circ$ were made for all flap configurations. A relatively large number (10 to 12) of equally spaced thrust values were set in the static tests to obtain a good definition of the variation of aerodynamic characteristics with static thrust. Static-turning angles and thrust-recovery efficiency for the jet flow were determined from the measurements of normal and axial forces $\left(\delta_j = \tan^{-1}\frac{F_N}{F_A} \text{ and } \eta = \frac{\sqrt{F_N^2 + F_A^2}}{T}\right)$. The thrust used in computing the thrust recovery efficiency was computed for each data point from the static calibration of each engine and summed to obtain the total thrust. The method of computing thrust-recovery efficiency does not account for installation losses and, therefore, does not represent the thrust efficiency normally associated with jet-engine installations. Since the basis for the efficiency parameter $\eta$ is the static thrust without flaps, $\eta$ can therefore be considered to represent the effects of flaps and the associated jet turning on the thrust recovery.

## Aerodynamic Tests

Wind-on aerodynamic tests of the model at an angle of attack of $0^\circ$ were made for all the model configurations and thrust settings investigated in the static tests. Longitudinal aerodynamic characteristics were obtained from tests through an angle-of-attack range of approximately $-4^\circ$ to $24^\circ$ and were conducted with power off and several values of thrust which were held constant as the angle of attack was varied. Nominal values of $C_\mu$ investigated were 1.0, 2.0, 3.0, and 4.0 for most of the tests. Configurations with stabilizer incidence angles of $0^\circ$ and $\pm 5^\circ$ and horizontal tail off were investigated to assess longitudinal trim capabilities and the aerodynamic performance of the wing and high-lift system.

Lateral-stability derivatives were obtained from tests conducted through the angle-of-attack range with the model sideslipped $\pm 5^\circ$ for the configuration having the rectangular exhaust nozzles and the horizontal tail at $-5^\circ$ incidence.

## Corrections

Jet-boundary corrections for the influence of the closed tunnel boundaries were determined from reference 7 and applied to the measured data.

# PRESENTATION OF RESULTS

The data which present the results obtained in this investigation are given in the figures as follows:

## DISCUSSION

### Static Data for Model With D-Nozzles

Basic data obtained over the range of static thrust, which show effects of flap deflection and modification to the model on the static turning and thrust recovery efficiency, are given in figure 4. These results are summarized in figure 27(a) as plots of normal force and axial

force, nondimensionalized by the static thrust. The static-turning and thrust-recovery efficiency are indicated by the rays and circular segments, respectively. The spread of the data points for a given configuration indicates the variance of $\delta_j$ and $\eta$ over the thrust range. (See also fig. 4.)

Test results for the clean wing $(\delta_f = 0^o)$ show that the flow was turned approximately $7^o$ with no flap deflection because the flow remained attached to the upper surface and was deflected to the approximate slope of the airfoil near the trailing edge. Deflection of the flap to $35^o$ increased the static turning at moderate and high thrust to approximately $30^o$ with thrust-recovery efficiencies varying from 0.91 to 0.97. Although substantial flow turning was obtained with the $35^o$ flap deflection, the amount of static turning achieved was significantly less than the sum of the flap deflection and the turning at $\delta_f = 0^o$. The static-turning efficiency of the flap can be considered as the static turning provided at a deflected condition $\delta_j$ in relation to the turning that should have been obtained, $\delta_f + \delta_{j,o}$, where $\delta_{j,o}$ is the turning at $\delta_f = 0^o$ expressed as $\frac{\delta_j}{\delta_f + \delta_{j,o}}$. Values of flap static-turning efficiency are summarized for all the configurations investigated in figure 28.

Static-turning angles obtained for the basic $50^o$ flap configuration were only slightly greater than the turning obtained with $\delta_f = 35^o$. (See fig. 27(a).) This lack of additional turning with $\delta_f = 50^o$ indicated that the flow was detaching from the forward part of the flap and that the radius of turn of the flap was too small for the relatively thick jet from the D-nozzles. Addition of the upper surface bump ahead of the flap provided about $10^o$ additional turning (fig. 27(a)); however, the turning was still much less than the flap should provide with fully attached flow. Addition of the external turning vane with the $50^o$ flap deflection provided very good turning (up to $52^o$), but the thrust-recovery efficiency was greatly reduced (probably by the additional drag on the turning vane).

Deflection of the flap to $65^o$ provided turning angles that varied from about $15^o$ to $25^o$ as the thrust varied; this variation indicated that the deflection was much too high for the combination of flap turning radius (see figs. 4(a) and 27(a)) and jet-sheet thickness provided by the D-nozzles. Some tests were made to assess the sensitivity of the $65^o$ flap deflection configuration to modifications in view of the very poor turning performance. Addition of the upper surface bump provided increasing turning angles up to about $\delta_j = 50^o$ as the thrust increased, but higher thrust values caused an abrupt loss in turning and in thrust-recovery efficiency. (See fig. 4(b).) The test data for the $65^o$ deflection indicated that the flow was detaching well forward on the flap; a test was made to determine whether opening the flap gaps in the double-slotted flap could improve the flow turning. The data obtained with the upper surface bump on and the flap gap open, however, showed slightly less turning than the basic $\delta_f = 65^o$ without the bump.

## Longitudinal Aerodynamic Characteristics of Model With D-Nozzles

Characteristics at an angle of attack of $0^o$.- The variations of lift coefficient and drag coefficient with thrust coefficient at an angle of attack of $0^o$ are presented in figure 5 for the same configurations and thrust settings investigated in the static tests. These characteristics are presented as an aid in assessing the extent that the static turning data are indicative of the nature of the characteristics to be expected in the aerodynamic tests.

A comparison of the static data of figures 4 and 27 with the wind-on aerodynamic data of figure 5 leads to the observation that the static data are generally indicative of the aerodynamic results at an angle of attack of $0^o$ in that configurations having the highest static turning also provided the highest lift coefficients at a given thrust. Lift coefficients for $\delta_f = 50^o$ with the upper surface bump (fig. 5(c)) showed somewhat higher values of lift than the basic $\delta_f = 35^o$ configuration (fig. 5(a)) for $C_\mu$ values less than 2.5, as would be expected from the static-turning data. The lift coefficients at high thrust coefficients were, however, essentially the same for both flap configurations, even though appreciably higher static turning was shown for the $50^o$ flap with the upper surface bump (fig. 4(c)).

Effects of flap deflection for basic model.- Basic data which present the aerodynamic characteristics over the angle-of-attack range for constant values of $C_\mu$ are presented in figures 6 to 9. Effects of flap deflection from these data are summarized for $C_\mu = 4$ for the basic model in figure 29.

Effects of flap deflection on the lift characteristics over the angle-of-attack range show the characteristics that could be inferred from the data at $\alpha = 0^o$ (fig. 5), except that the losses in lift coefficient for $\delta_f = 50^o$ and $\delta_f = 65^o$ were much more pronounced at moderate and high angles of attack in relation to the $\delta_f = 35^o$ configuration. An overall assessment of the effects of flap deflection for the basic model with D-nozzles suggests that flap configurations that show low static turning will also have poor powered-lift characteristics for aerodynamic (forward-speed) conditions.

Effects of modifications to basic model.- Effects of the upper surface bump and the external vane on the aerodynamic characteristics through the angle-of-attack range are summarized in figure 30 for $\delta_f = 50^o$ at $C_\mu = 2.0$. Attempts were made to obtain data at $C_\mu = 4$ over the angle range with the external vane, but the extended exposure of the vane to the high velocities in the jet caused failure of the vane attachment screws. The summary presented in figure 30, therefore, is limited to a value of $C_\mu = 2$.

The summary results of figure 30 show improvements in lift characteristics about as would be expected from the improvements in static turning (fig. 27(a)) that were associated with adding the upper surface bump and the turning vane to the $50^o$ flap configuration. The relatively low turning efficiency of the model with the bump, and the low thrust-recovery efficiency obtained with the external vane, suggested that fundamental configuration changes were needed to obtain good high-lift performance on this model.

The most effective basic configuration changes that could be envisioned were reducing the jet height along with increasing the jet spreading, and the use of a more gentle turning radius at the flap knee. The nacelle afterbodies were modified to provide the widest rectangular nozzles feasible with the engine spacing and nozzle exit area of the original model. A simple radius flap was also constructed for tests of the model with the rectangular nozzles.

## Static Data for Model With Rectangular Nozzles

Basic flap.- Basic data obtained over the range of static thrust which show effects of deflection of the basic two-element flap on the static turning and thrust-recovery efficiency are given in figure 10. These results are summarized in figure 27(b) as plots of normal force and axial force nondimensionalized by the static thrust.

Static data for the clean wing $\left(\delta_f = 0^o\right)$ show that the flow was turned approximately $5^o$ with no flap deflection and the thrust-recovery efficiency was about 0.99 (figs. 10(a) and 27(b)). Deflection of the flap to $35^o$ provided static-turning angles up to about $37^o$ with about 97-percent thrust-recovery efficiency. Increasing the flap deflection to $50^o$ increased the static turning to approximately $49^o$ with about 94-percent thrust-recovery efficiency. The $65^o$ flap deflection gave around $60^o$ turning in the lower half of the thrust range (fig. 10(a)); however, progressive flow detachment was indicated with increasing thrust as evidenced by the decreasing values of turning. The indication of flow detachment and the overall relatively low thrust-recovery efficiencies (73 to 84 percent) obtained suggest that the $65^o$ flap deflection would not perform nearly as well in the aerodynamic tests as the lower flap deflections.

Radius flap.- Basic static data for the model with the radius flap are given in figure 11 and summarized in figure 27(b). An important characteristic evident in the static turning for the radius flap is the lack of appreciable variations in $\delta_j$ with increasing thrust above about 450 N for all flap deflections tested. This characteristic and the relatively high and invariant level of thrust-recovery efficiency suggest that the jet flow was fairly well stabilized over the radius flap even though the full turning that would be expected for the indicated deflections was not achieved. The turning effectiveness of the radius flap was about two-thirds for all flap deflections investigated; for example, about $40^o$ turning was achieved with the $60^o$ deflection.

Twin-engine power simulation.- Static tests were made with either the inboard engines or the outboard engines shut off to simulate power effects for a twin-engine arrangement with the engines located close inboard or outboard. Results of these static tests are presented in figure 10(c) for $50^o$ deflection of the basic flap and in figure 11(c) for two deflections of the radius flap. The data show that approximately $10^o$ greater turning was achieved with only the outboard engines operating than with only the inboard engines operating. Thrust-recovery efficiencies were also significantly higher with only the outboard engines operating.

A comparison of data obtained for only two engines operating with the data for all four engines indicates that there was considerable interaction between the inboard and outboard engines when the four engines operated together (fig. 10(c)). This interaction is also evidenced by the fact that the static turning for the inboard and outboard engines only was not additive; the static turning for the outboard engines alone was around 90 percent of the turning achieved for all engines operating. Thrust-recovery efficiencies for the inboard engines alone were appreciably lower than those obtained with outboard engines only, the latter being only slightly lower than with all engines operating. These results suggest that if the static data are indicative of aerodynamic characteristics, the lift coefficient obtained with only the outboard engines operating should be about the same as the lift coefficient $\left(\text{at } \alpha = 0^{\circ}\right)$ obtained with four engines operating at one-half the thrust coefficient for outboard engines alone. The aerodynamic data at $\alpha = 0^{\circ}$ presented in figures 12(c) and 13(c) essentially support this observation.

Effects of wedges.- An internal wedge was installed in the inboard engine exit nozzles (see fig. 2(c)) in order to eliminate the separation of the spread exhaust flow over the outboard nozzle. Effects of this wedge which eliminated the internal flare of the outboard side of the inboard nozzle are given in figures 10(b) and 11(b) for static conditions. The static data obtained with and without the wedges showed increased static turning and a small reduction in static thrust-recovery efficiency with the wedges installed for all flap-deflected configurations. The decision to leave the wedges in the inboard nozzles for the remainder of the tests was based on the improved static turning. Aerodynamic data obtained with and without the wedges installed (figs. 12(b) and 13(b)) also showed small improvements in $C_L$ with the wedges installed.

## Longitudinal Aerodynamic Characteristics of Model With Rectangular Nozzles

Effects of flap deflection at $\alpha = 0^{\circ}$.- Effects of flap deflection over the $C_\mu$ range at $\alpha = 0^{\circ}$ are presented in figures 12 and 13. These aerodynamic data generally reflect the trends shown in the static-turning data with respect to effects of flap deflection for both the basic flap and the radius flap, except for the $65^{\circ}$ basic flap deflection. The lift coefficients for $\delta_f = 65^{\circ}$ (fig. 12) would be expected to be higher than those for $\delta_f = 50^{\circ}$ at low and moderate thrust because the static-turning angles were significantly higher (fig. 10). The values of $C_L$ obtained for $\delta_f = 65^{\circ}$ were lower than for either the $50^{\circ}$ or the $35^{\circ}$ flap deflections throughout the range of $C_\mu$. These results indicate that the flow over $65^{\circ}$ deflected flap was relatively unstable, and forward speed caused detachment throughout the $C_\mu$ range, possibly in the same manner as increased thrust caused the loss of turning for the static case. The conclusion may be made, therefore, that at $\alpha = 0^{\circ}$, the turning radius

at the flap knee was too small for the 65° flap deflection to turn the jet flow from the aspect-ratio-6 rectangular nozzles as well as from the D-nozzles.

Effect of flap deflection over angle-of-attack range.- Basic data presenting the effects of angle of attack at constant thrust coefficients on the longitudinal characteristics of the model with different deflections of the basic flap and the radius flap are given in figures 14 and 15. Effects of flap deflection are summarized for $C_\mu = 4$ in figures 31 and 32.

The aerodynamic characteristics over the angle-of-attack range summarized in figures 31 and 32 reflect the overall characteristics shown in the aerodynamic data at $\alpha = 0^\circ$ except for the 65° deflection of the basic flap. Fairly high values of $C_L$ were obtained at high angles of attack with $\delta_f = 65^\circ$, and the stall indicated at lower thrust coefficients (fig. 14(d)) was delayed or eliminated at the highest $C_\mu$ values. Even though no stall was apparent up to the highest angle of attack investigated for $C_\mu = 4$, the drag polars for the 65° flap indicate the effects of some flow breakdown by the sudden increase of $C_D$ at $C_L$ values above about 5.8 $(C_\mu = 4)$ and by the complete separation of its drag polar from those of other flap deflections, as summarized in figure 31. These drag data indicate that the 65° deflection was providing significant aerodynamic turning of the jet sheet as evidenced by the fairly high value of $C_L$ reached $(C_L \approx 7)$ and by the positive drag values at the highest lift coefficients (fig. 31). This aerodynamic turning was, however, apparently accompanied by considerable flow separation.

The drag polars for the radius flap presented in figure 32 appear to describe an extensive envelope as defined by the overall level of the polars for each flap deflection and the overlap of polars. An envelope of this nature is indicated also, to a somewhat lesser definition, for the basic flap at deflections less than 65° (fig. 31). It could be reasoned that different flap deflections having drag polars that lie in a common envelope may also have similar or related aerodynamic turning efficiency in the same manner as well-designed unpowered flap systems.

Analyses of the lift and drag characteristics of other powered-lift configurations have been made by use of the assumption that the static turning and static thrust-recovery efficiency also applied for the aerodynamic coefficients. The results of this investigation have shown, however, that the static characteristics cannot always be used to infer the aerodynamic characteristics of an upper surface blown flap configuration, and improved analysis techniques are needed to gain a better understanding of the relationships of static and aerodynamic data.

## Lateral-Stability Derivatives of Model With Rectangular Nozzles

Static lateral-stability derivatives for the model with rectangular nozzles are presented in figure 26 for power off and two thrust coefficients.

Effective dihedral.- Positive effective dihedral $\left(-C_{l_\beta}\right)$ was indicated for all deflections of the basic flap throughout the range of angle of attack and thrust coefficients investigated. The variation of $C_{l_\beta}$ with angle of attack was relatively small except around $20^\circ$ for the two highest flap deflections where an abrupt increase in $-C_{l_\beta}$ occurred, followed by an abrupt decrease. The application of power generally increased the effective dihedral, and the data for $C_\mu = 4$ do not show the abrupt change in $C_{l_\beta}$ at high angles that was in the power-off results.

Static directional stability.- The static directional-stability characteristics presented in figure 26(a) show increasing values of $C_{n_\beta}$ as the angle of attack increased up to about $12^\circ$ for the power-off condition. Values of $C_{n_\beta}$ decreased as the angle of attack increased above about $12^\circ$ to neutral or very low stability at the highest angles of attack investigated. The application of power caused significant increases in directional stability throughout the angle-of-attack range for the flap deflections investigated. An abrupt loss of directional stability occurred around an angle of attack of $15^\circ$, and this loss was followed by an abrupt increase to around an angle of attack of $20^\circ$. These changes in directional stability are most likely caused by effects of flap deflection inasmuch as the data obtained with the flap undeflected (figs. 26(a) and 26(d)) did not show these abrupt variations.

A fairly substantial endplate effect of the horizontal tail on the vertical tail in sideslip was indicated in the power-off directional-stability data of figure 26(a) where values of $C_{n_\beta}$ obtained with the horizontal tail on were consistently higher than those with the horizontal tail removed. The application of power (figs. 26(b) and 26(c)) caused an appreciable reduction in the endplate effect at low angles of attack; at the highest thrust (fig. 26(c)), the horizontal tail had an unfavorable effect on $C_{n_\beta}$ up to about $4^\circ$. At higher angles of attack (above $7^\circ$), the favorable endplate effect with power on was much greater than that for the zero-thrust condition (fig. 26(a)).

Some knowledge of the vertical-tail contribution to $C_{n_\beta}$ is needed to gain an understanding of the endplate effects of the horizontal tail, but the needed vertical-tail-off data were not obtained. The tail contribution, therefore, cannot be determined. The longitudinal characteristics at zero sideslip (fig. 20), however, provide some indications of flow anomalies that are probably pertinent; pitching moments with the $-5^\circ$ stabilizer setting are of interest inasmuch as this setting was used in the lateral-stability tests. The results of figure 20 indicate that the horizontal tail was operating at or near stall at angles of attack near $0^\circ$ when the stabilizer was set at $-5^\circ$, and increasing thrust appeared to aggravate this behavior. It is highly probable that effects of flow separation and the associated pressure field on the underside of the downward-lifting horizontal tail were responsible for the loss of endplate effect on the vertical tail. It may be reasoned, furthermore, that the loss of endplate effect shown in the directional-stability data probably would not have occurred with the horizontal tail set at $+5^\circ$ incidence instead of the $-5^\circ$ used.

## SUMMARY OF RESULTS

The results obtained in a low-speed investigation of the power-on static-turning characteristics and powered-lift aerodynamic performance of a four-engine upper surface blown transport configuration may be summarized as follows:

1. Static turning characteristics generally were indicative of the powered-lift performance to be expected; however, aerodynamic results obtained with the D-nozzles and high flap deflections did not show the performance expected from the static data.

2. The overall results obtained on the model with the D-nozzles indicated that the turning radius associated with the higher flap deflection was too small to maintain attached flow of the relatively thick jet efflux from the D-nozzles.

3. Thinning and spreading of the jet efflux by the use of aspect-ratio-6 rectangular nozzles provided significant improvements in powered-lift performance; however, the $65^{\circ}$ basic flap deflection provided less maximum lift than the $35^{\circ}$ or $50^{\circ}$ deflections with power on.

4. Maximum lift coefficients of about 6.3 were obtained with the rectangular nozzles at a thrust coefficient of 2.0 for both the basic $50^{\circ}$ flap deflection and the $90^{\circ}$ radius flap. Positive drag was indicated for lift coefficients greater than 5.5. The highest lift coefficients obtained with these flap deflections were about 9.3 at a thrust coefficient of 4.0.

5. Longitudinal trim of the complete model could be obtained for most conditions within the $\pm 5^{\circ}$ range of stabilizer incidence tested. The model was longitudinally unstable at high thrust and high angles of attack for many conditions, and some forward transfer of the moment reference would be required to provide positive static margins for all conditions. Trim could be obtained with the forward transfer within the test range of stabilizer settings, except for the $90^{\circ}$ radius flap at thrust coefficients of 3.0 and 4.0.

6. Positive effective dihedral $\left(-C_{l_\beta}\right)$ was indicated for the model with rectangular nozzles for all deflections of the basic flap and thrust conditions investigated. The addition of power generally caused minor increases in effective dihedral, except at high angles of attack where the power-off data for the high flap deflections showed an abrupt increase in negative values of $C_{l_\beta}$.

7. Increasing positive static directional stability was indicated up to an angle of attack of about $12^{\circ}$ with power off. The static directional stability decreased as the angle of attack increased above about $12^{\circ}$, and about neutral stability was shown for the high flap deflections above an angle of attack of $20^{\circ}$. The application of power significantly increased the static directional stability throughout the test angle-of-attack range at all flap deflections.

Langley Research Center
National Aeronautics and Space Administration
Hampton, Va. 23665
October 8, 1975

## REFERENCES


1. Smith, Charles C., Jr.; Phelps, Arthur E., III; and Copeland, W. Latham.: Wind-Tunnel Investigation of a Large-Scale Semispan Model With an Unswept Wing and an Upper-Surface-Blown Jet Flap. NASA TN D-7526, 1974.
2. Phelps, Arthur E., III; and Smith, Charles, C., Jr.: Wind-Tunnel Investigation of an Upper Surface Blown Jet-Flap Powered-Lift Configuration. NASA TN D-7399, 1973.
3. Phelps, Arthur E.; Letko, William; and Henderson, Robert L.: Low-Speed Wind-Tunnel Investigation of a Semispan STOL Jet Transport Wing-Body With an Upper-Surface Blown Jet Flap. NASA TN D-7183, 1973.
4. Johnson, William G., Jr.: Aerodynamic and Performance Characteristics of Externally Blown Flap Configurations. STOL Technology, NASA SP-320, 1972, pp. 43-54.
5. Hoad, Danny R.: Comparison of Aerodynamic Performance of Several STOL Concepts. STOL Technology, NASA SP-320, 1972, pp. 111-119.
6. Mechtly, E. A.: The International System of Units – Physical Constants and Conversion Factors (Second Revision). NASA SP-7012, 1973.
7. Heyson, Harry H.: Linearized Theory of Wind-Tunnel Jet-Boundary Corrections and Ground Effect for VTOL-STOL Aircraft. NASA TR R-124, 1962.

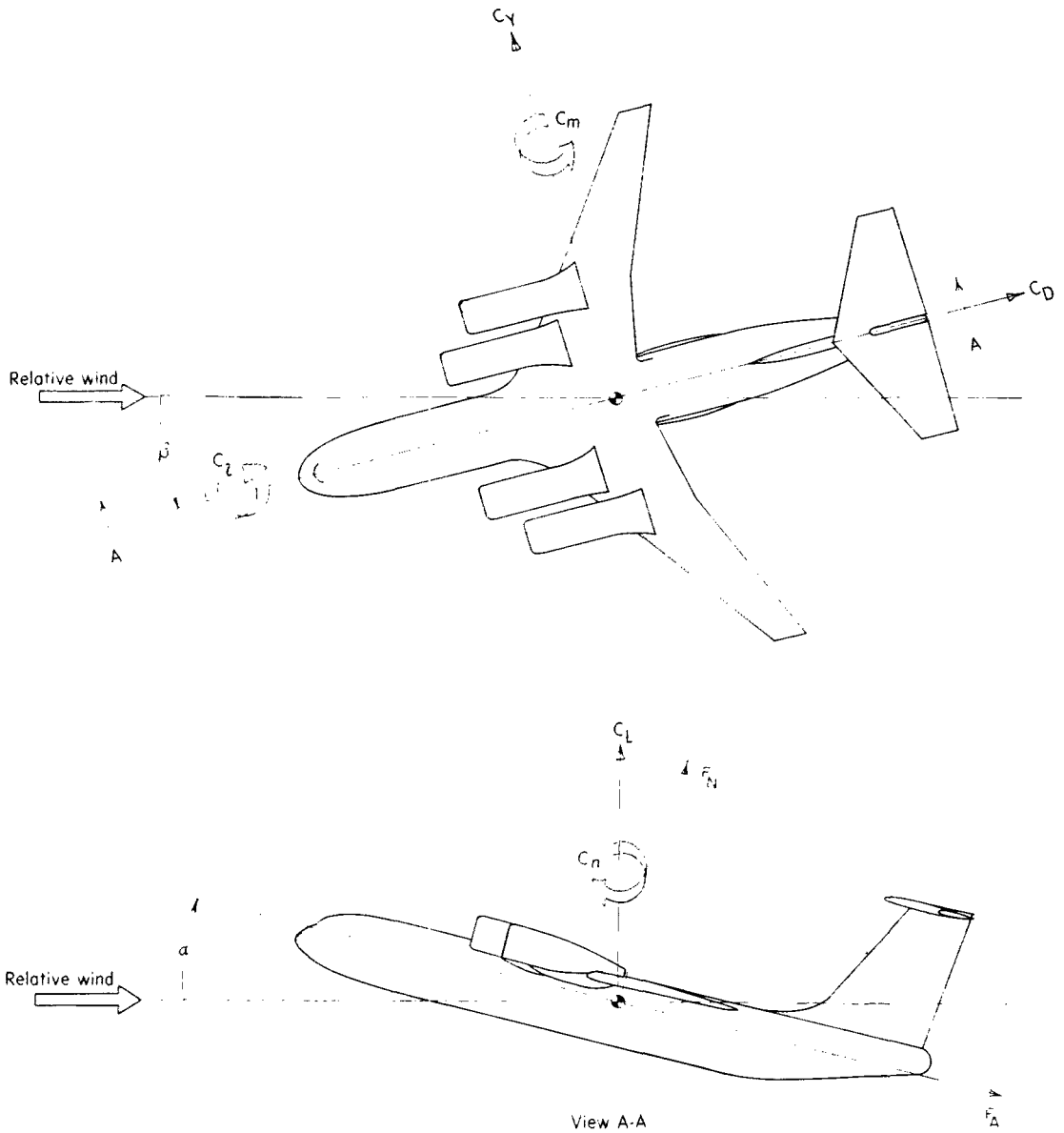


Figure 1.- System of axes used in presentation of data.

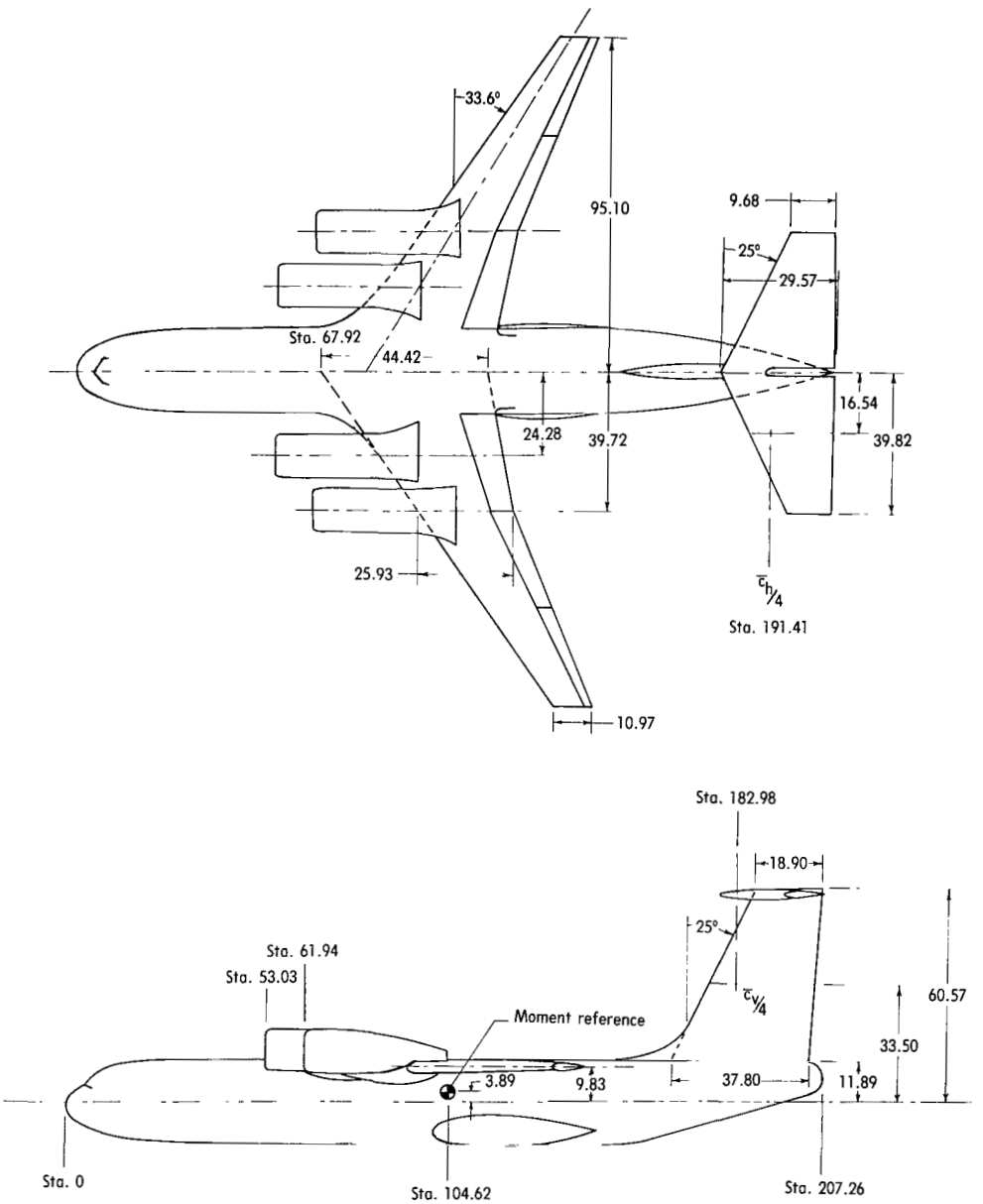


(a) General arrangement and principal dimensions of model with rectangular exhaust nozzles.

Figure 2.- Geometric characteristics of upper surface blown model. All dimensions are in centimeters.

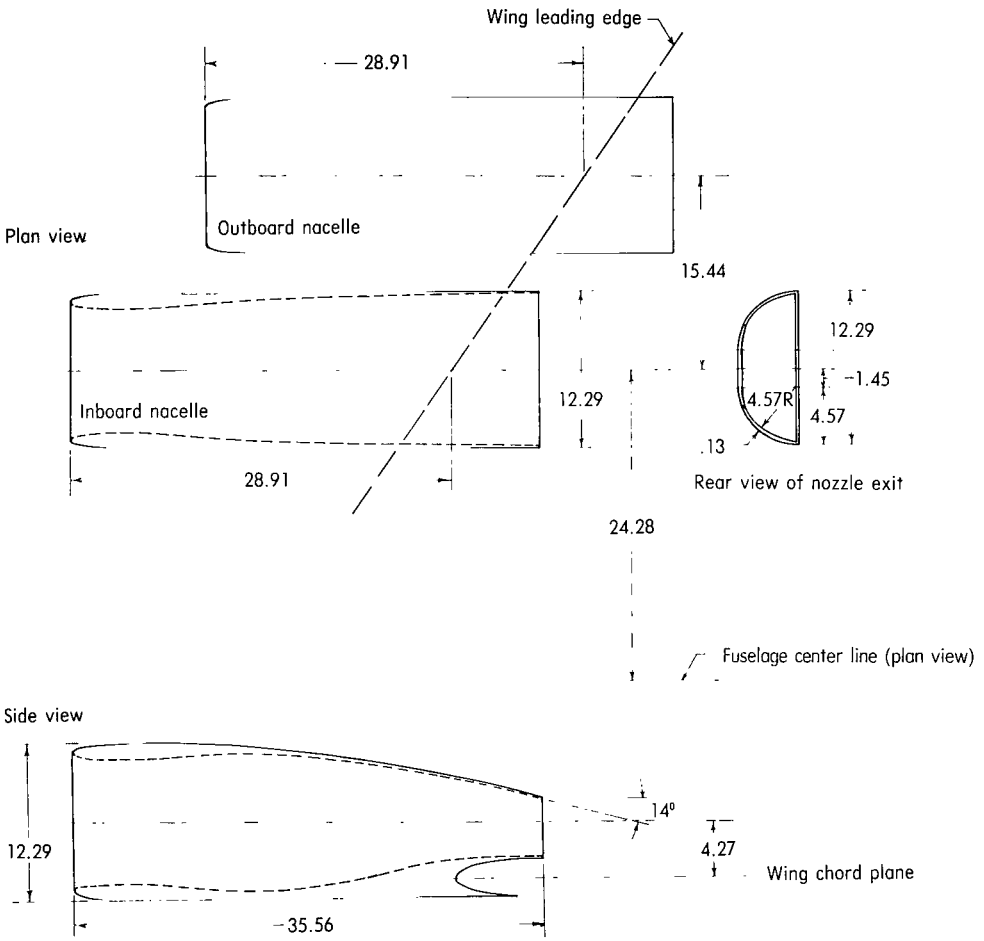


(b) Details of nacelles. D-nozzles.

Figure 2.- Continued.

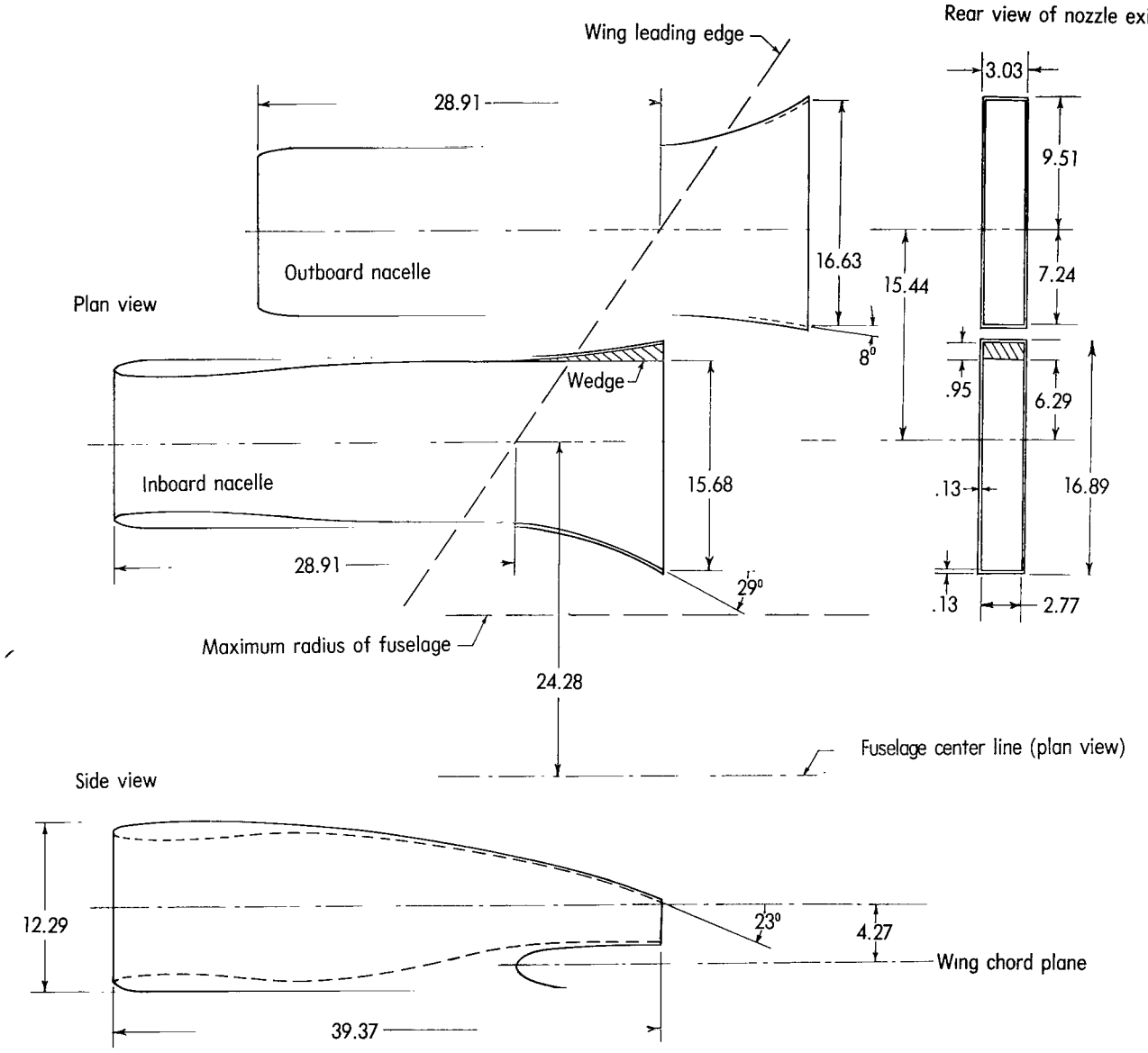


(c) Details of nacelles. Aspect-ratio-6 rectangular nozzles.

Figure 2.- Continued.

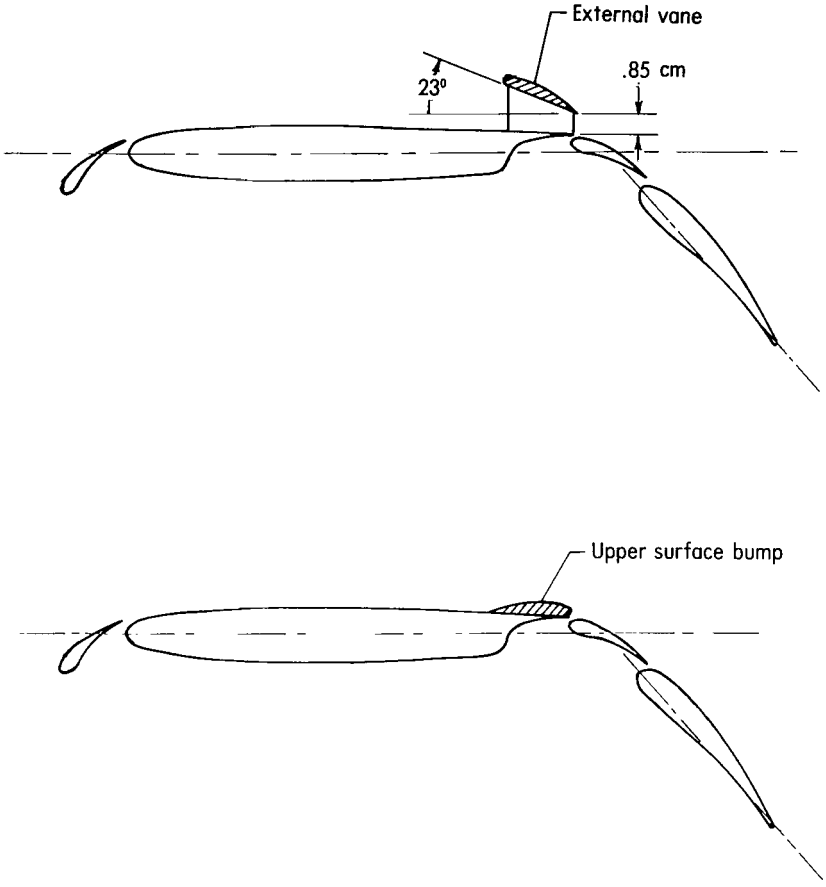


(d) Modifications tested on model with D-nozzles.

Figure 2.- Continued.

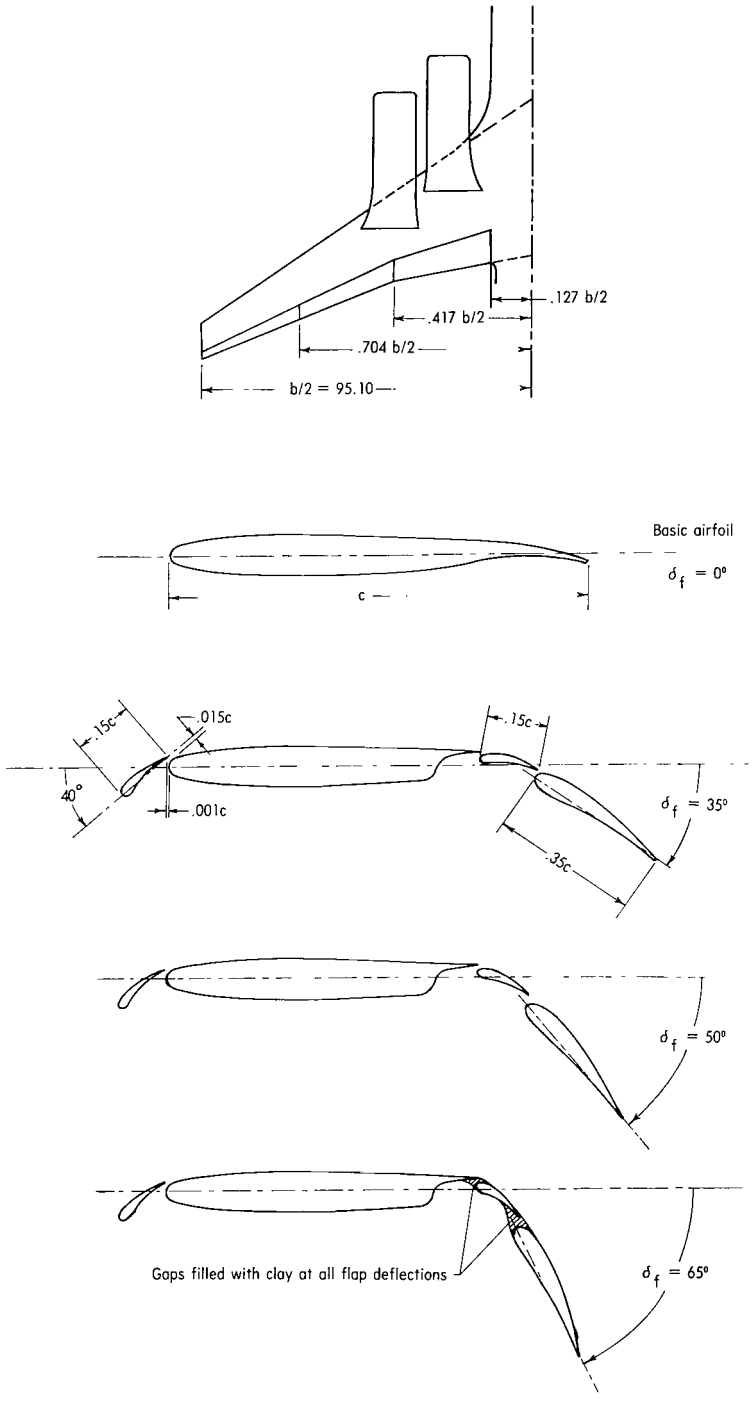


(e) Basic high-lift system with leading-edge slat and double-slotted flap.

Figure 2.- Continued.

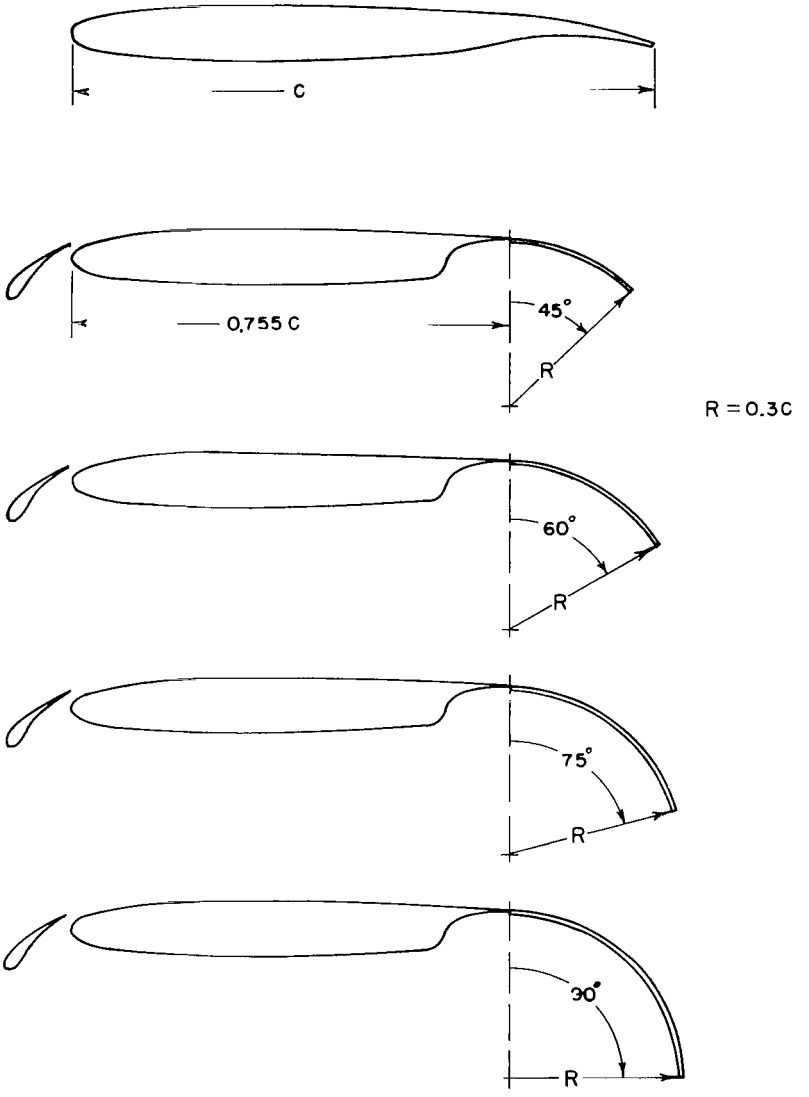


(f) Radius flap high-lift system.

Figure 2.- Concluded.

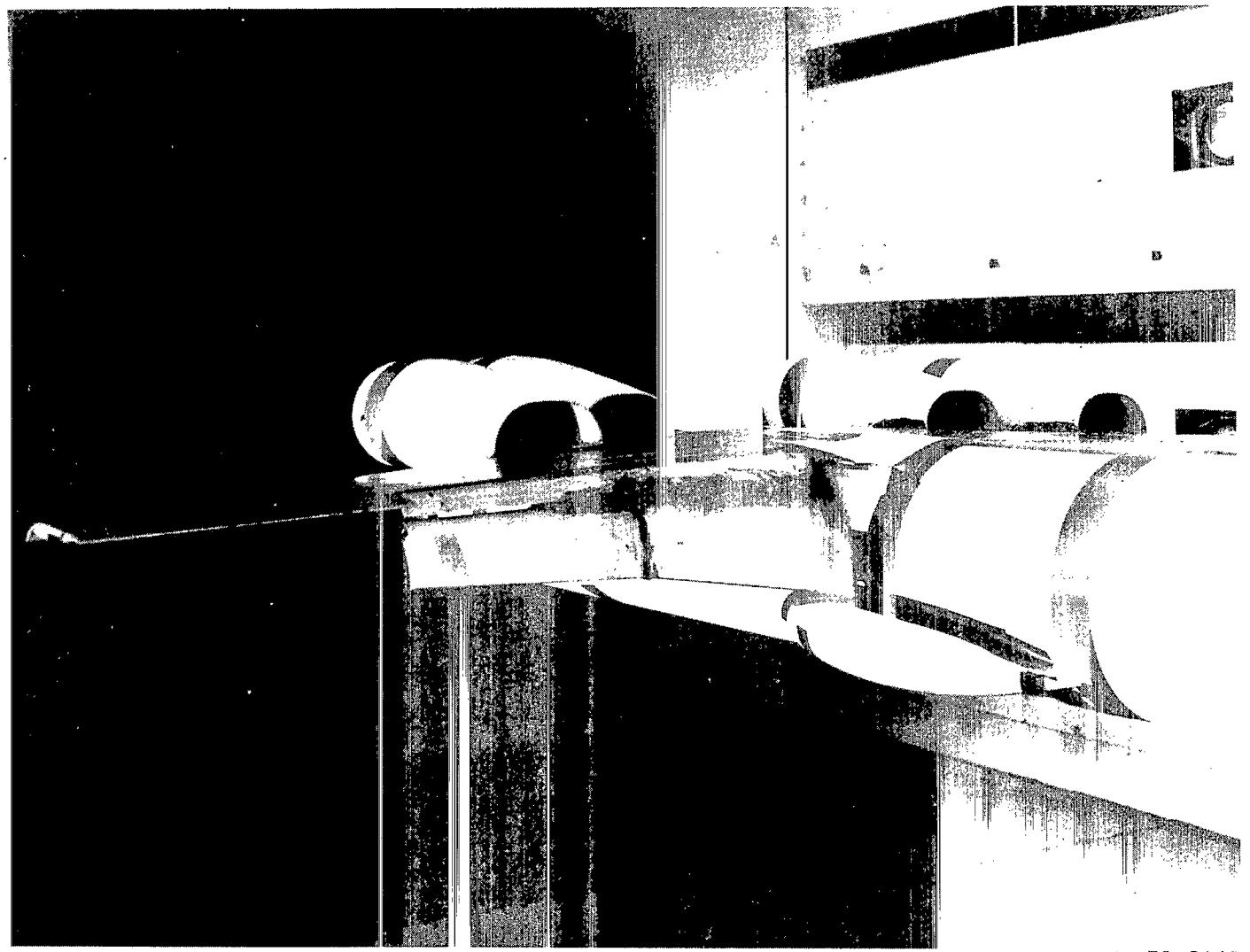

L-72-5148

(a) Model with D-nozzles and basic flap deflected 65°.

Figure 3.- Photographs of upper surface blown model in the Langley V/STOL tunnel.

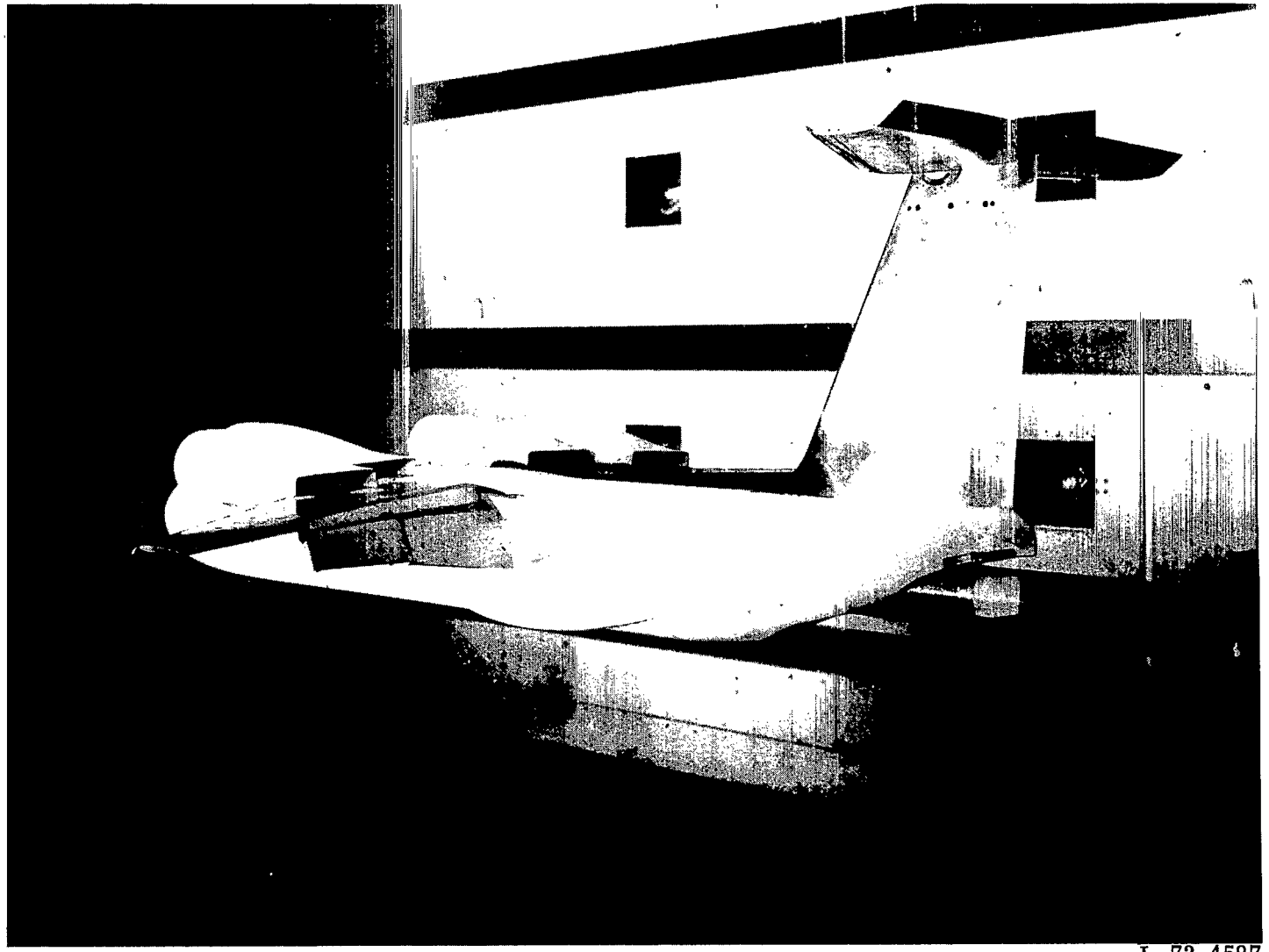

L-73-4587

(b) Model with aspect-ratio-6 rectangular exhaust nozzles and basic flap deflection $65^{o}$.

Figure 3.- Continued.

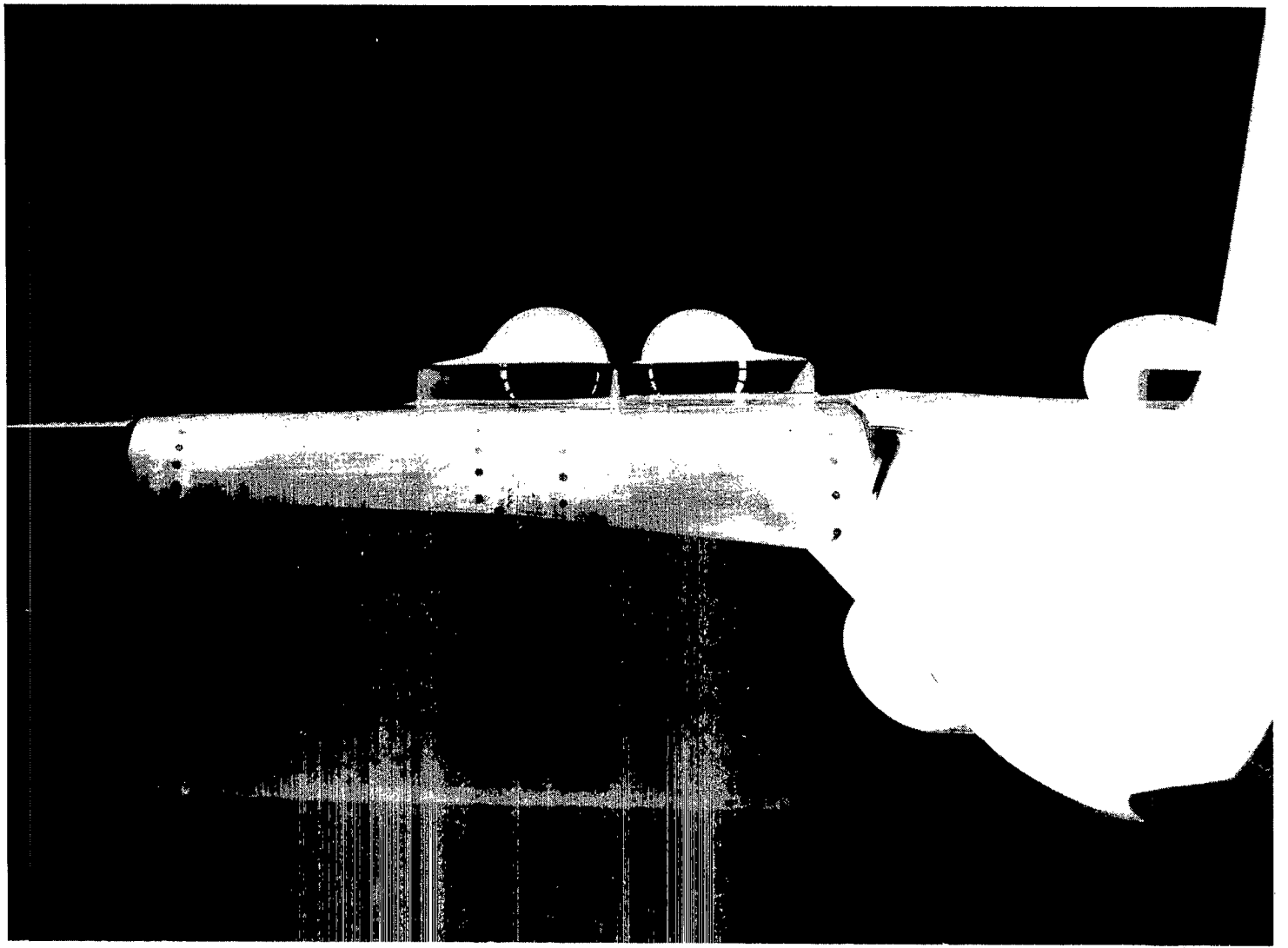

L-73-4586

(c) Model with aspect-ratio-6 rectangular exhaust nozzles and the $90^{o}$ radius flap.

Figure 3.- Concluded.

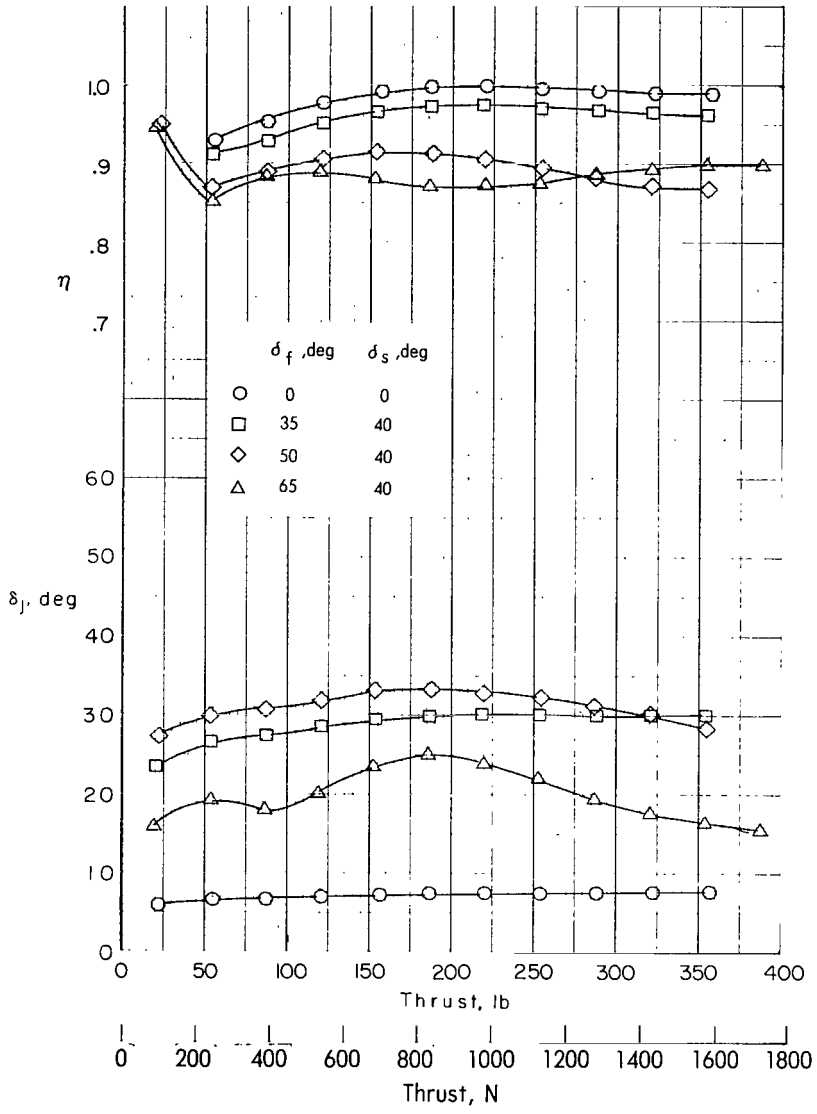


(a) Effect of flap deflection on the basic model.

Figure 4.- Variation of static-turning angle and static-thrust-recovery efficiency with static thrust for the model with D-nozzles. $\alpha = 0^{o}$.

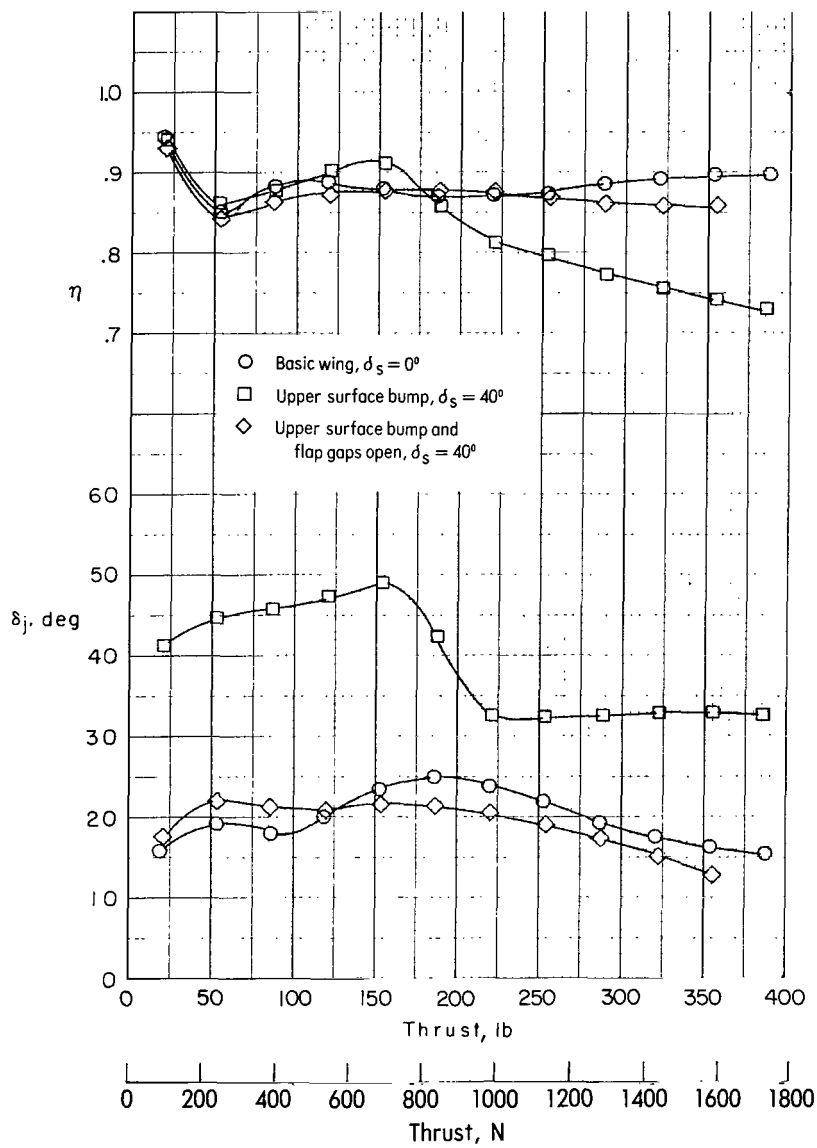


(b) Effect of modifications to the model. $\delta_f = 65^o$.

Figure 4.- Continued.

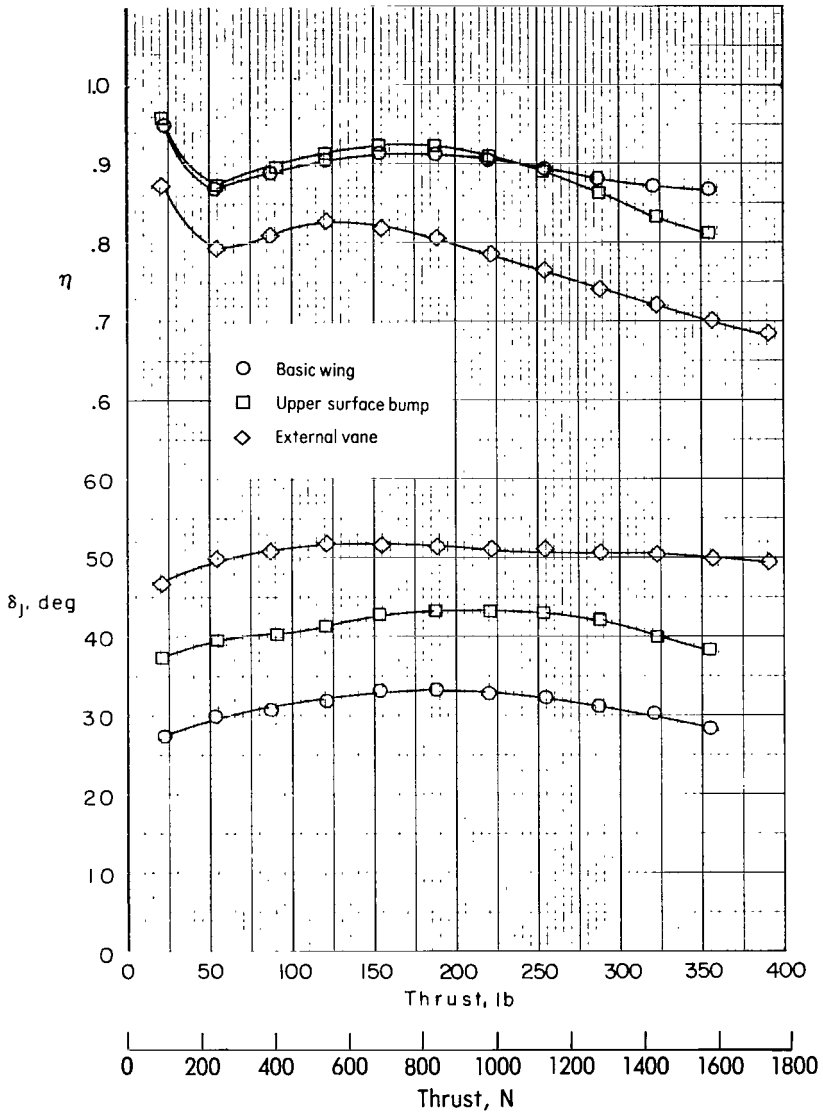


(c) Effect of modifications to the model. $\delta_f = 50^o$; $\delta_s = 40^o$.

Figure 4.- Concluded.

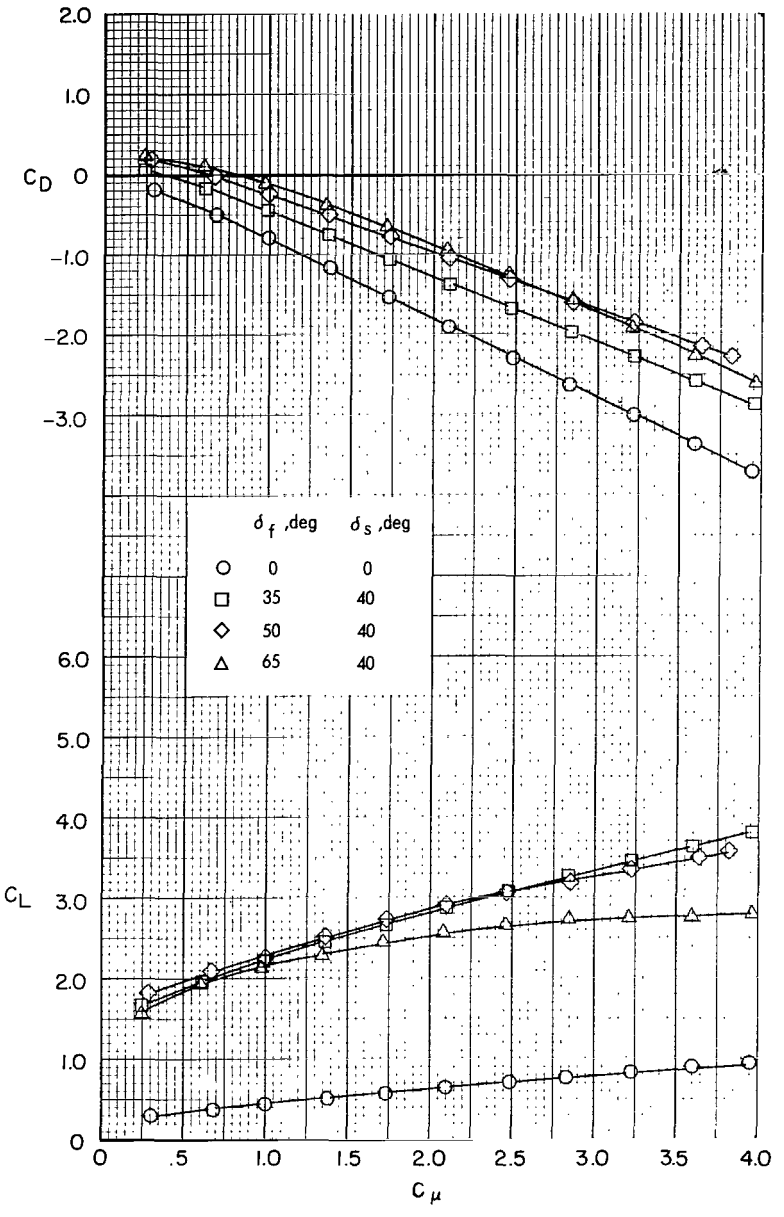


(a) Effect of flap deflection on basic model.

Figure 5.- Variations of lift and drag coefficients with thrust coefficient for the model with D-nozzles. $\alpha = 0^o$.

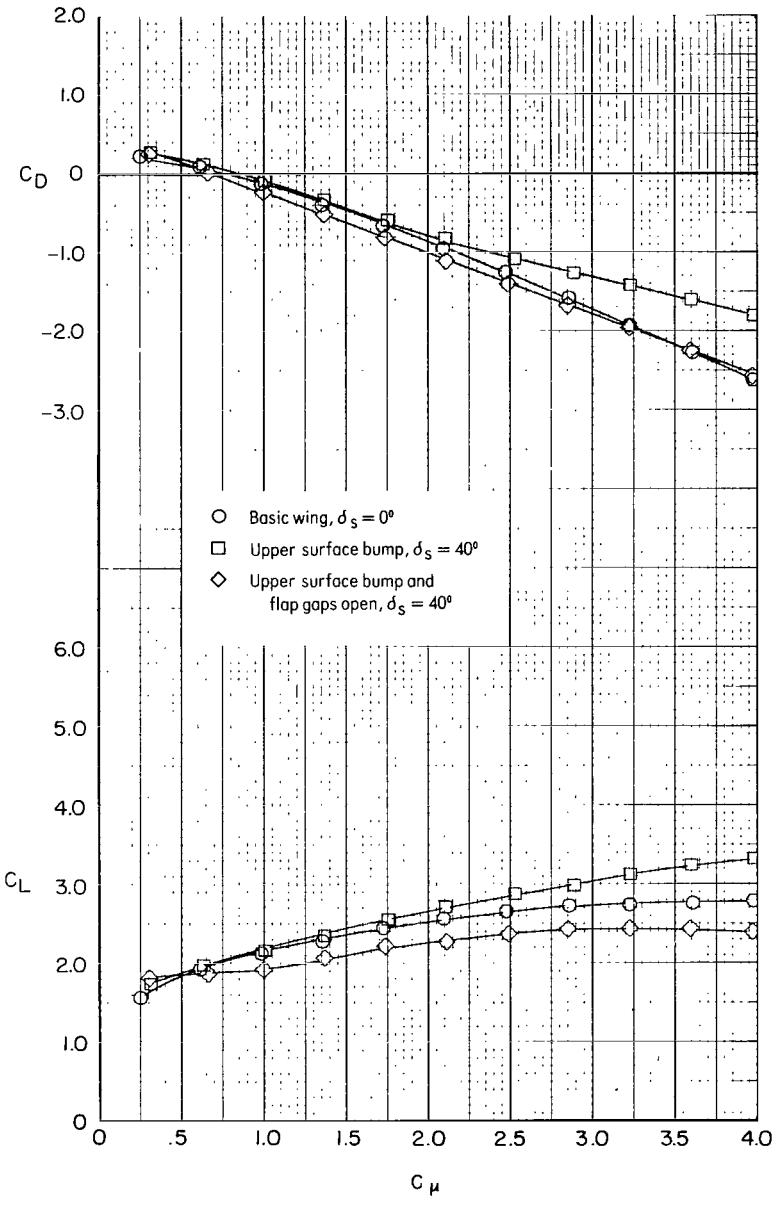


(b) Effect of modifications to the model. $\delta_f = 65^o$; $\delta_s = 40^o$.

Figure 5.- Continued.

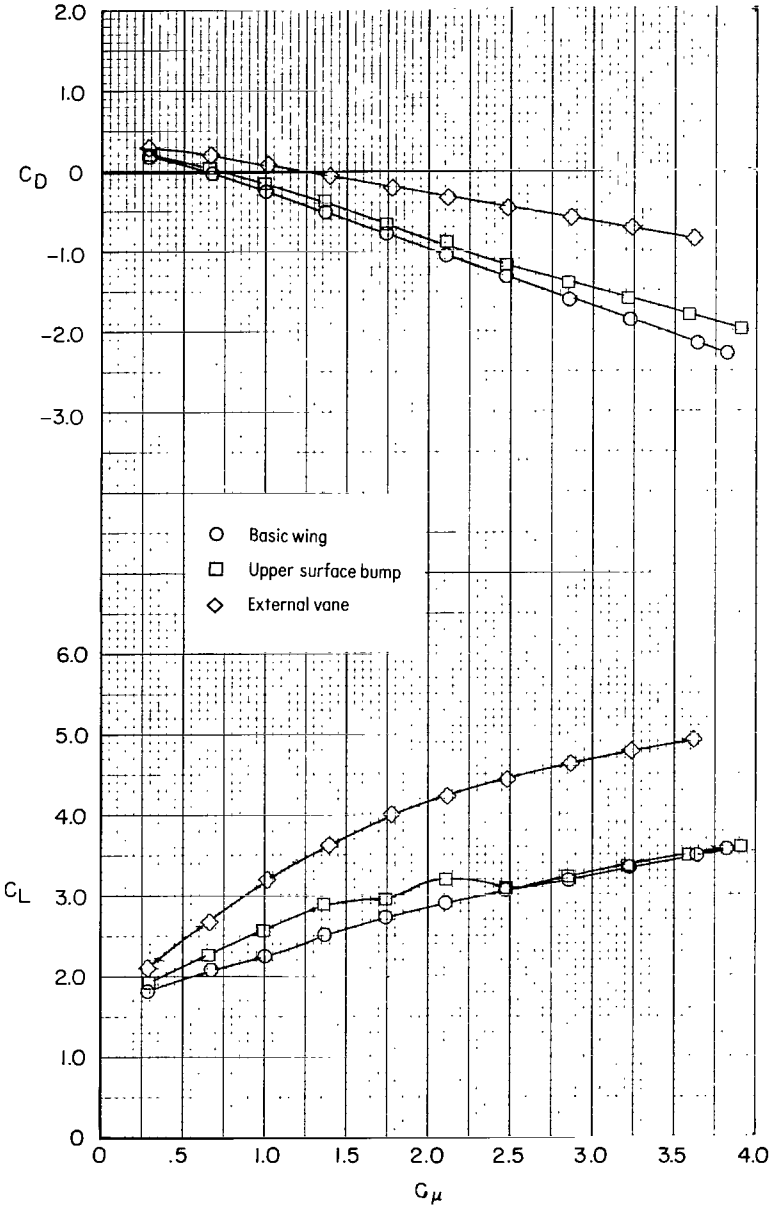


(c) Effect of modifications to the model. $\delta_f = 50^o$; $\delta_s = 40^o$.

Figure 5.- Concluded.

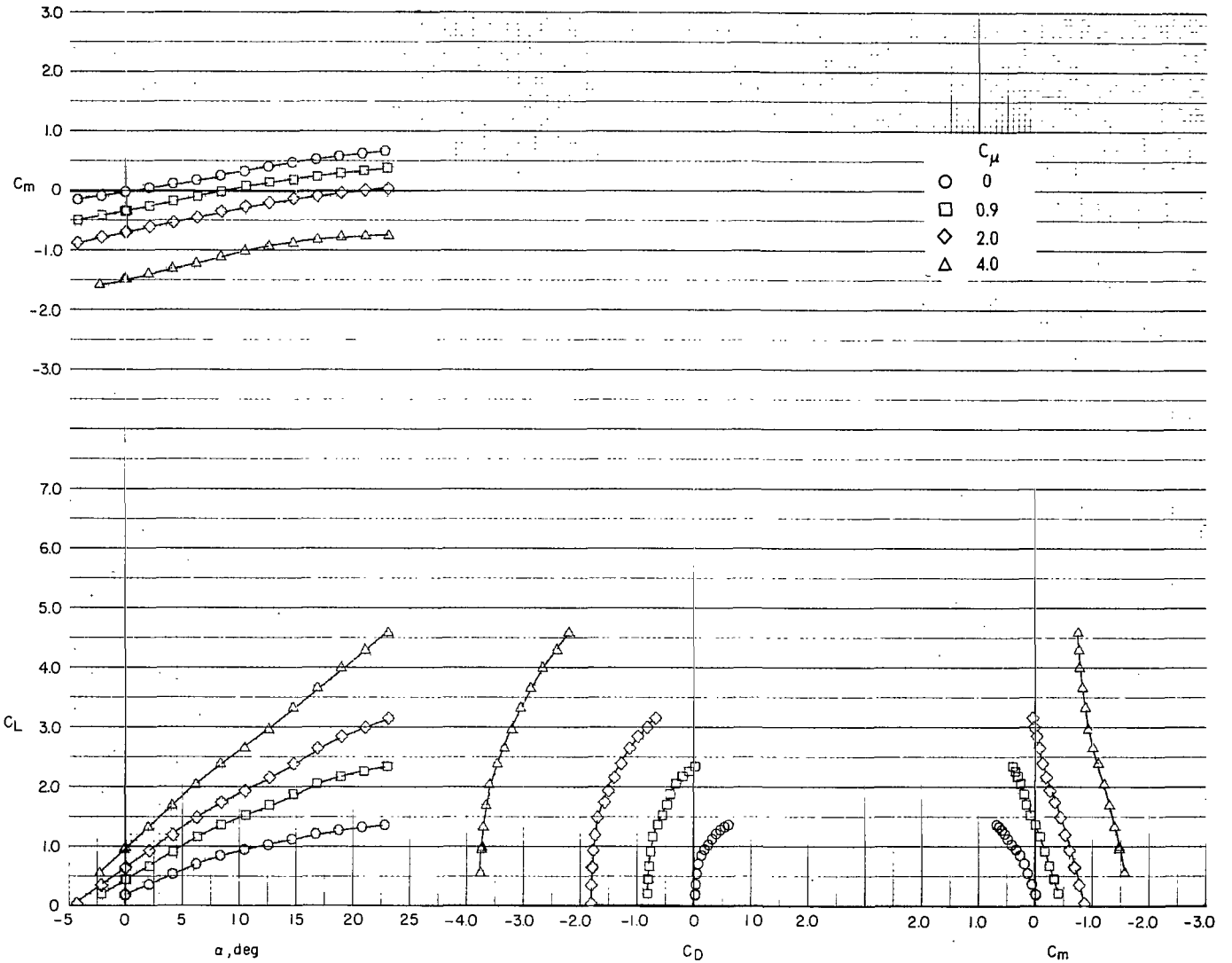


Figure 6.- Effect of angle of attack on the longitudinal aerodynamic characteristics of the model with D-nozzles for constant thrust conditions. Horizontal tail off; $\delta_f = 0^o$; $\delta_s = 0^o$.

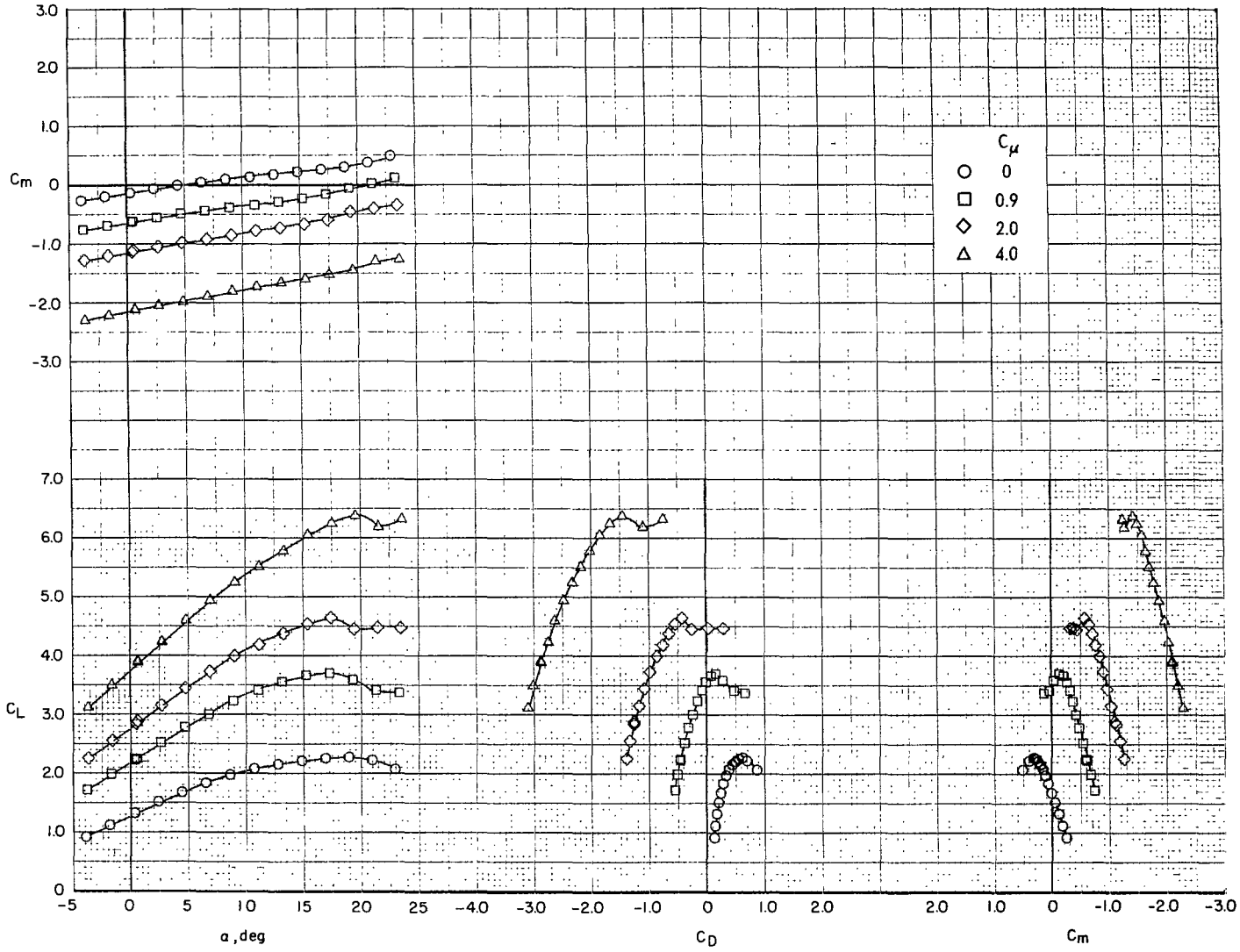


Figure 7.- Effect of angle of attack on the longitudinal aerodynamic characteristics of the model with D-nozzles for constant thrust conditions. Horizontal tail off; $\delta_f = 35^o$; $\delta_s = 40^o$.

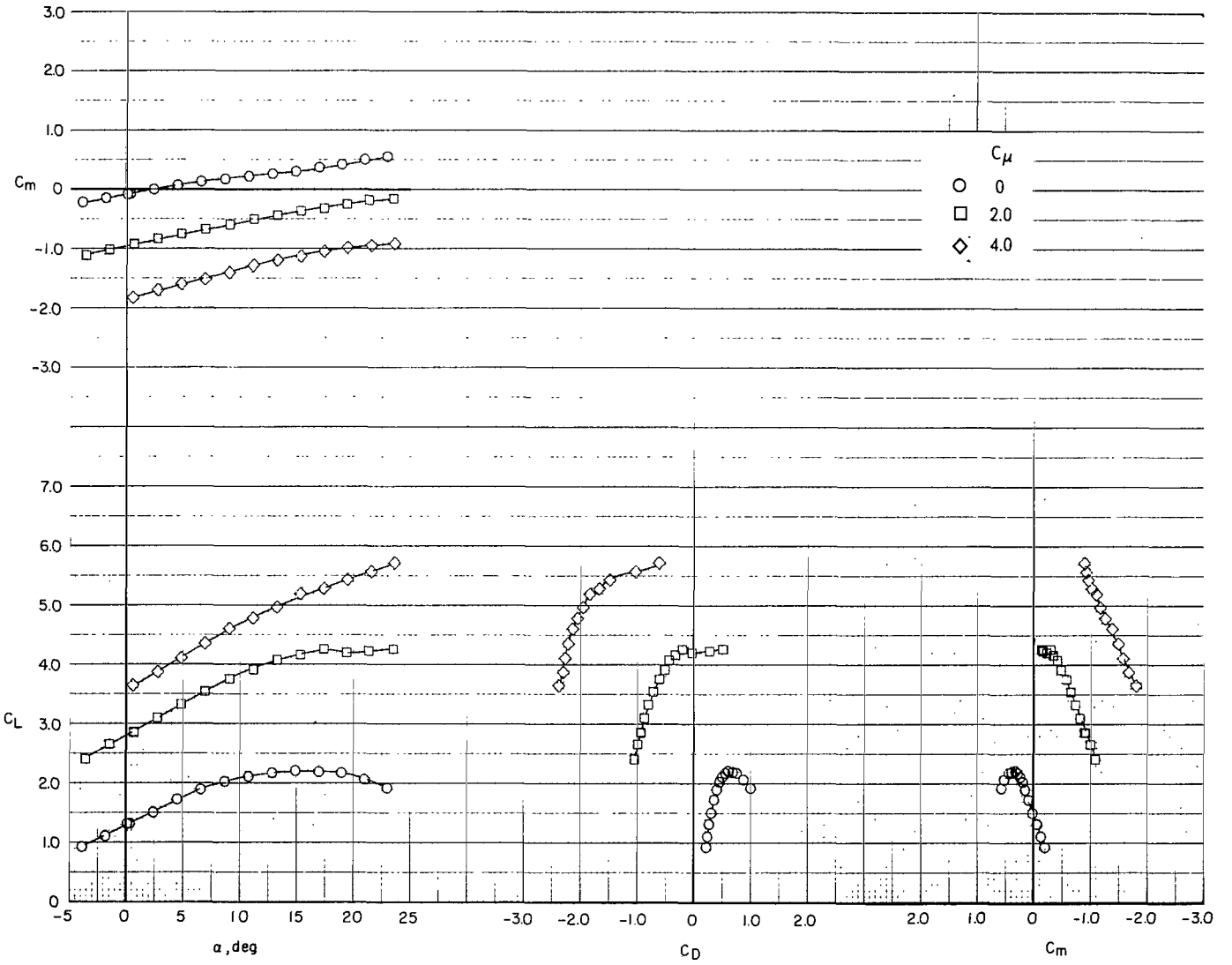


(a) Basic model.

Figure 8.- Effect of angle of attack on the longitudinal aerodynamic characteristics of the model with D-nozzles for constant thrust conditions. Horizontal tail off; $\delta_f = 50^o$; $\delta_s = 40^o$.

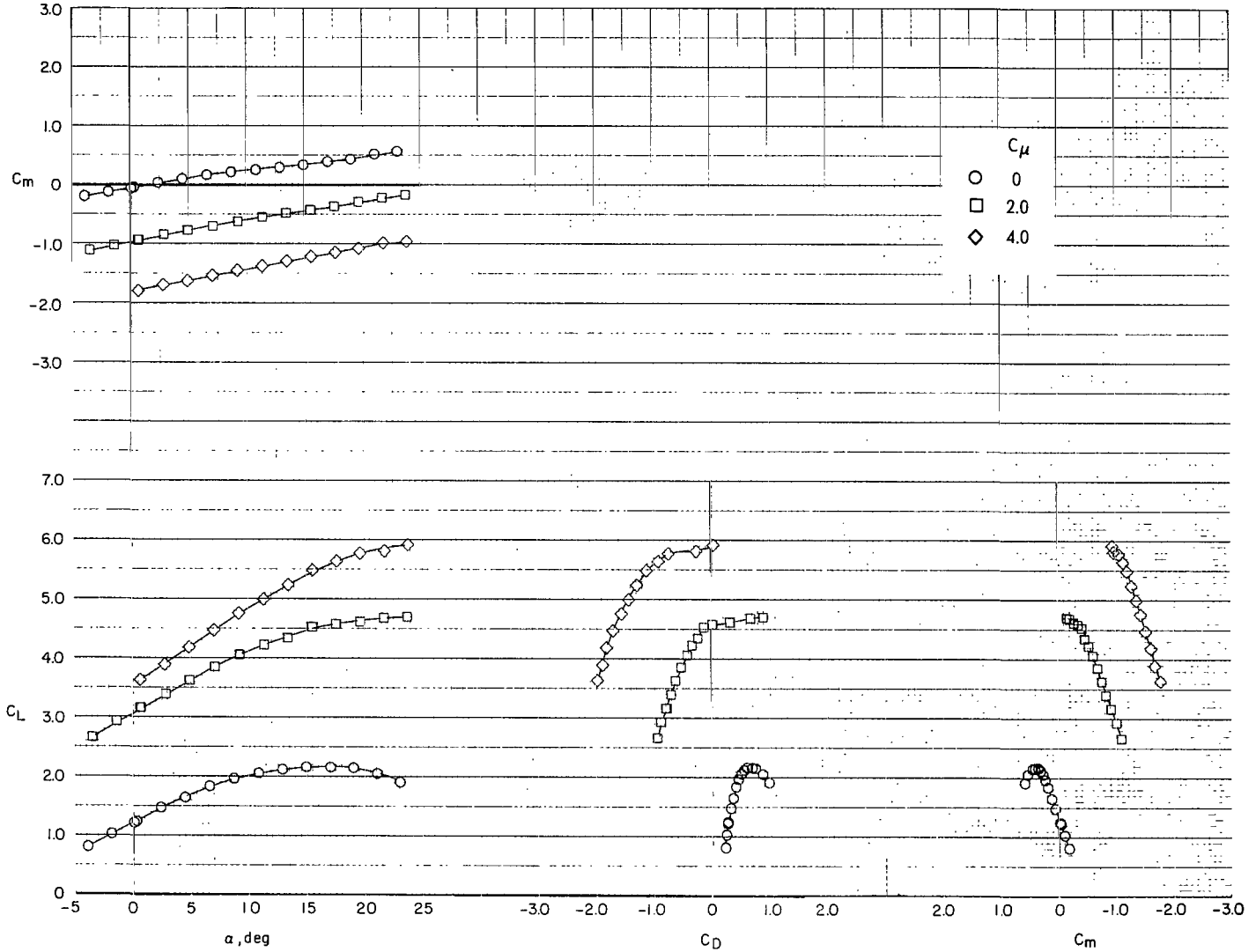


(b) Model with upper surface bump.

Figure 8.- Continued.

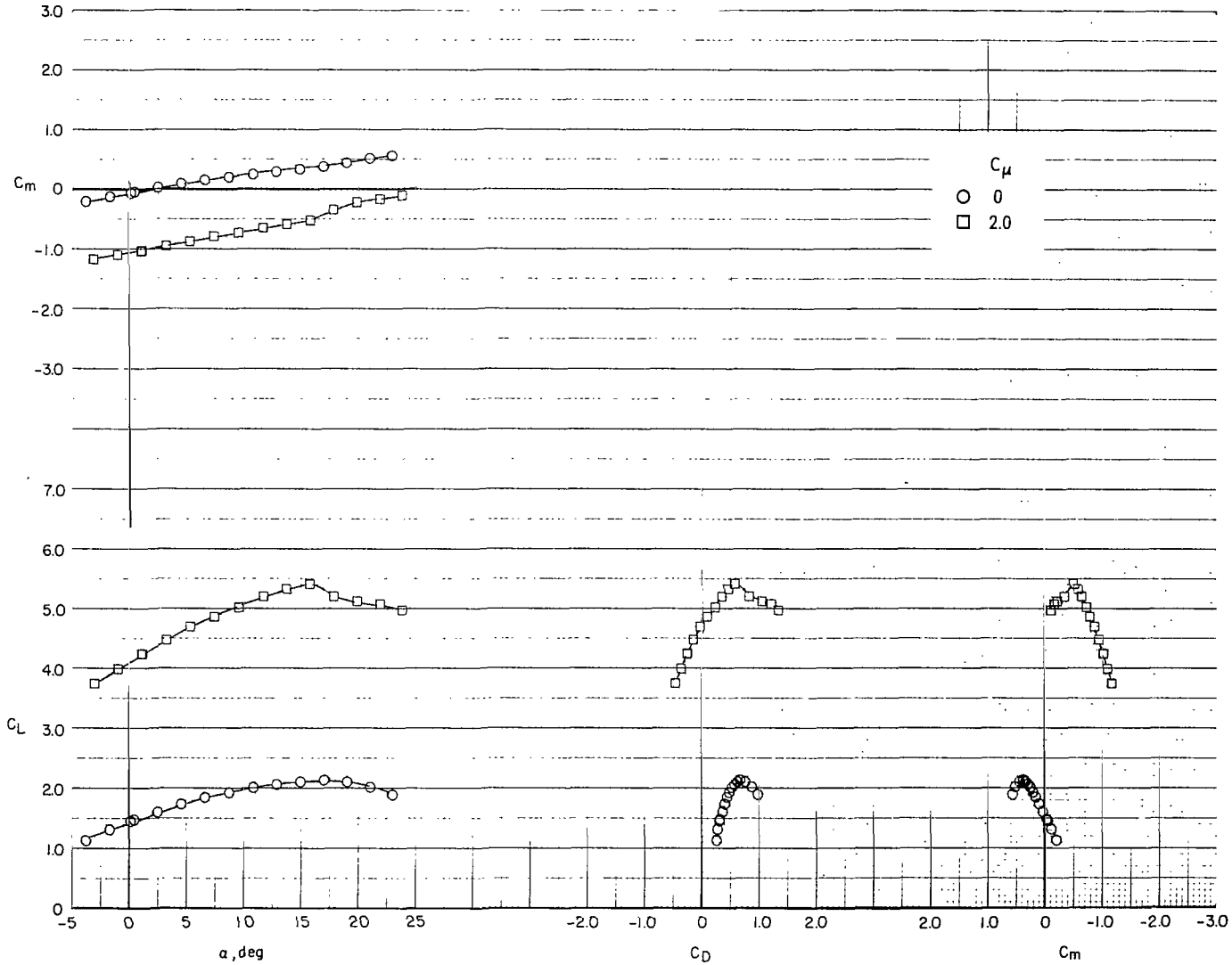


(c) Model with external vane.

Figure 8.- Concluded.

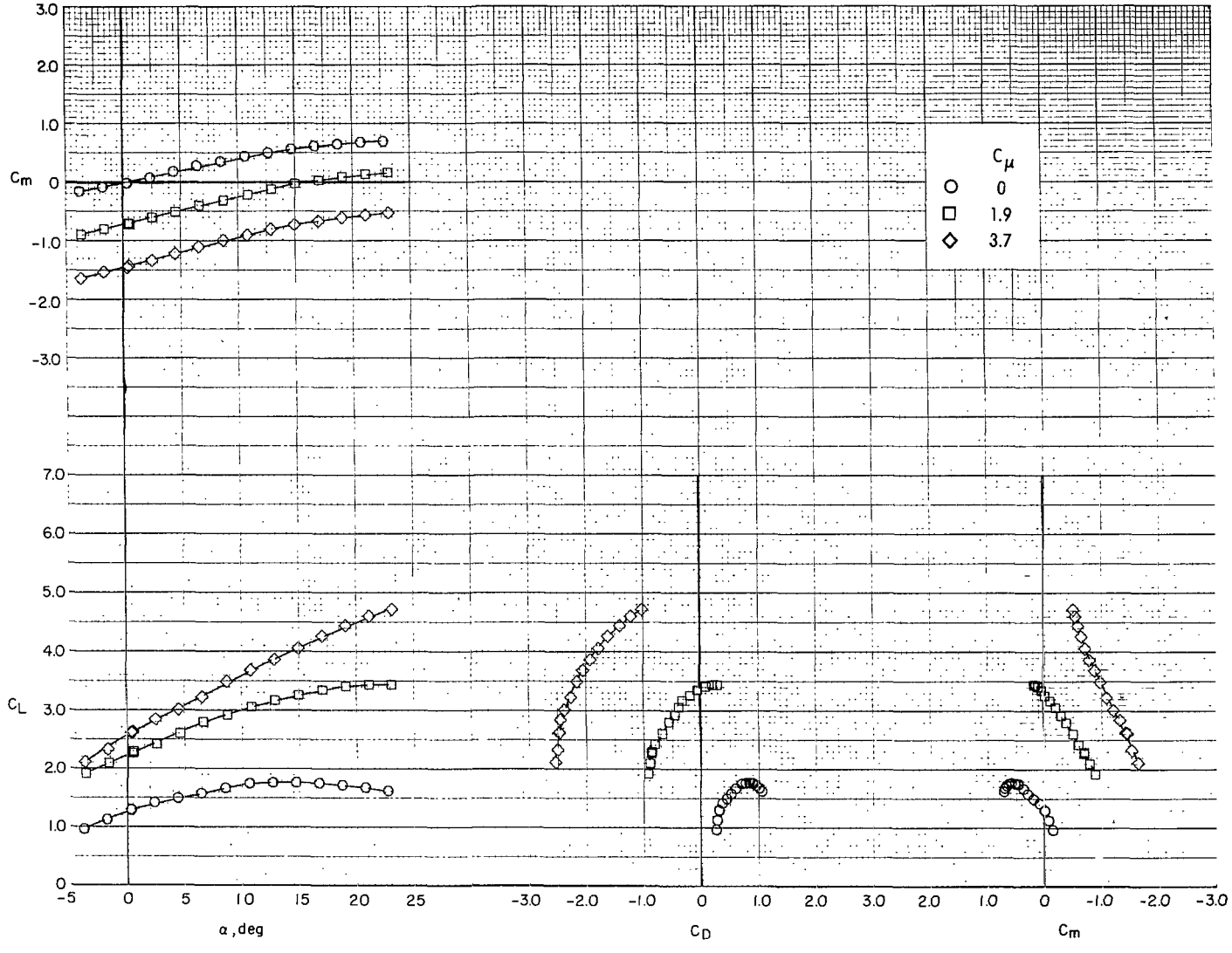


(a) Basic model; $\delta_s = 0^o$.

Figure 9.- Effect of angle of attack on the longitudinal aerodynamic characteristics of the model with D-nozzles for constant thrust conditions. Horizontal tail off; $\delta_f = 65^o$.

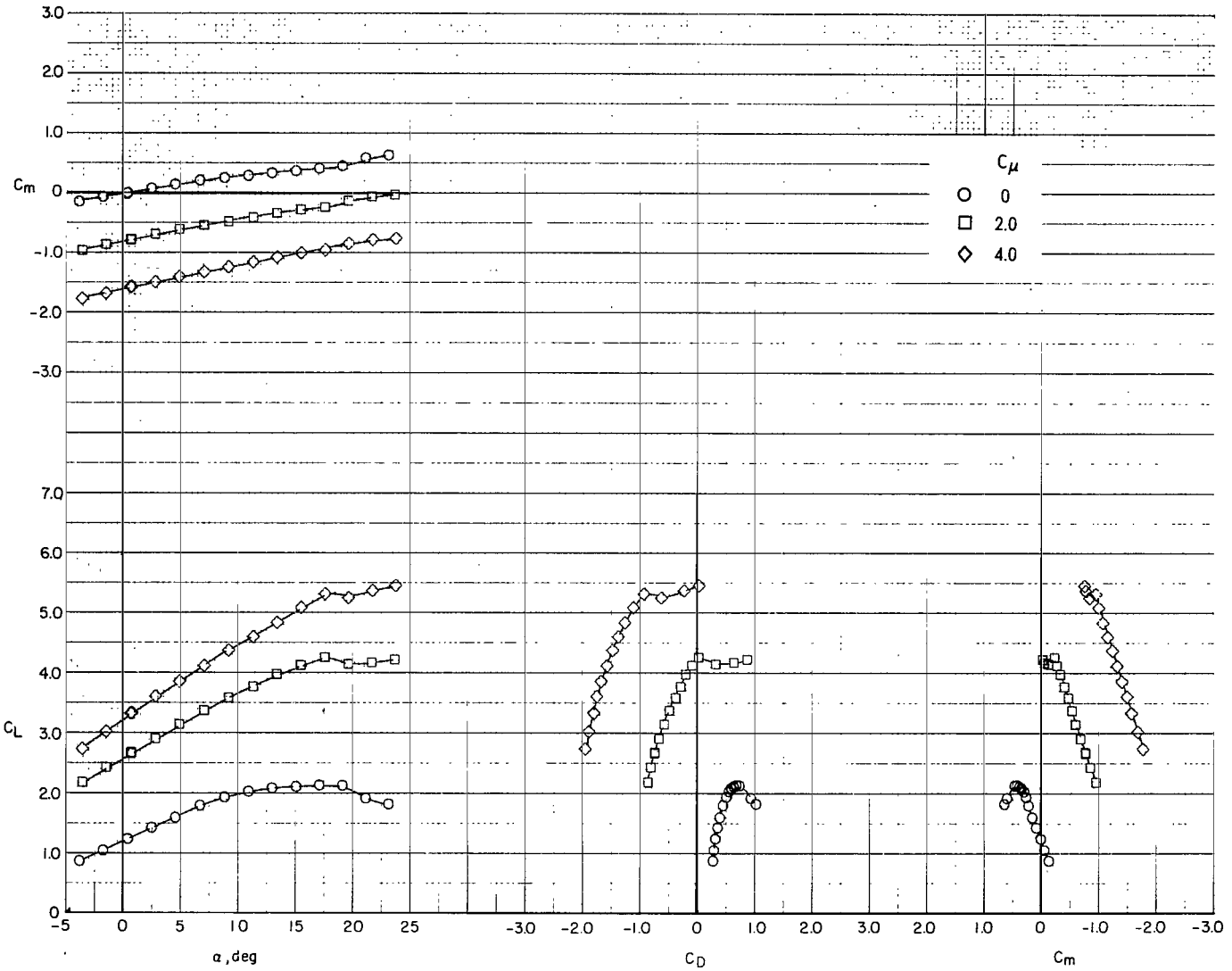


(b) Model with upper surface bump. $\delta_s = 40^o$.

Figure 9.- Continued.

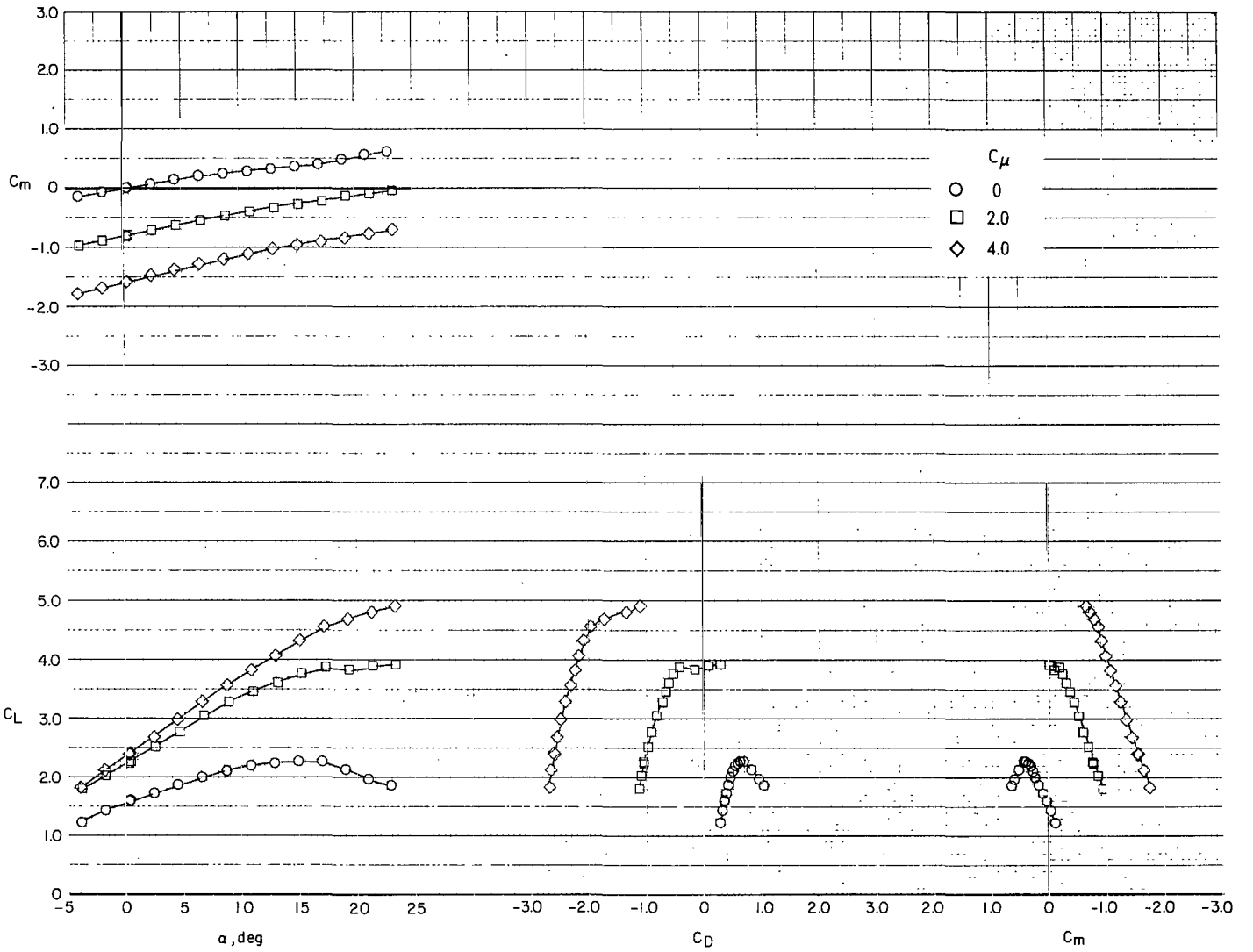


(c) Model with flap gaps open. $\delta_s = 40^o$.

Figure 9.- Concluded.

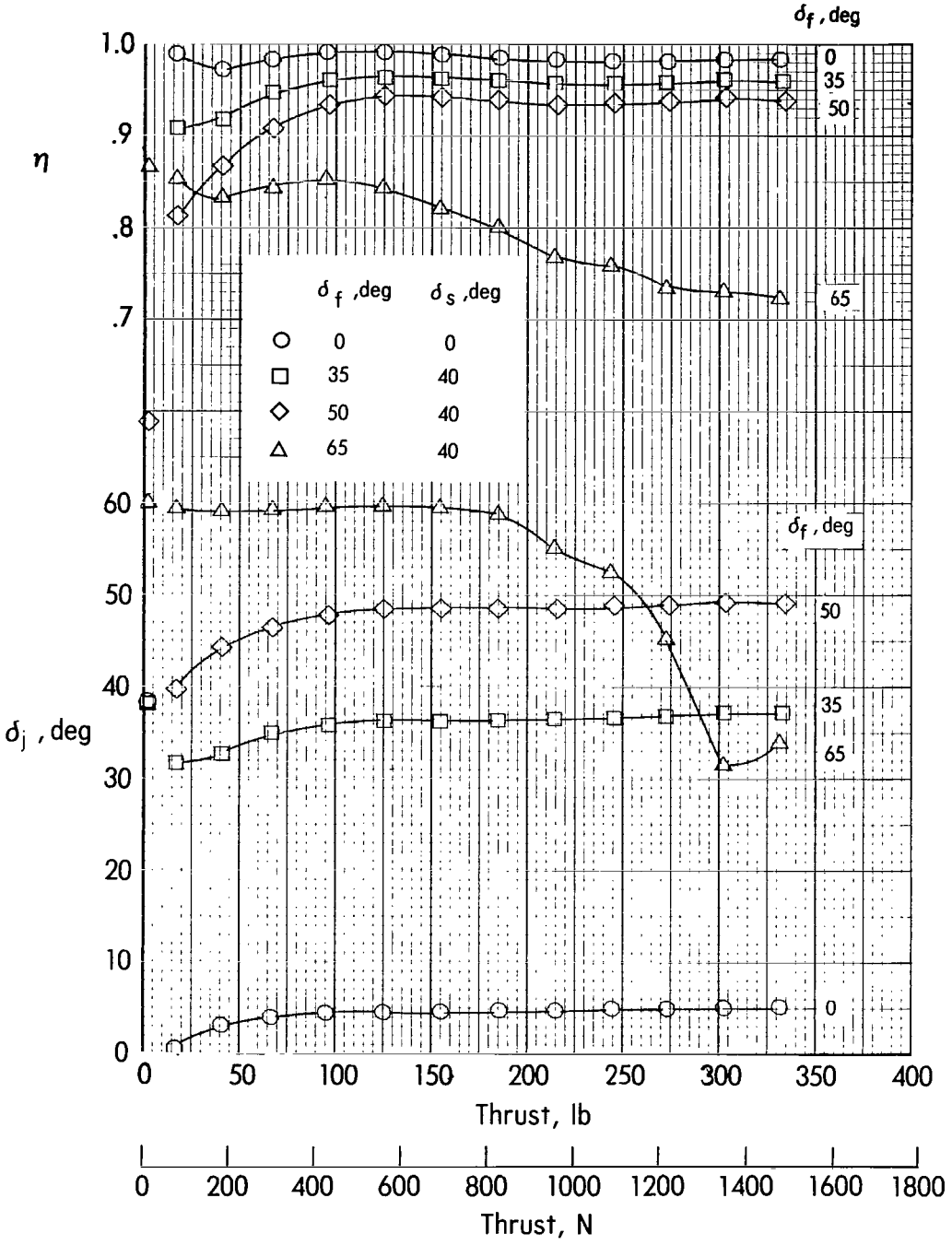


(a) Effect of basic flap deflection.

Figure 10.- Variation of static-turning angle and static-thrust-recovery efficiency with static thrust for the model with rectangular nozzles. $\alpha = 0^{o}$.

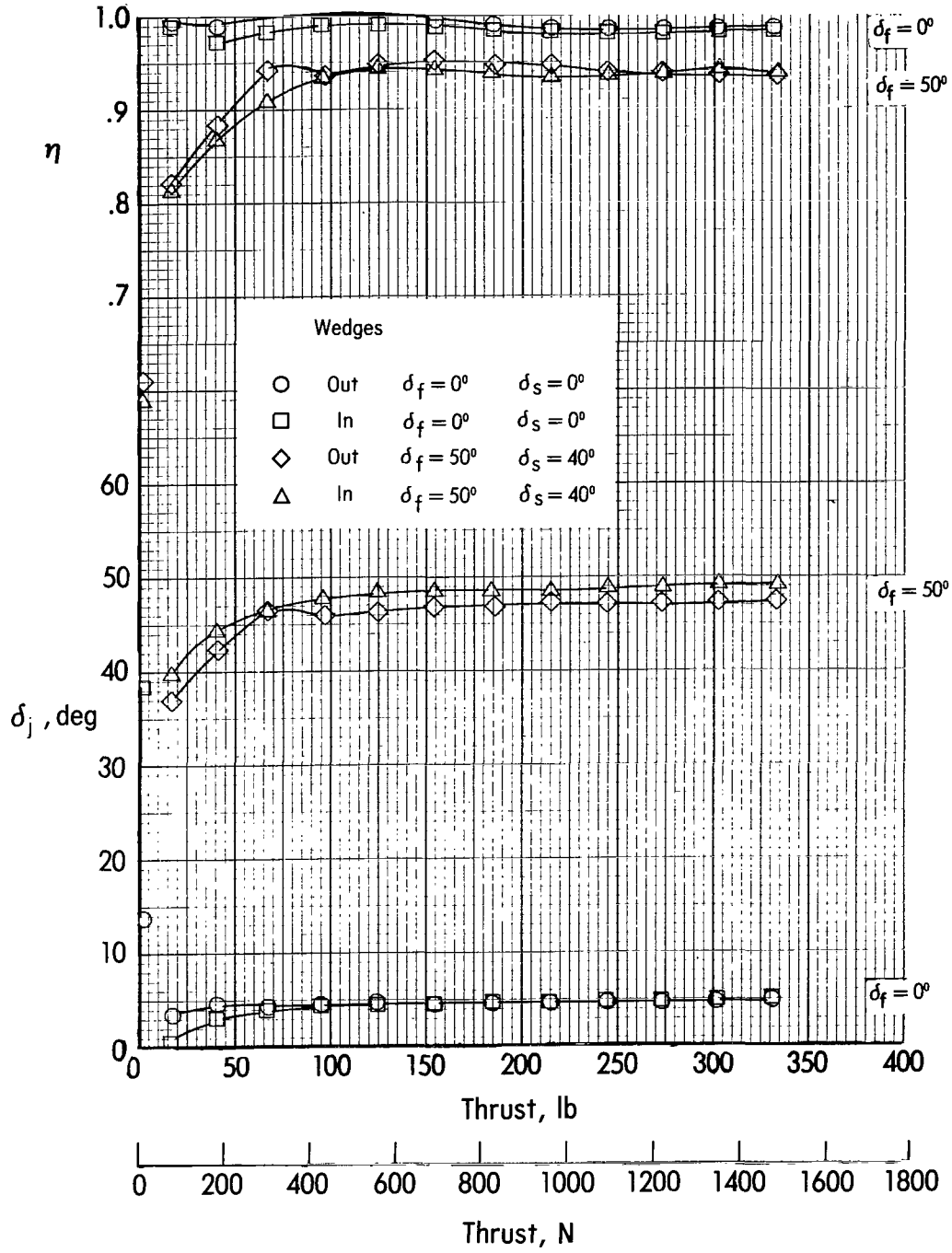


(b) Effect of wedges in the outboard side of the exit nozzles of the inboard nacelles.

Figure 10.- Continued.

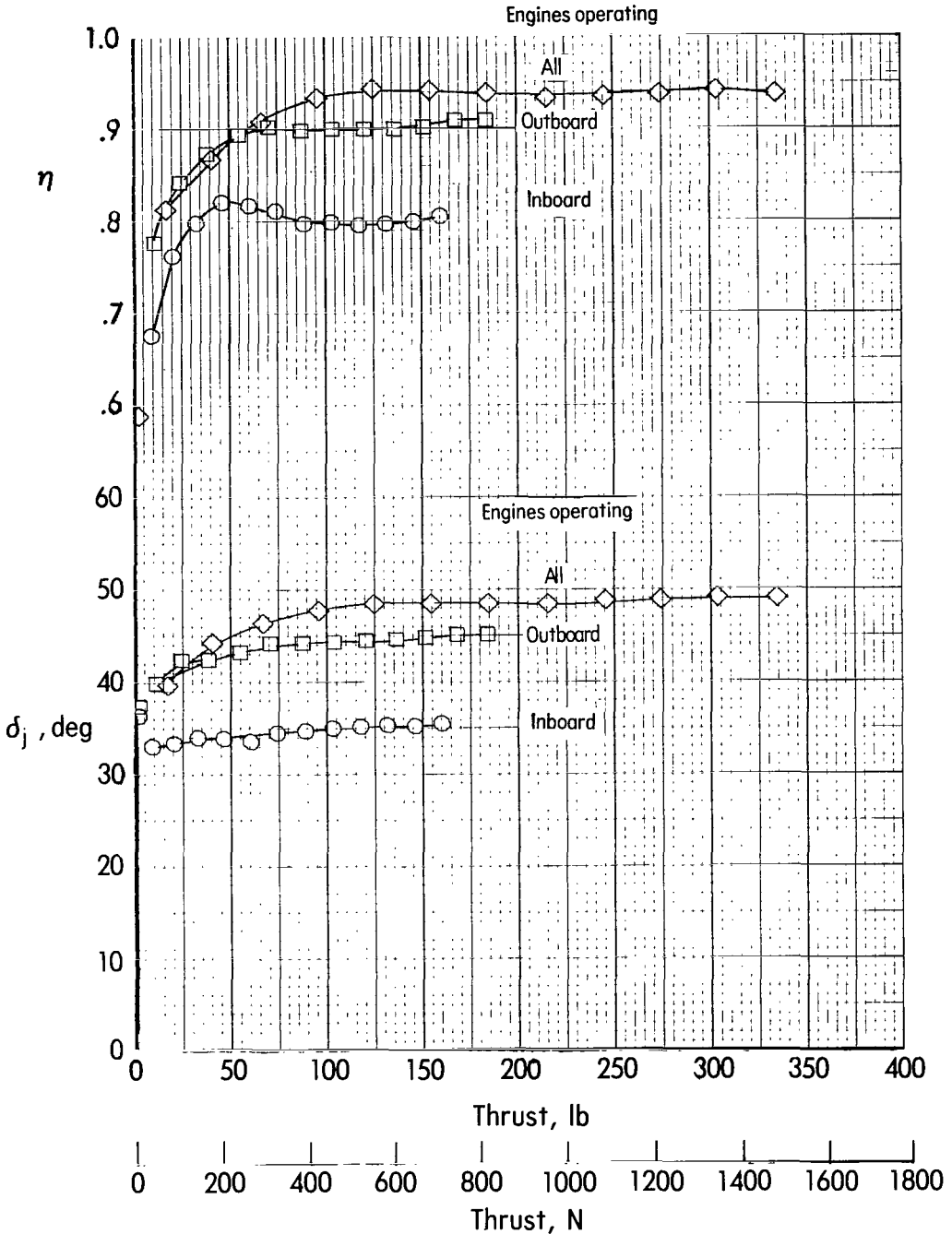


(c) Effect of twin-engine simulation. $\delta_f = 50^o$; $\delta_s = 40^o$.

Figure 10.- Concluded.

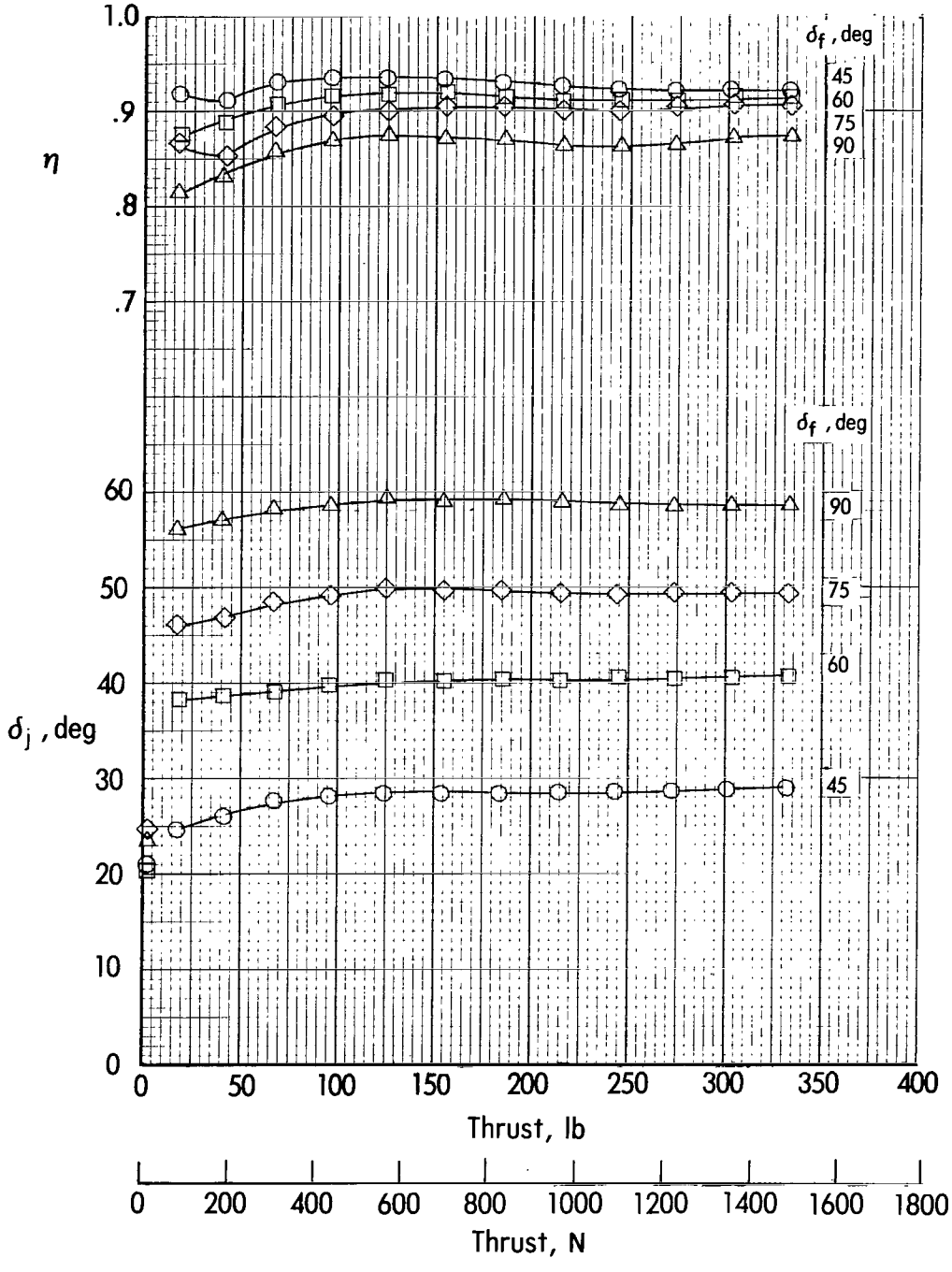


(a) Effect of radius flap deflection.

Figure 11.- Variation of static-turning angle and static-thrust-recovery efficiency with static thrust for the model with rectangular nozzles and the radius flap. $\alpha = 0^{o}$.

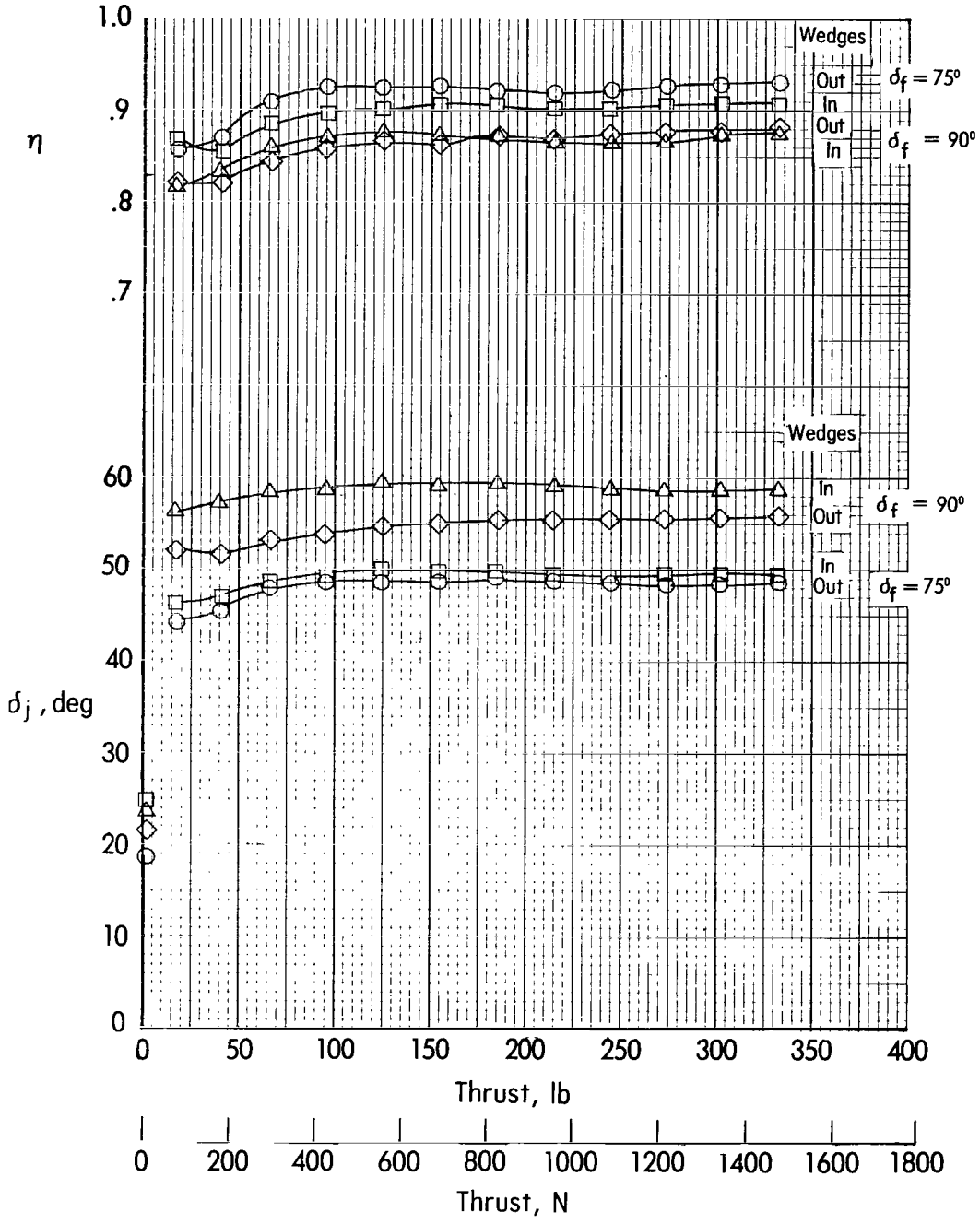


(b) Effect of wedges in the outboard side of the exit nozzles of the inboard nacelles.

Figure 11.- Continued.

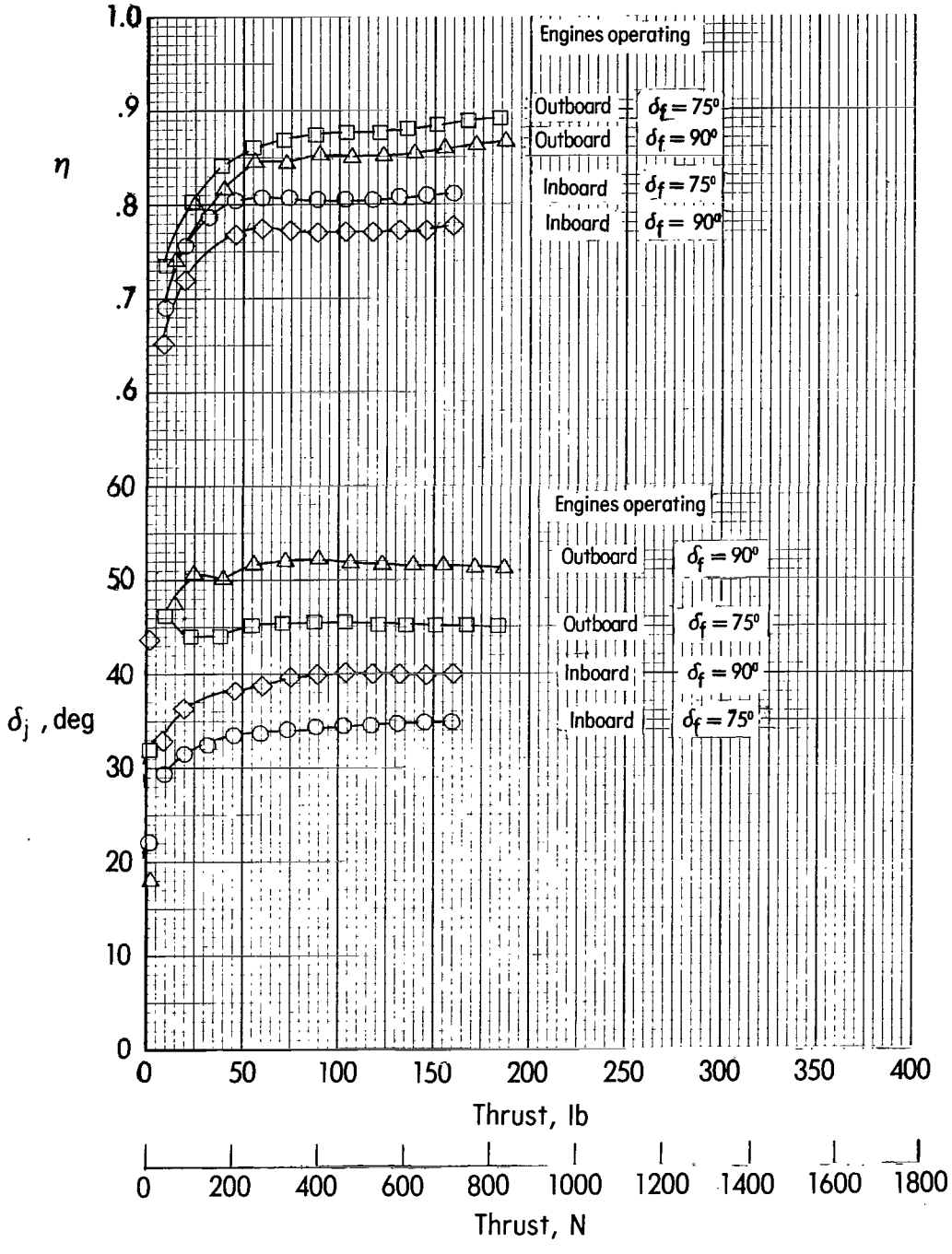


(c) Twin-engine simulation.

Figure 11.- Concluded.

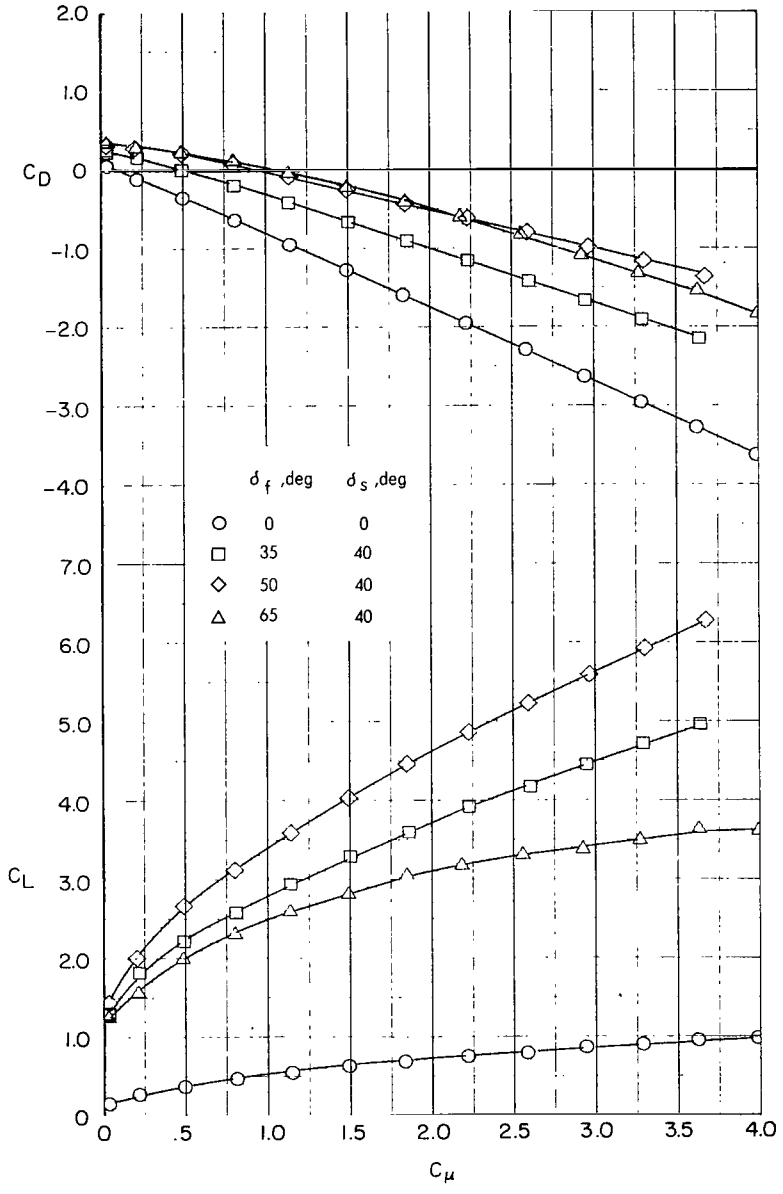


(a) Effect of basic flap deflection.

Figure 12.- Variation of lift and drag coefficients with thrust coefficient for the model with rectangular nozzles. $\alpha = 0^{o}$.

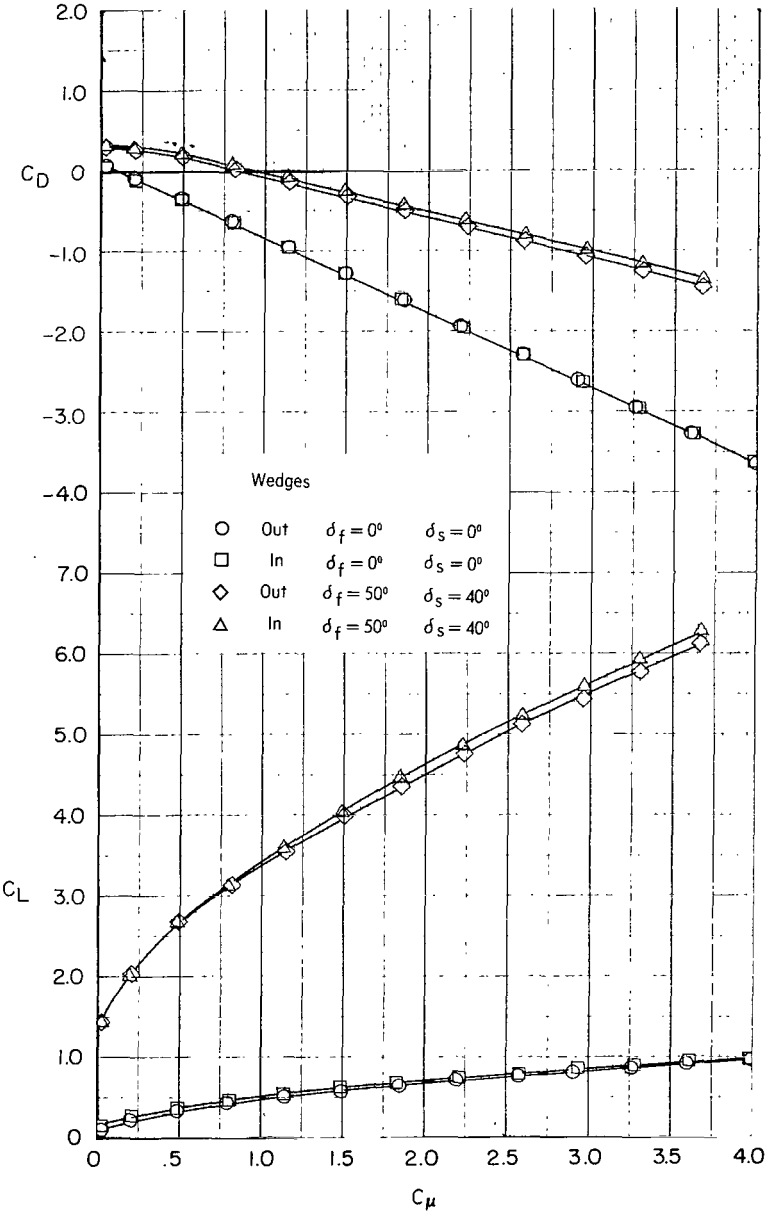


(b) Effect of wedges in the outboard side of the exit nozzles of the inboard nacelles. Basic flap.

Figure 12.- Continued.

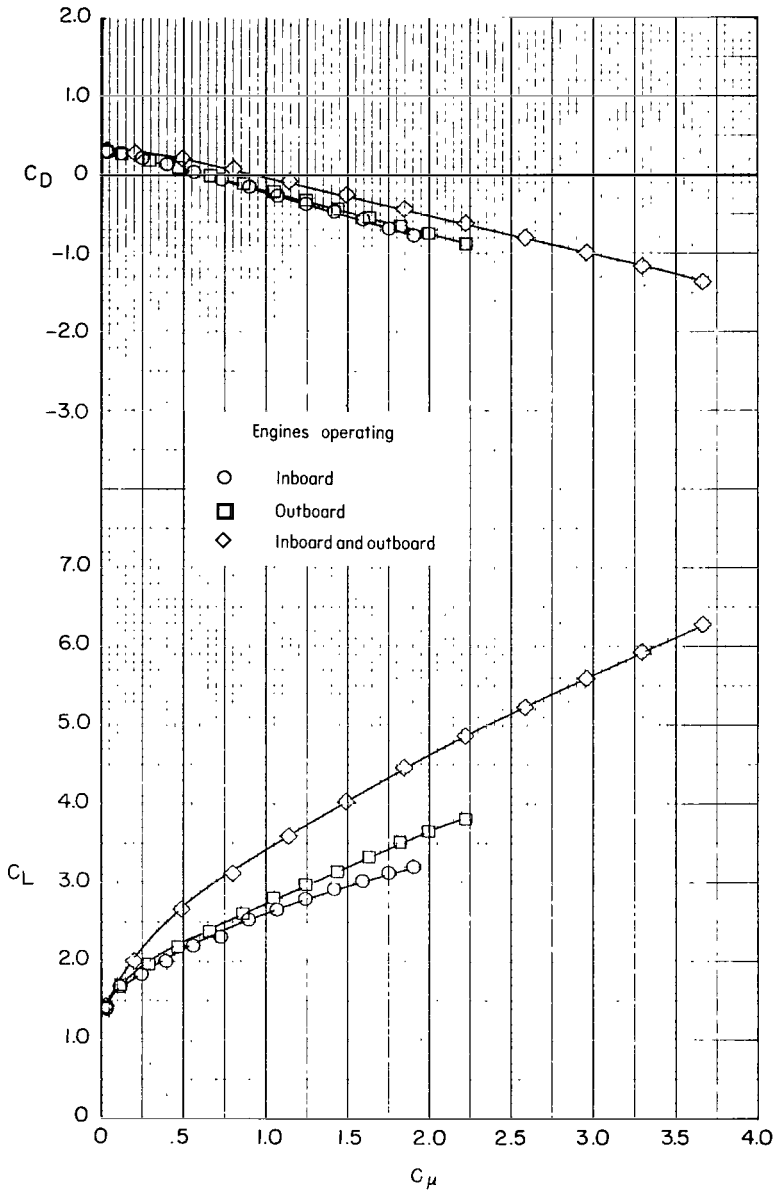


(c) Effect of twin-engine simulation. $\delta_f = 50^o$; $\delta_s = 40^o$.

Figure 12.- Concluded.

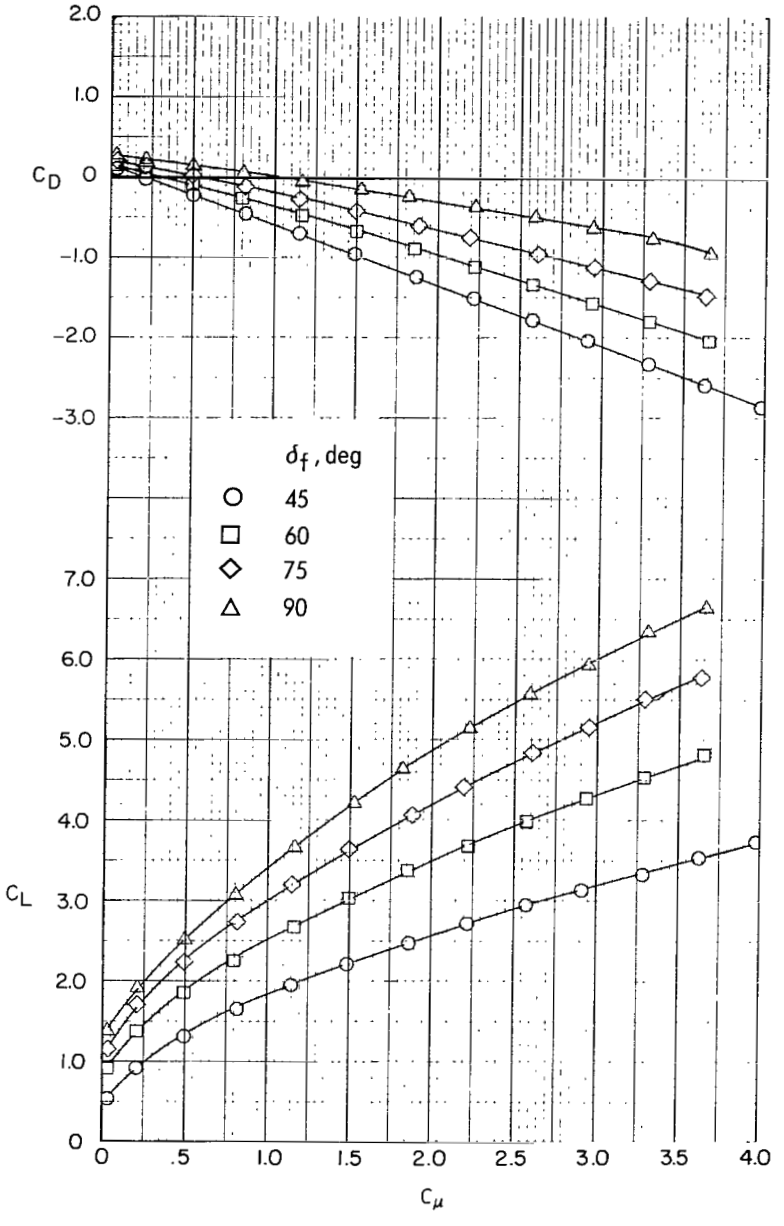


(a) Effect of radius flap deflection. $\delta_s = 40^o$.

Figure 13.- Variation of lift and drag coefficients with thrust coefficient for the model with rectangular nozzles and radius flap. $\alpha = 0^o$.

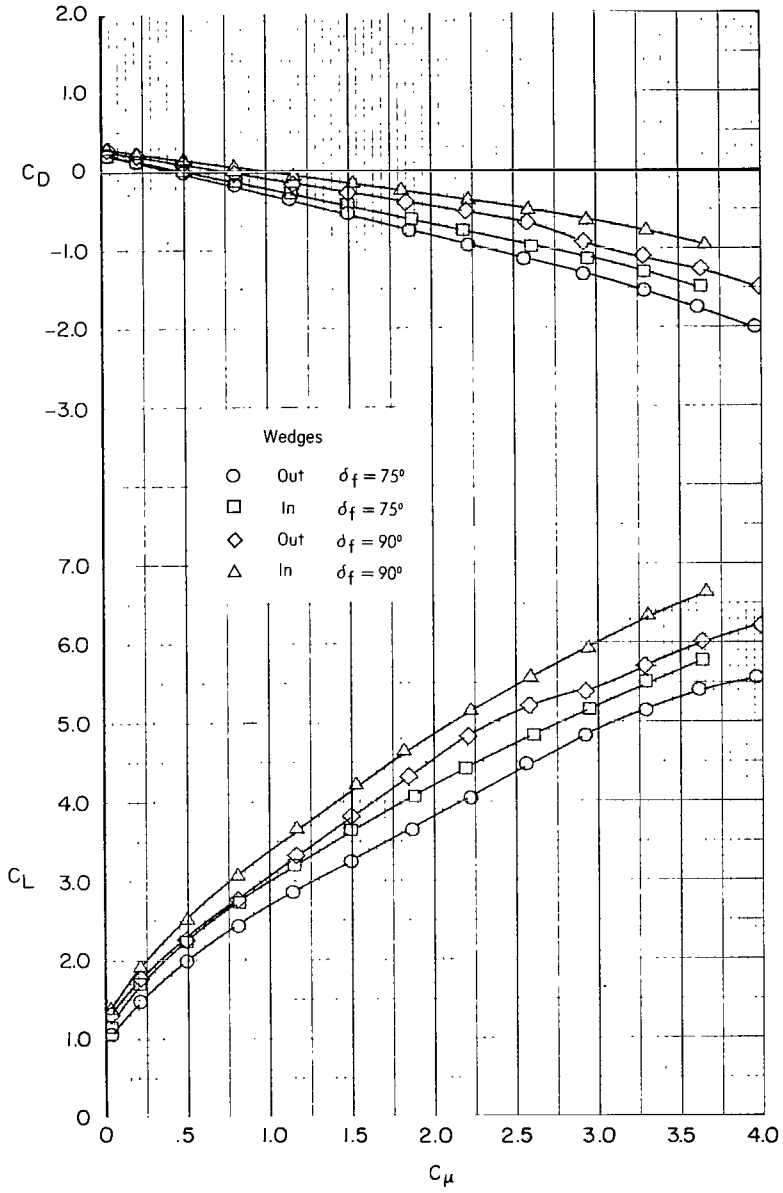


(b) Effect of wedges in the outboard side of exit nozzles of the inboard nacelles.

Figure 13.- Continued.

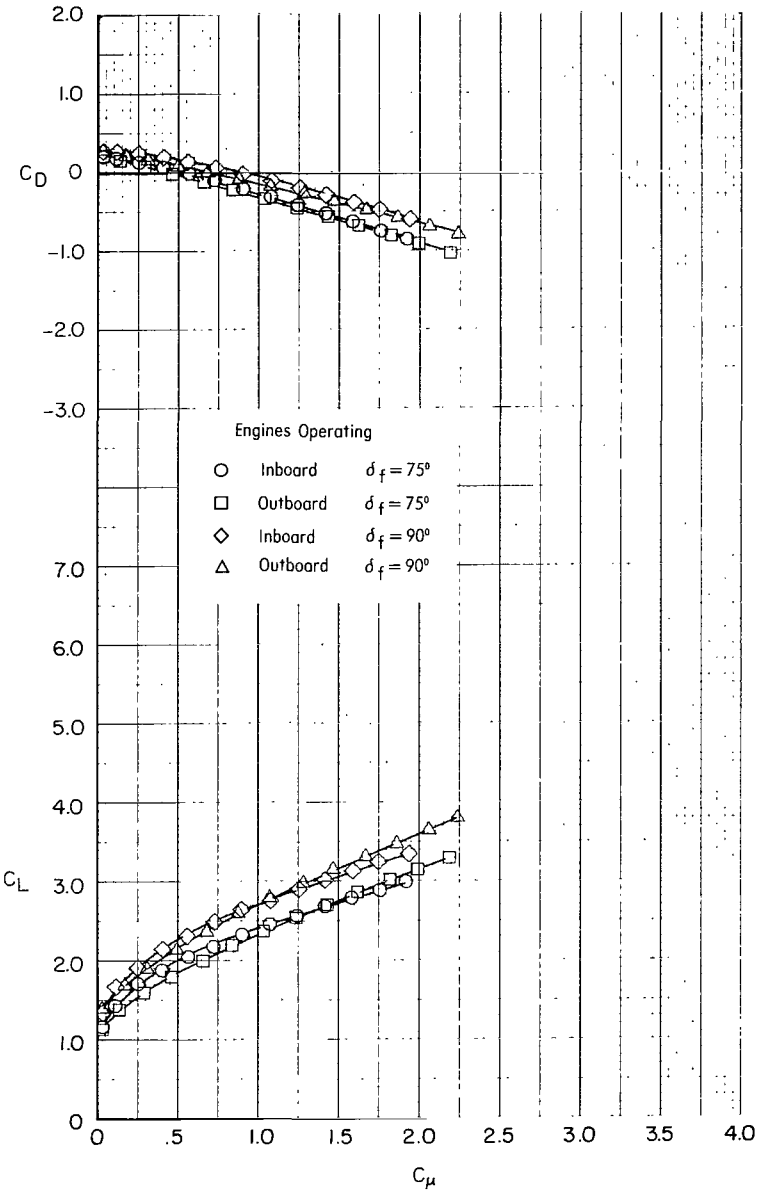


(c) Twin-engine simulation.

Figure 13.- Concluded.

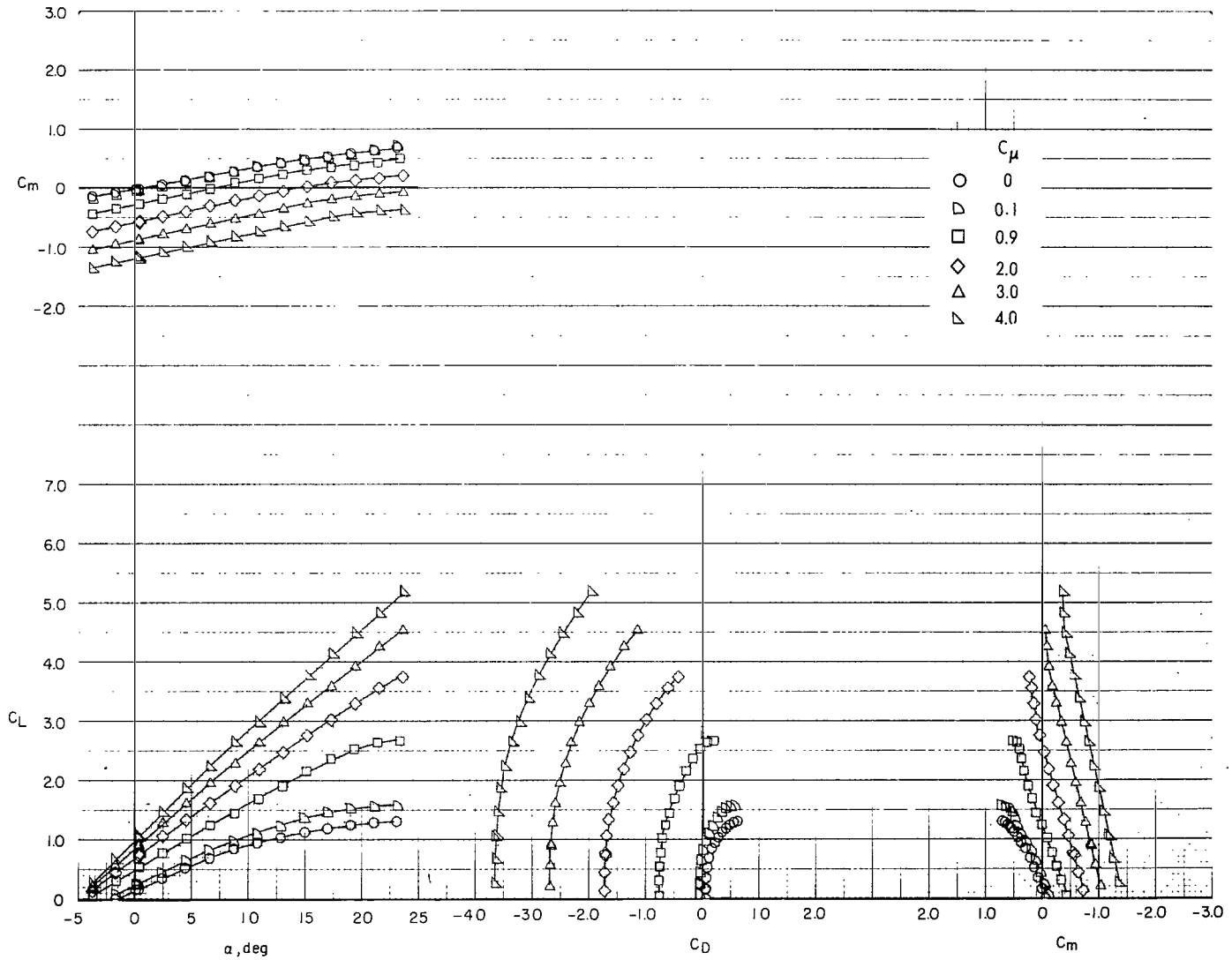


(a) $\delta_f = 0^o$; $\delta_s = 0^o$.

Figure 14.- Effect of angle of attack on the longitudinal aerodynamic characteristics of the model with rectangular nozzles for constant thrust conditions. Basic flap; horizontal tail off.

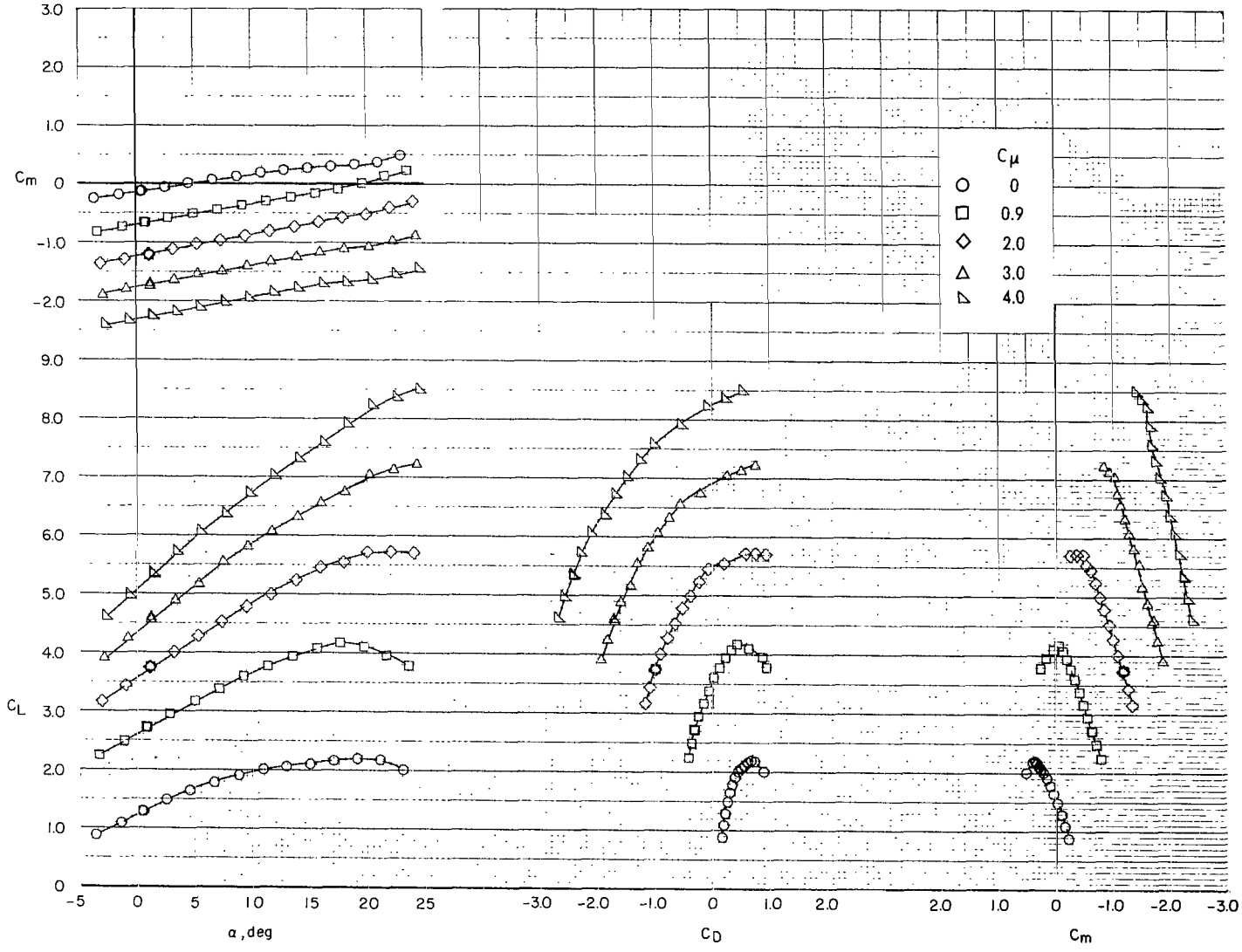


(b) $\delta_f = 35^o$; $\delta_s = 40^o$.

Figure 14.- Continued.

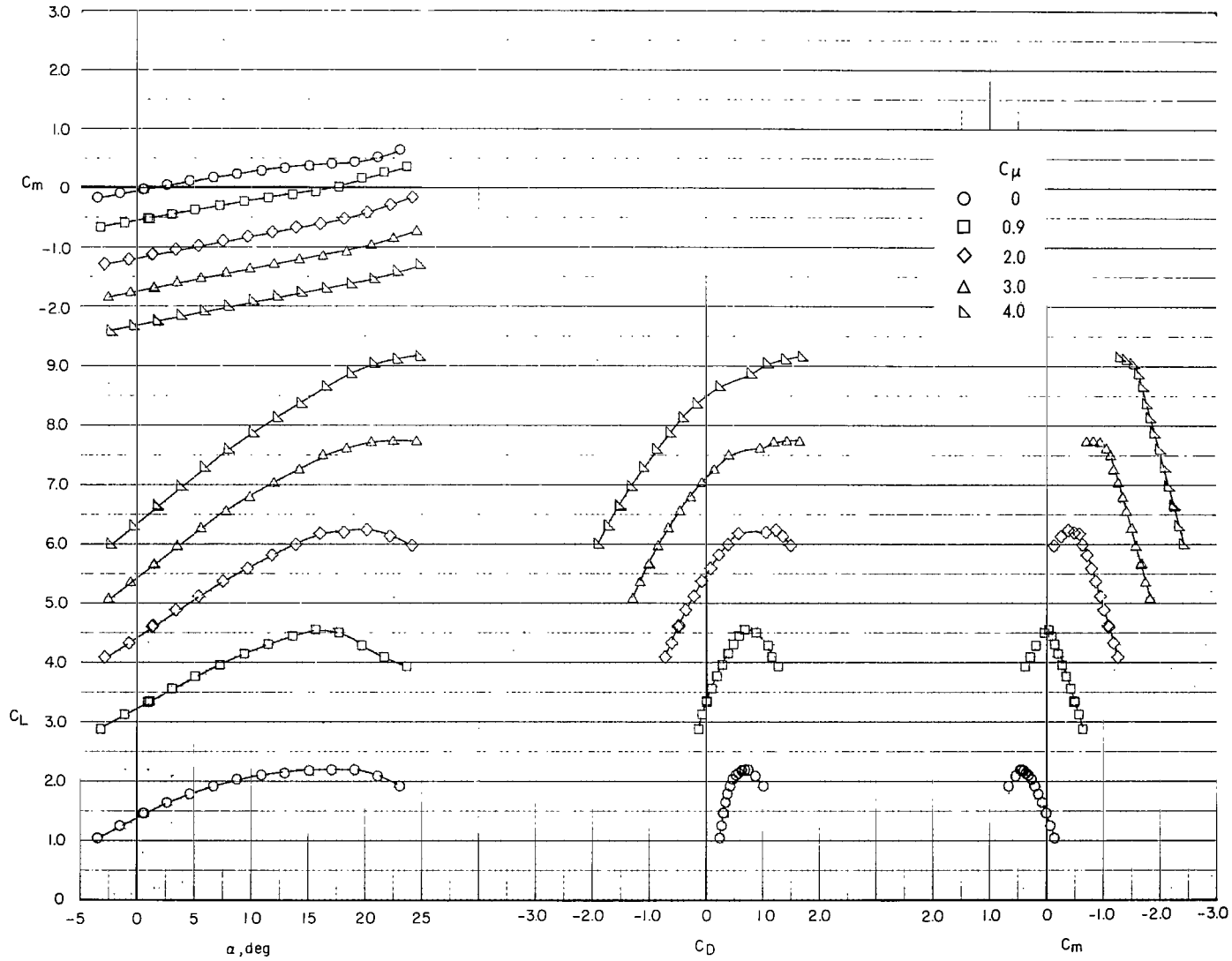


(c) $\delta_f = 50^o$; $\delta_s = 40^o$.

Figure 14.- Continued.

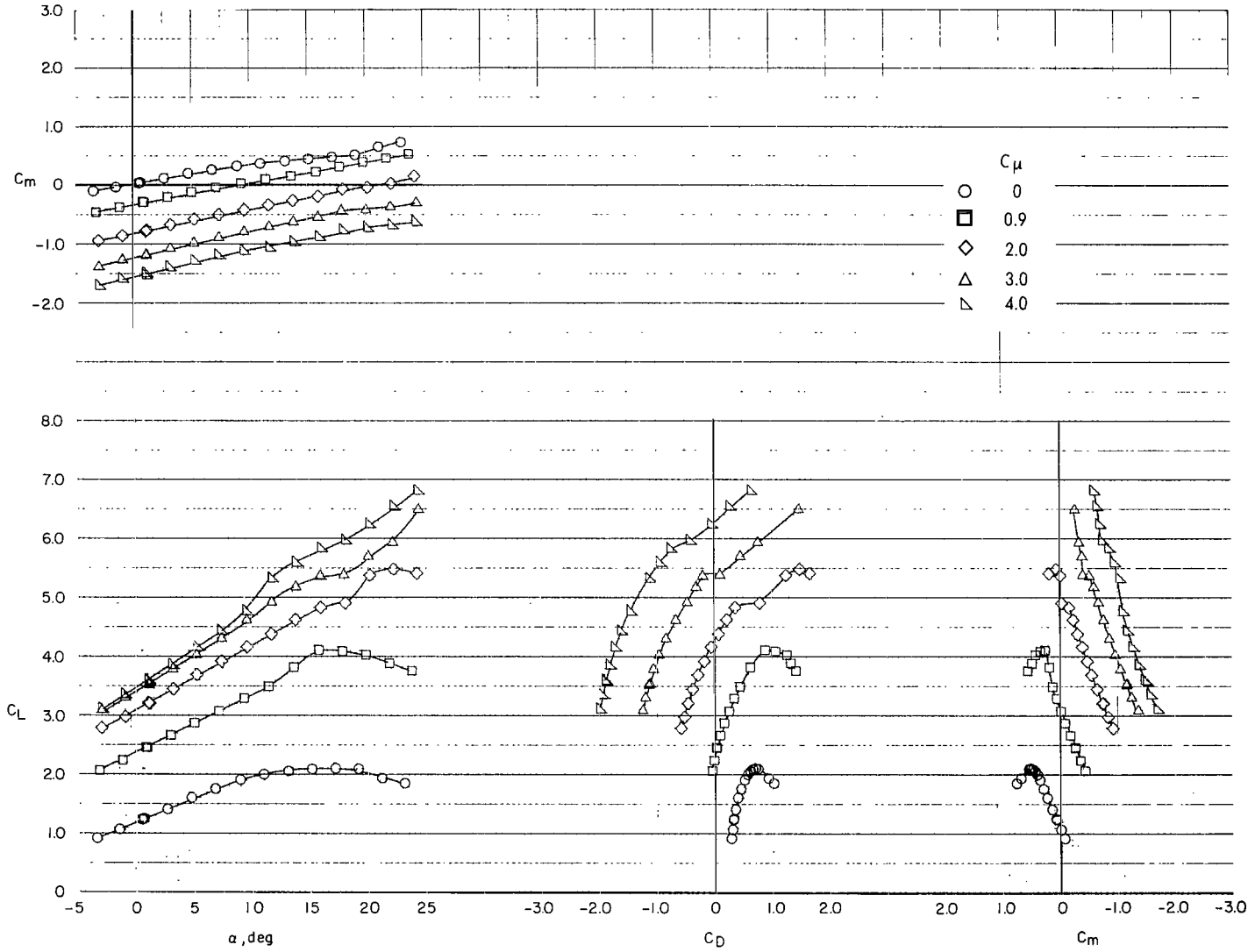


(d) $\delta_f = 65^o$; $\delta_s = 40^o$.

Figure 14.- Concluded.

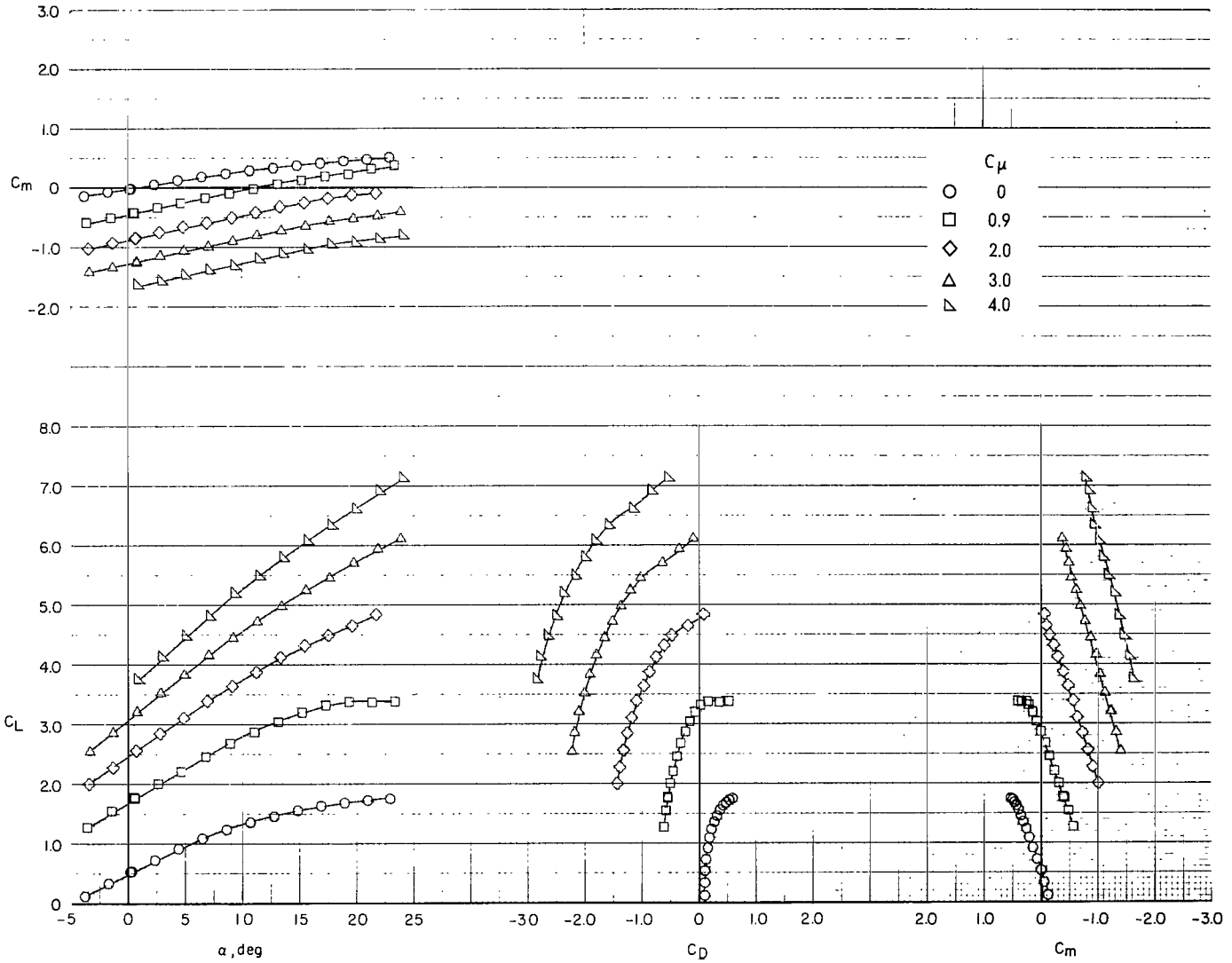


(a) $\delta_f = 45^o$; $\delta_s = 40^o$.

Figure 15.- Effect of angle of attack on the longitudinal aerodynamic characteristics of the model with rectangular nozzles for constant thrust conditions. Radius flap; horizontal tail off.

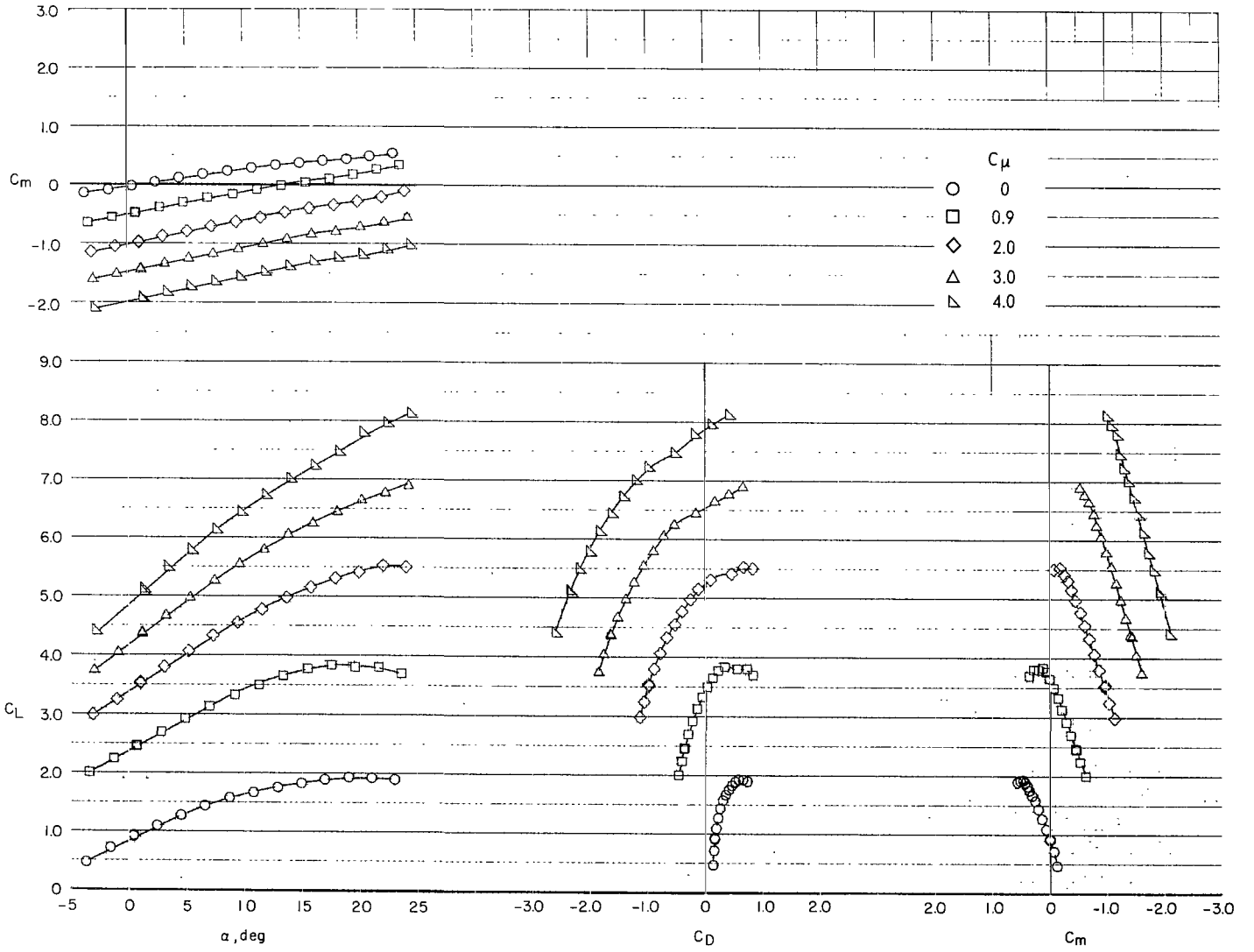


(b) $\delta_f = 60^o$; $\delta_s = 40^o$.

Figure 15.- Continued.

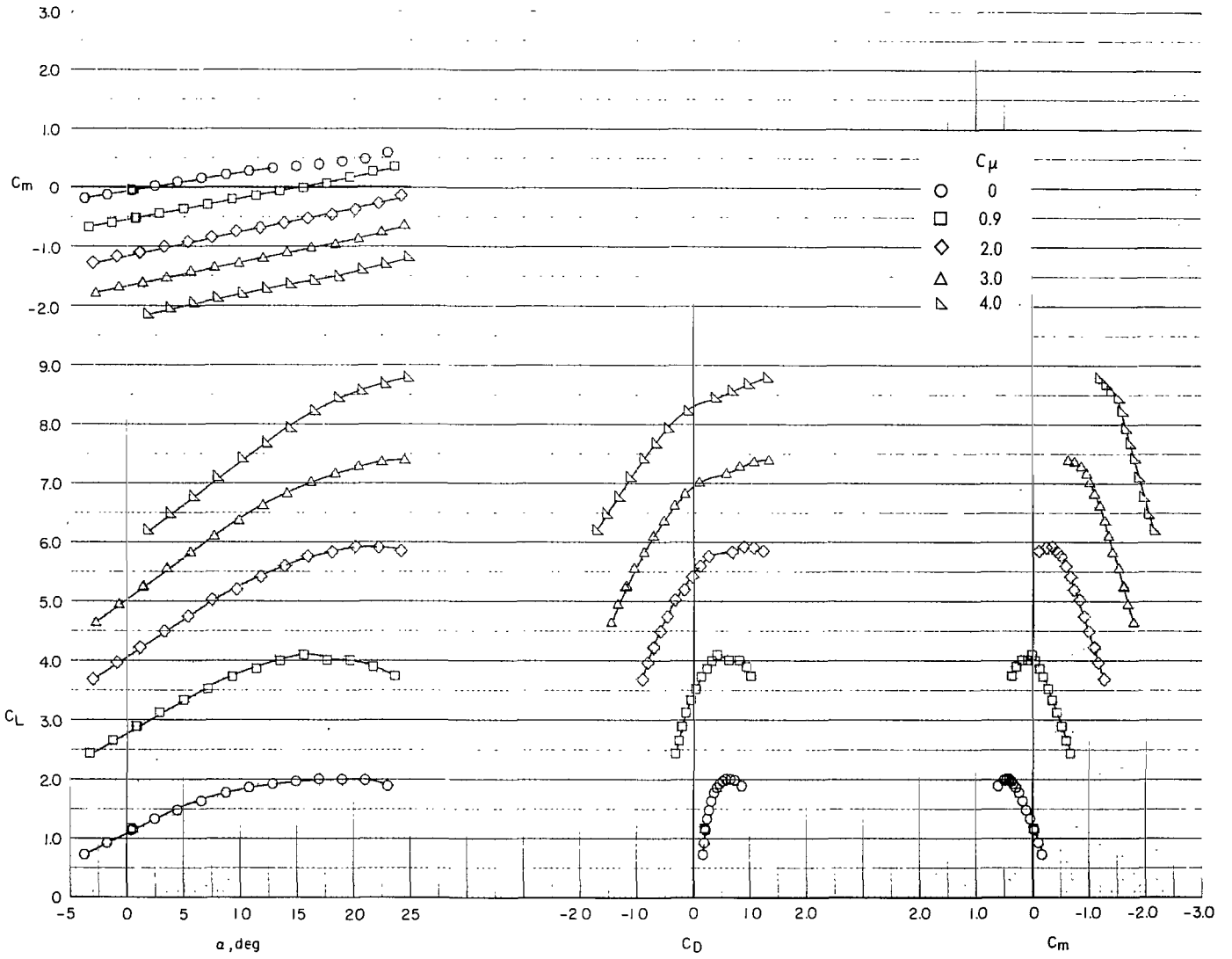


(c) $\delta_f = 75^o$; $\delta_s = 40^o$.

Figure 15.- Continued.

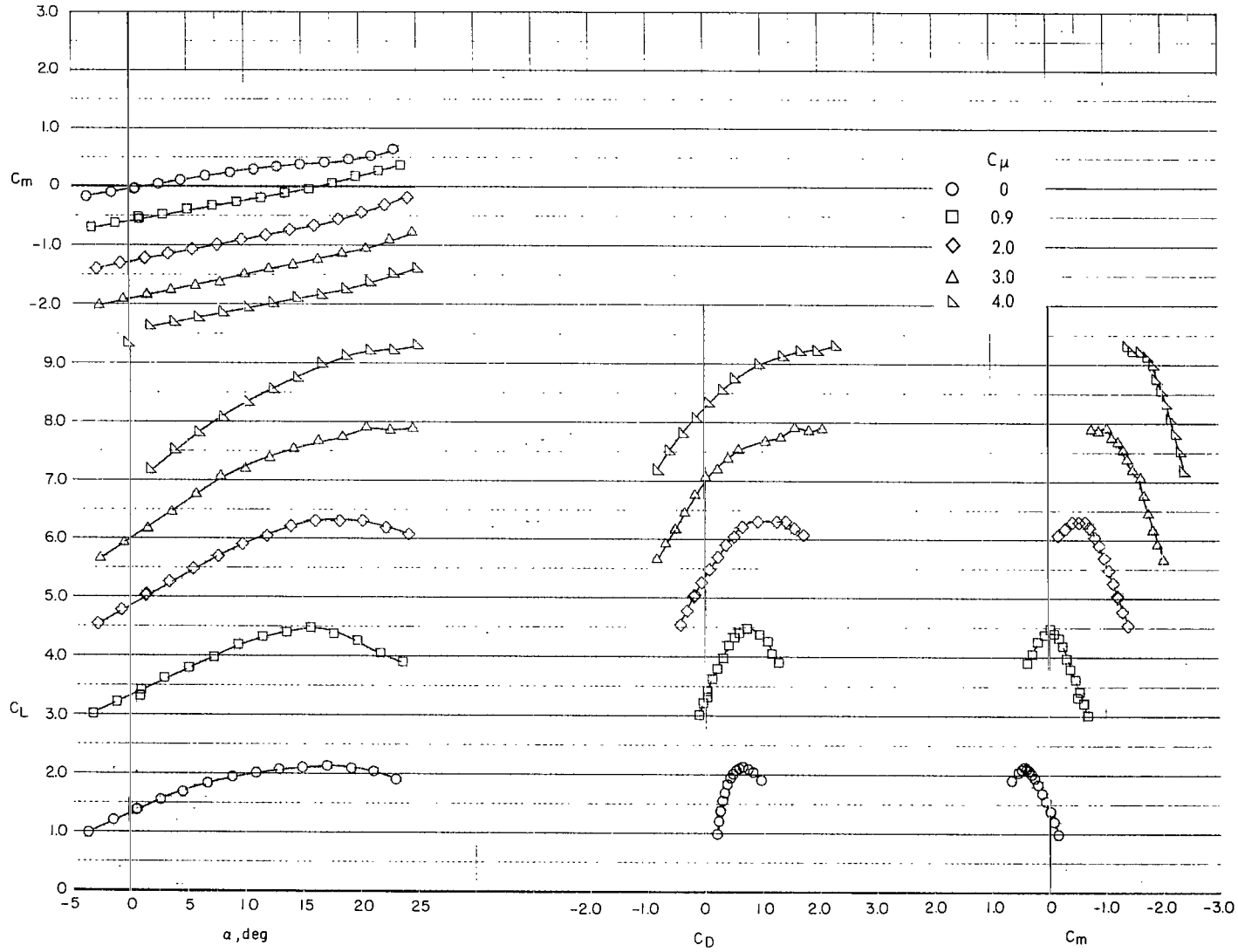


(d) $\delta_f = 90^o$; $\delta_s = 40^o$.

Figure 15.- Concluded.

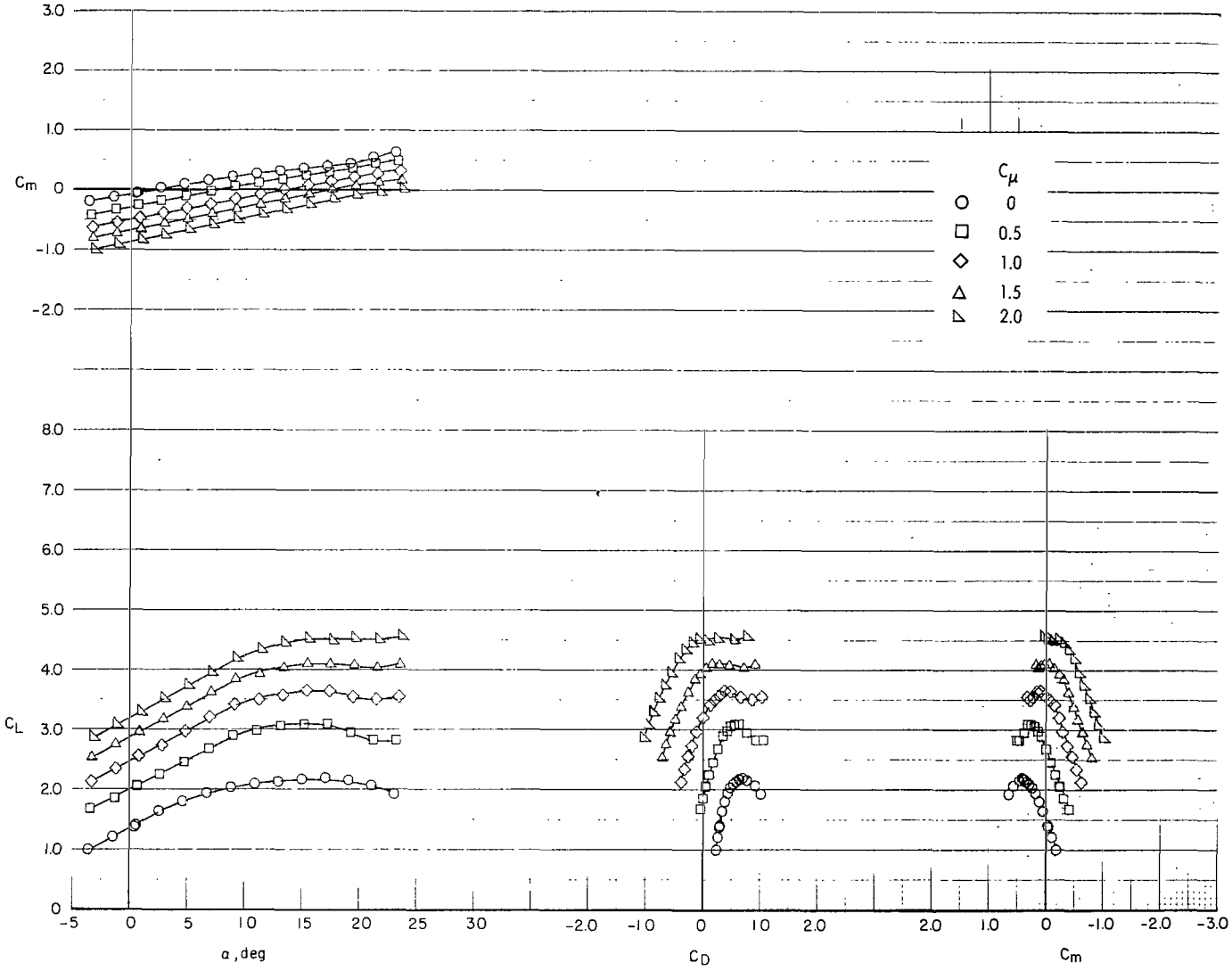


(a) Inboard engines alone.

Figure 16.- Effect of angle of attack on the longitudinal aerodynamic characteristics of the model with rectangular nozzles for constant thrust conditions with twin-engine operation simulated. Basic flap; $\delta_f = 50^o$; $\delta_s = 40^o$; horizontal tail off.

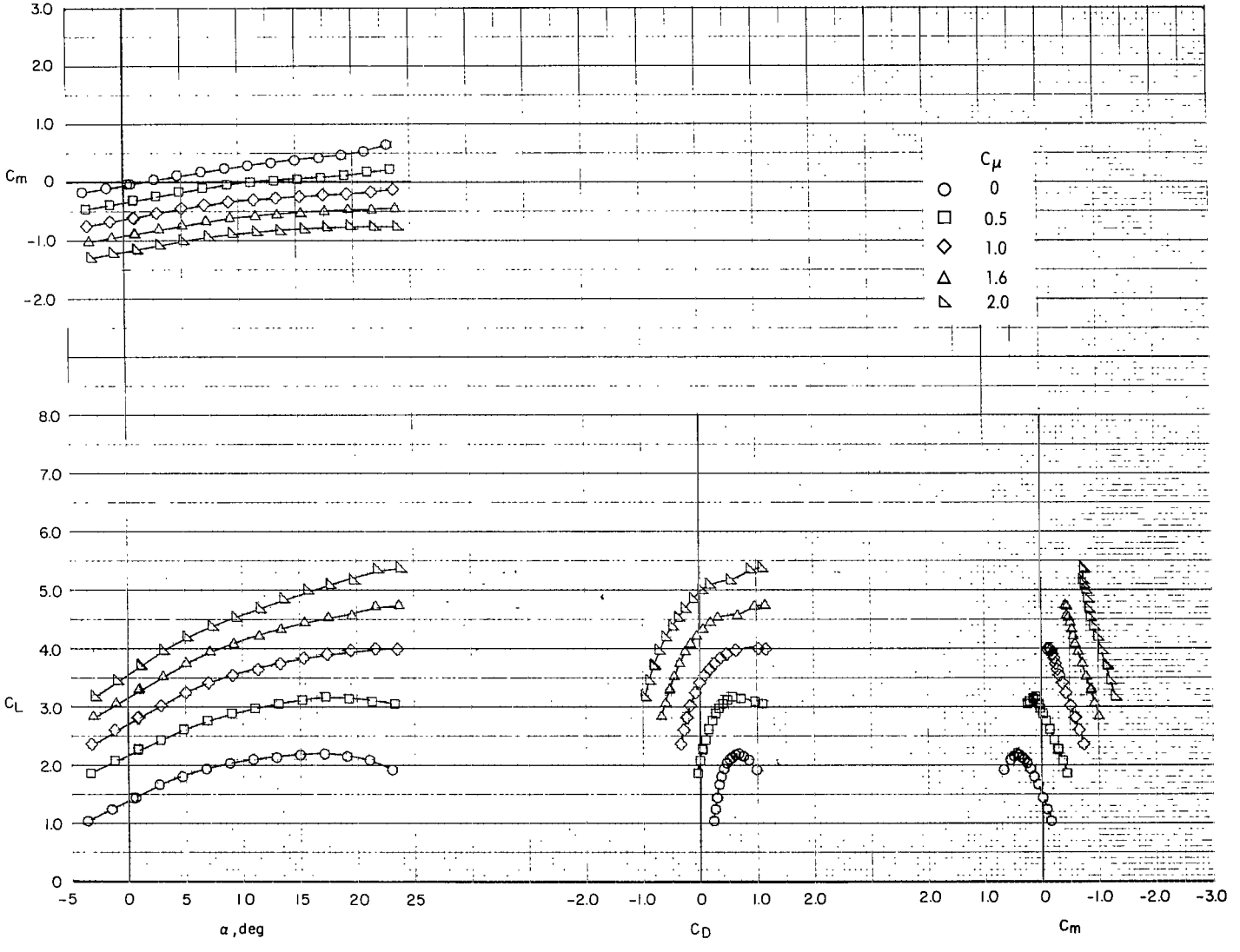


(b) Outboard engines alone.

Figure 16.- Concluded.

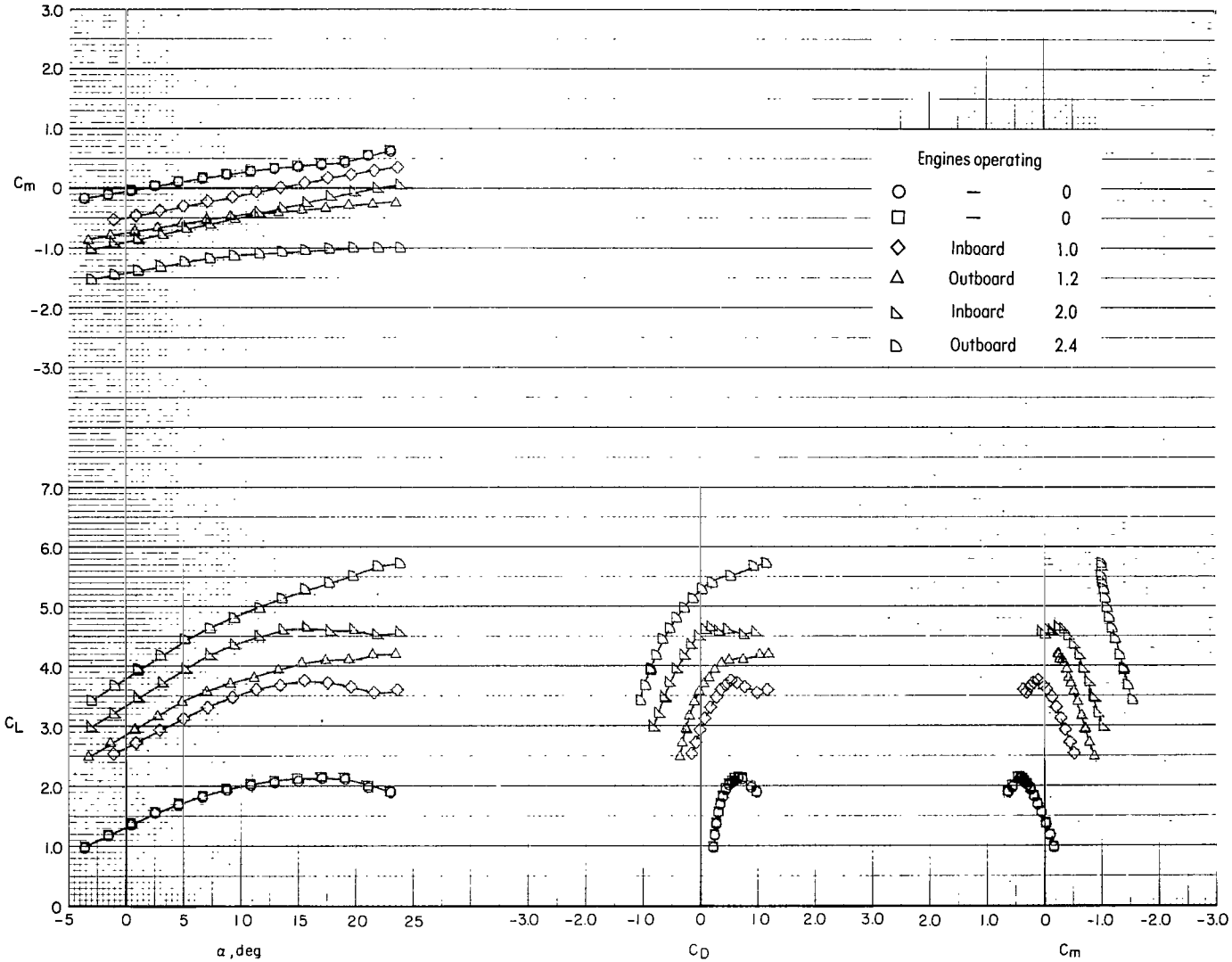


Figure 17.- Effect of angle of attack on the longitudinal aerodynamic characteristics of the model with rectangular nozzles for constant thrust conditions. Twin-engine simulation; radius flap; $\delta_f = 90^o$; $\delta_s = 40^o$; horizontal tail off.

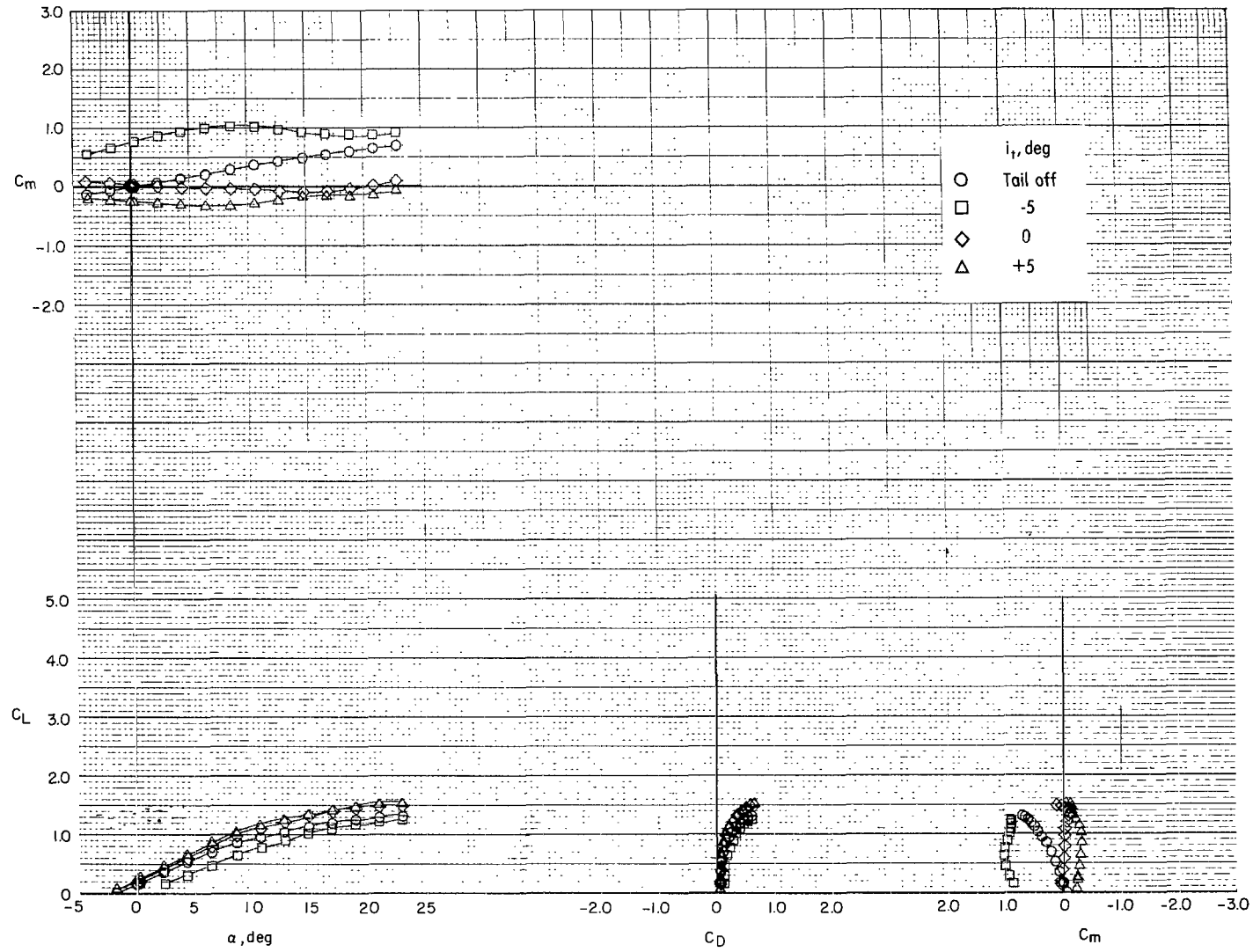


(a) $C_{\mu} = 0.$

Figure 18.- Effect of the horizontal-tail and stabilizer incidence on the longitudinal aerodynamic characteristics of the model with rectangular nozzles. Basic flap; $\delta_f = 0^o$; $\delta_s = 0^o$.

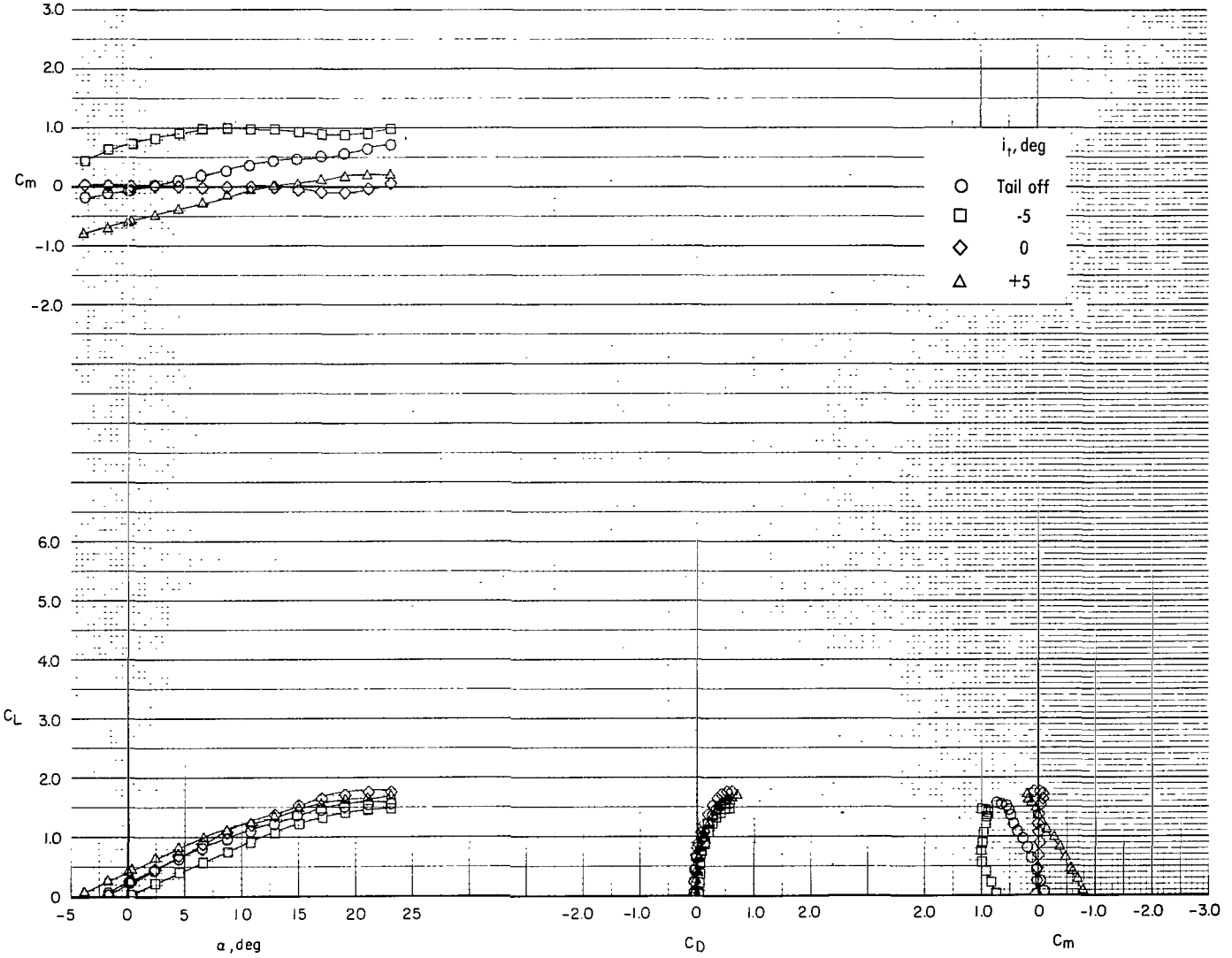


(b) $C_{\mu} = 0.1$.

Figure 18.- Continued.

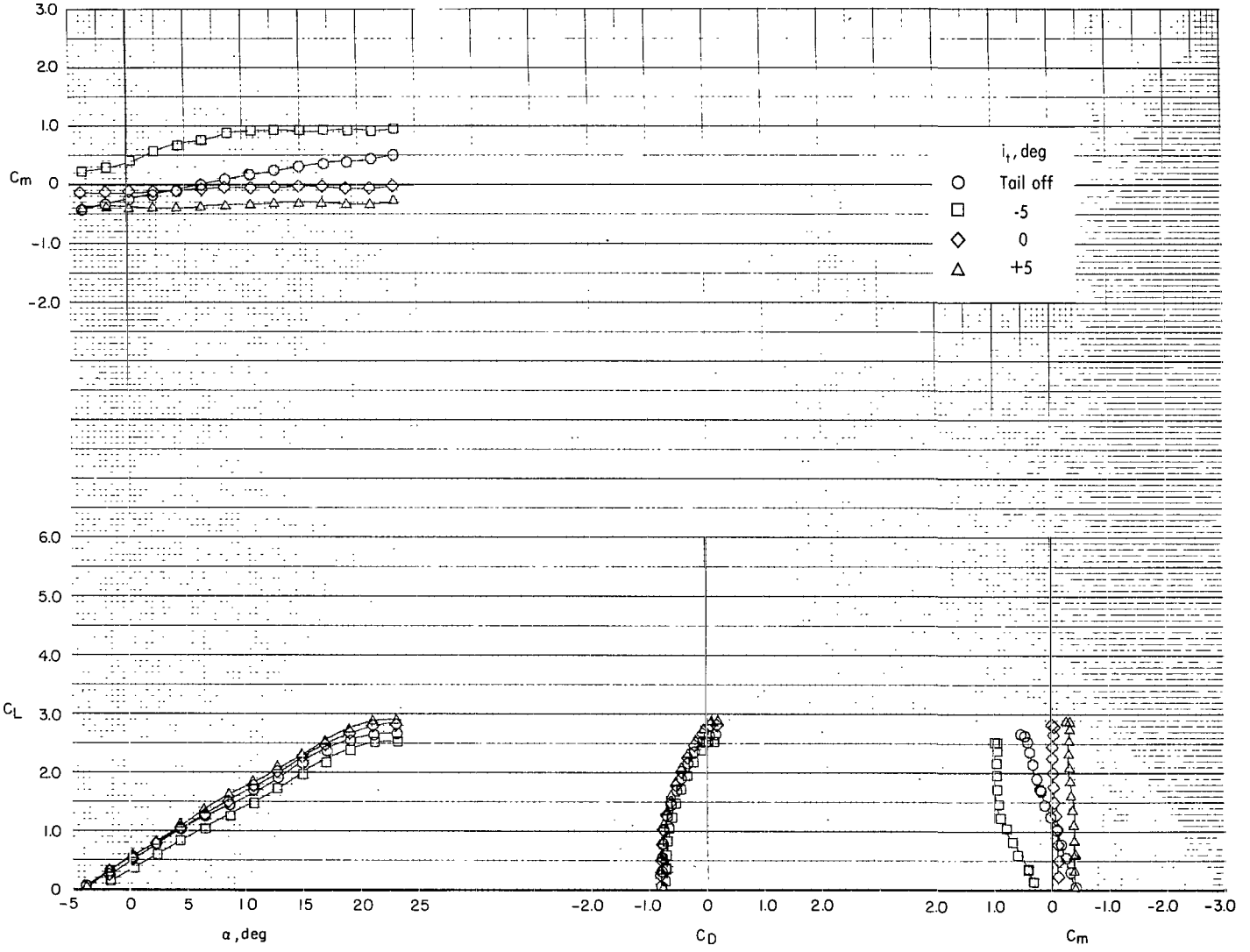


(c) $C_{\mu} = 1.0$.

Figure 18.- Continued.

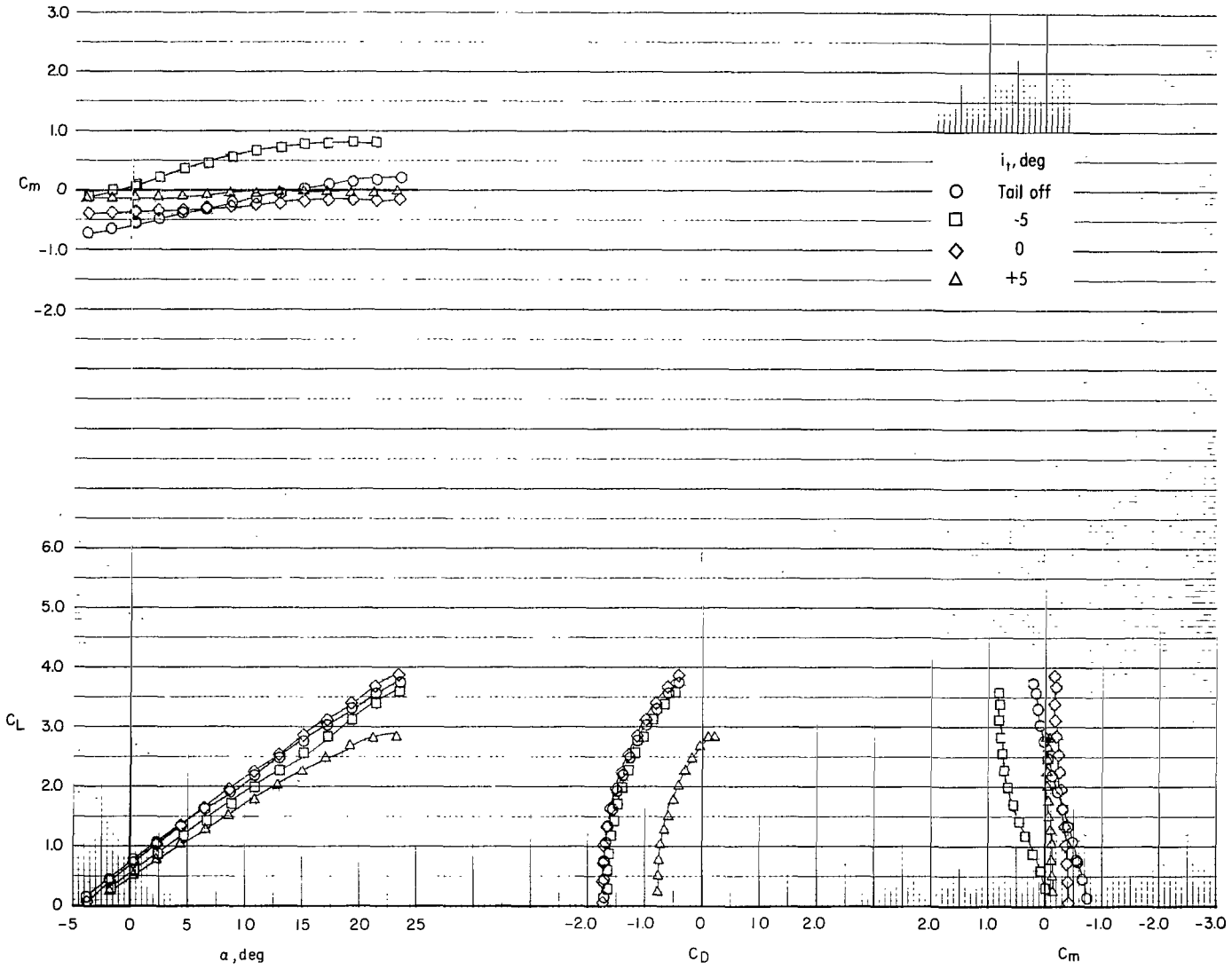


(d) $C_\mu = 2.0$.

Figure 18.- Concluded.

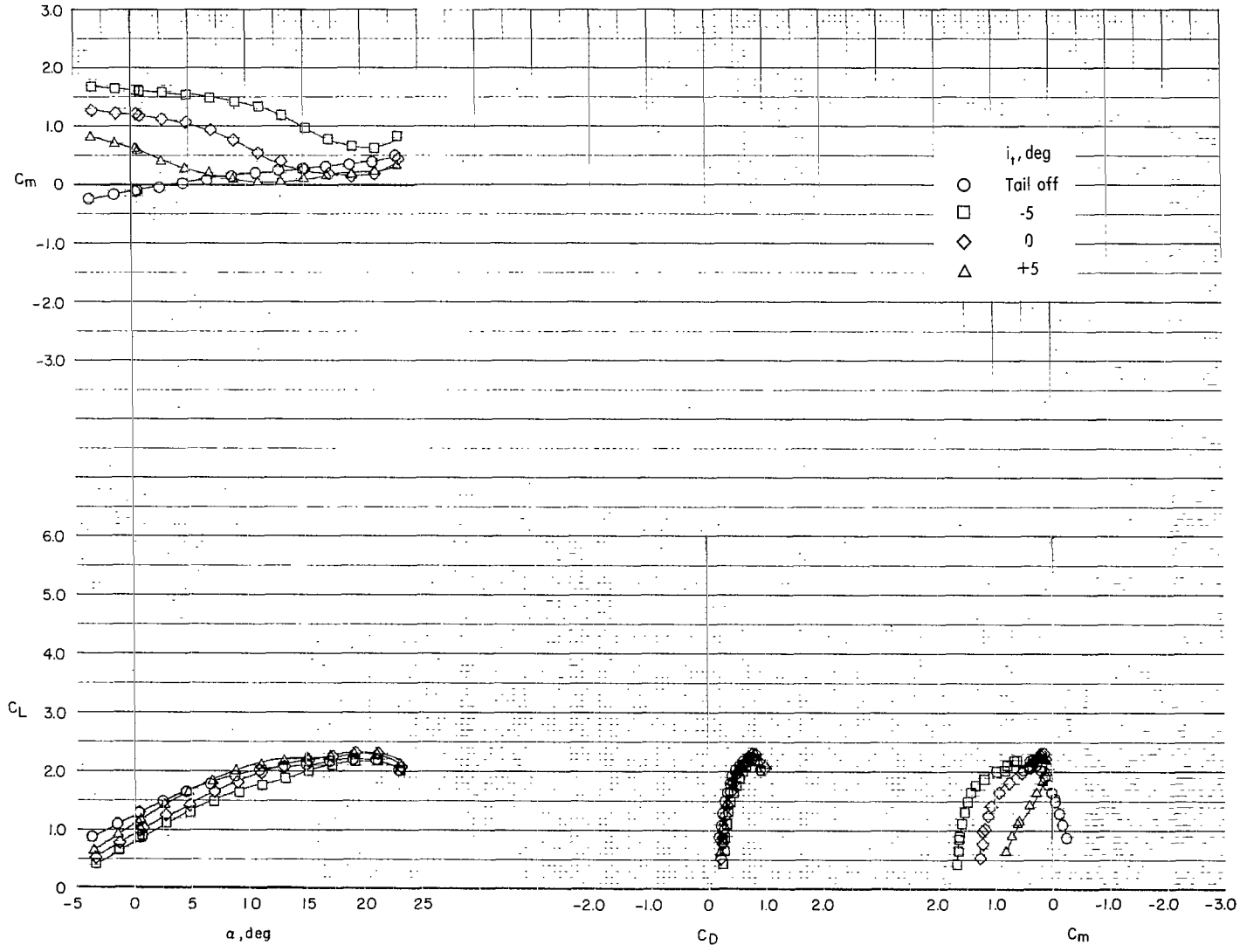


(a) $C_\mu = 0$.

Figure 19.- Effect of the horizontal-tail and stabilizer incidence on the longitudinal aerodynamic characteristics of the model with rectangular nozzles. Basic flap; $\delta_f = 35^o$; $\delta_s = 40^o$.

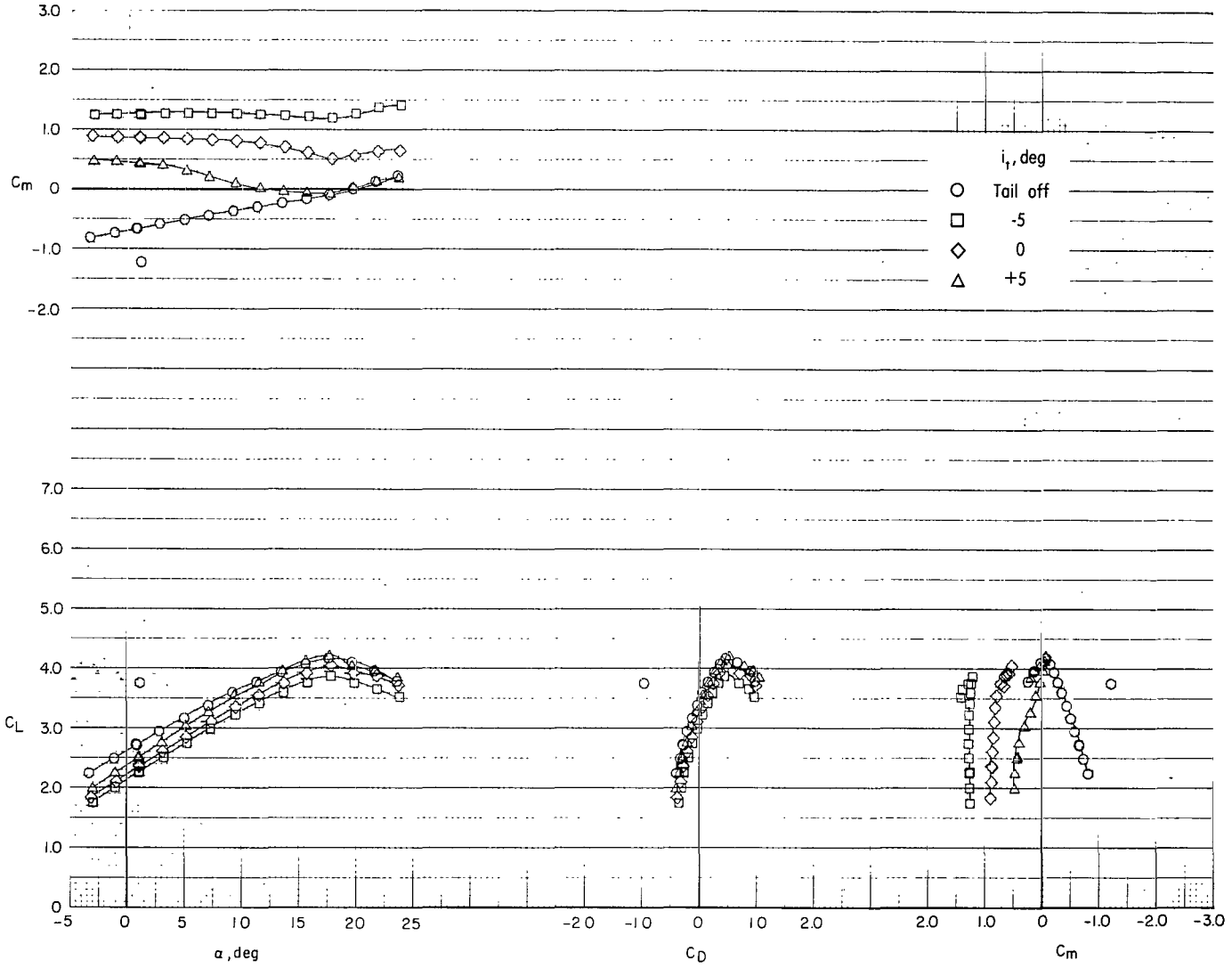


(b) $C_\mu = 1.0$.

Figure 19.- Continued.

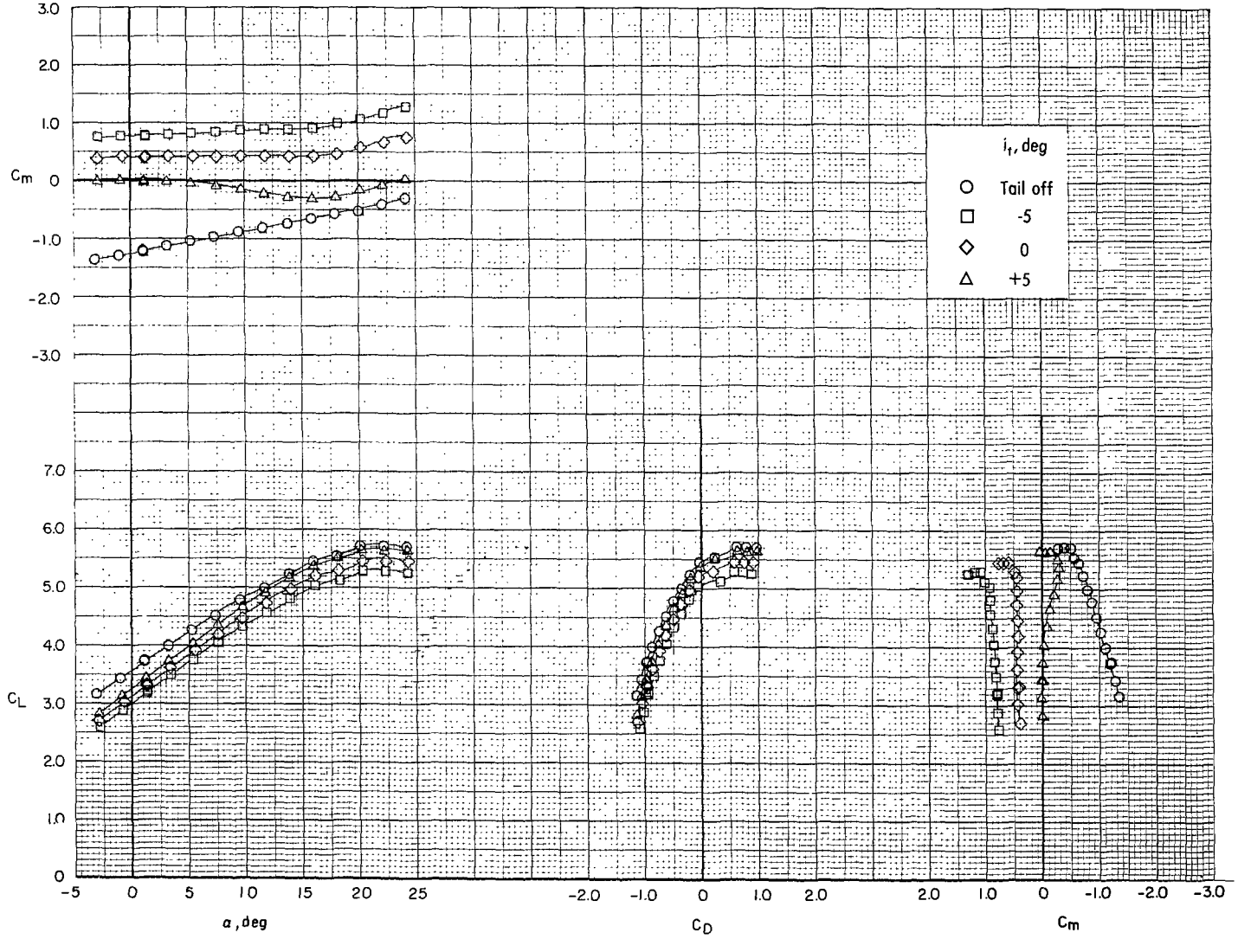


(c) $C_\mu = 2.0$.

Figure 19.- Continued.

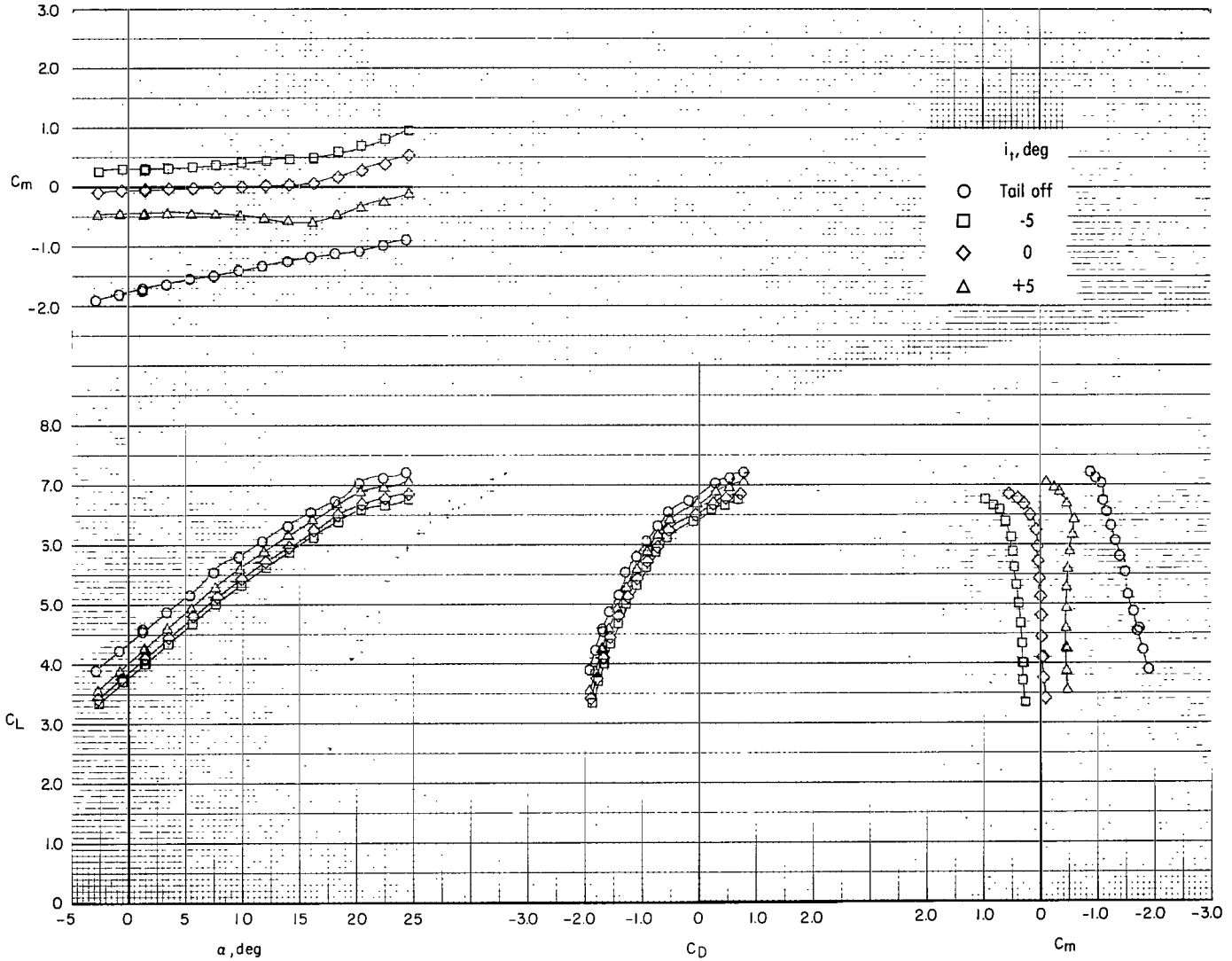


(d) $C_{\mu}^{'} = 3.0$.

Figure 19.- Continued.

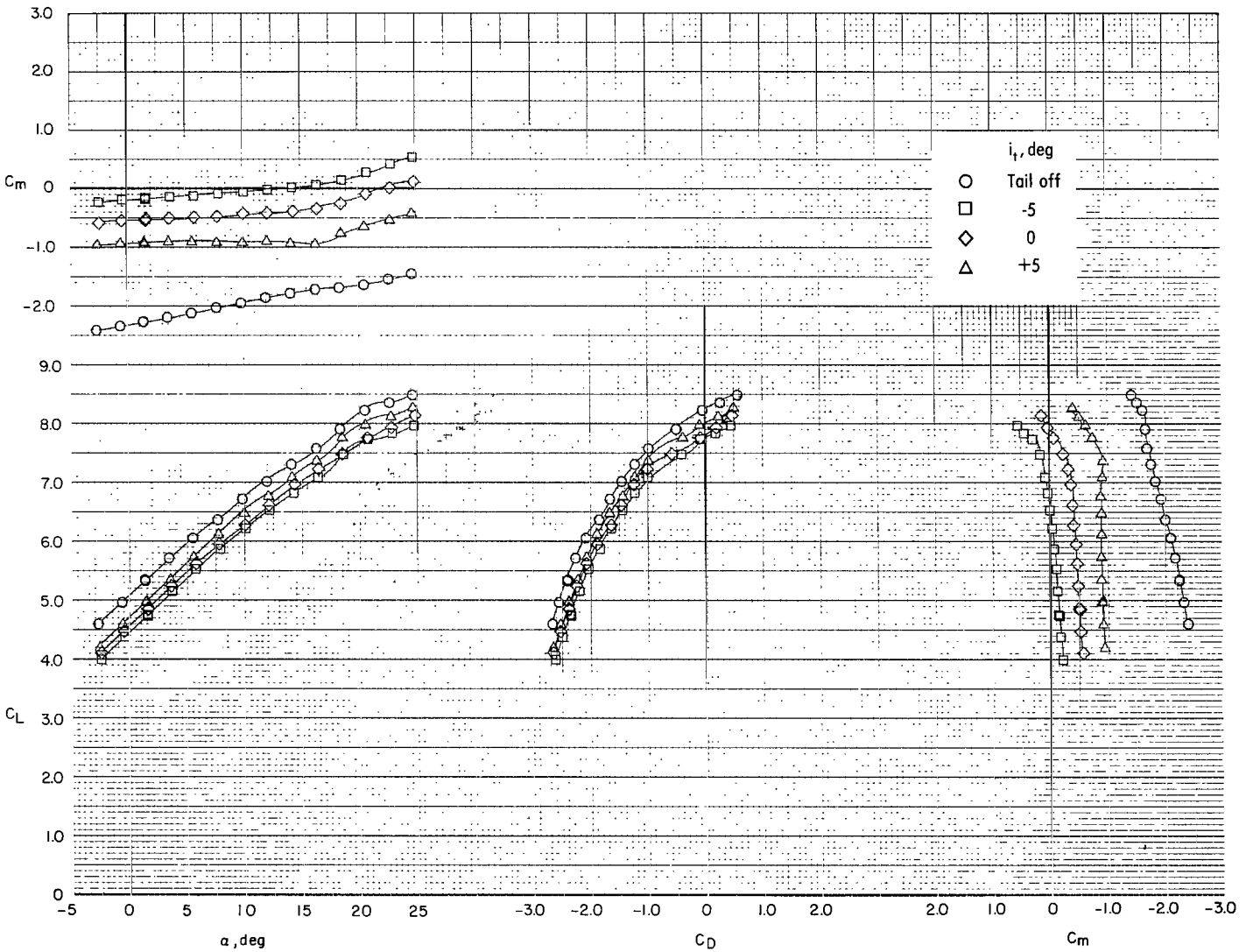


(e) $C_\mu = 4.0$.

Figure 19.- Concluded.

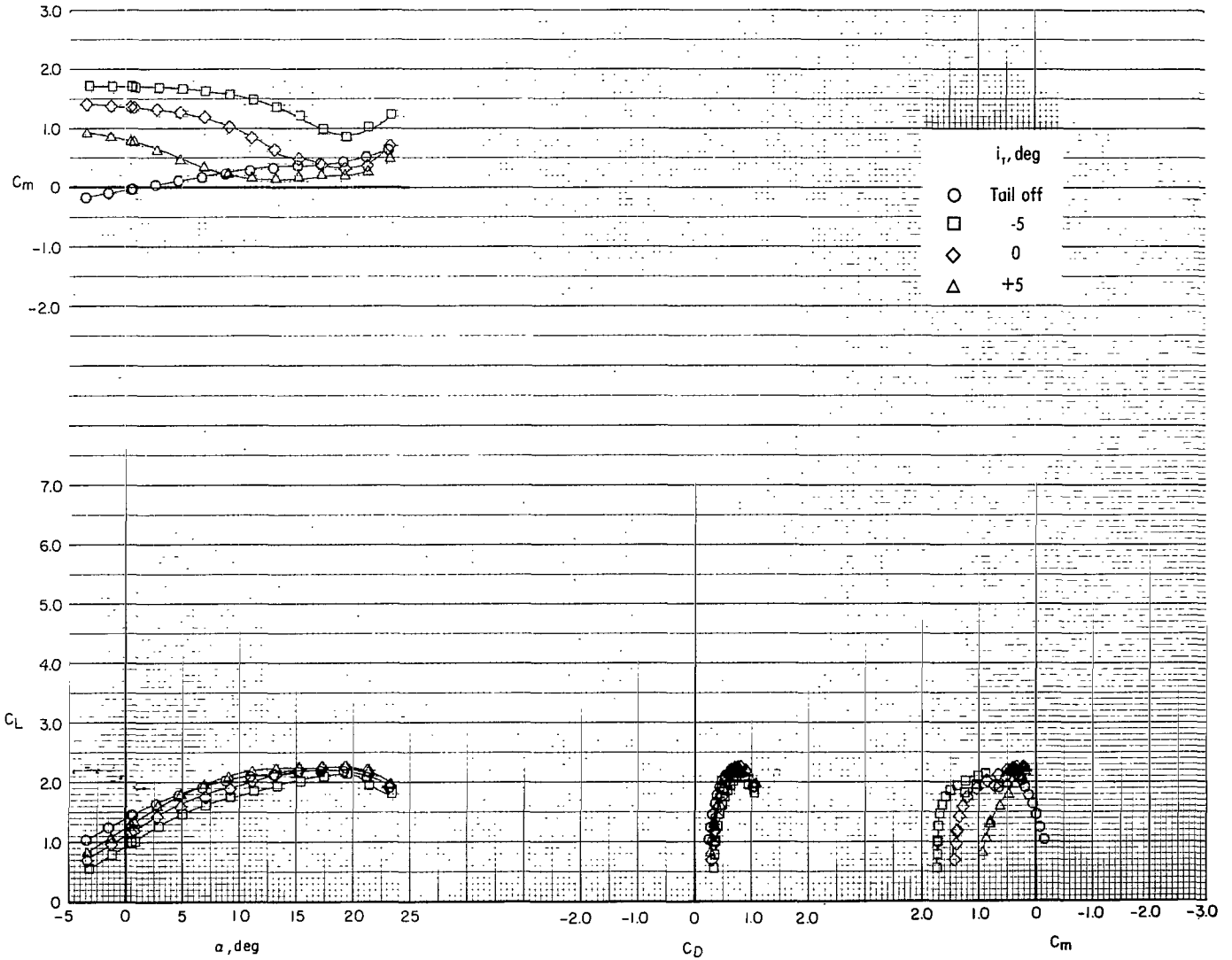


(a) $C_\mu = 0$.

Figure 20.- Effect of the horizontal-tail and stabilizer incidence on the longitudinal aerodynamic characteristics of the model with rectangular nozzles. Basic flap; $\delta_f = 50^o$; $\delta_s = 40^o$.

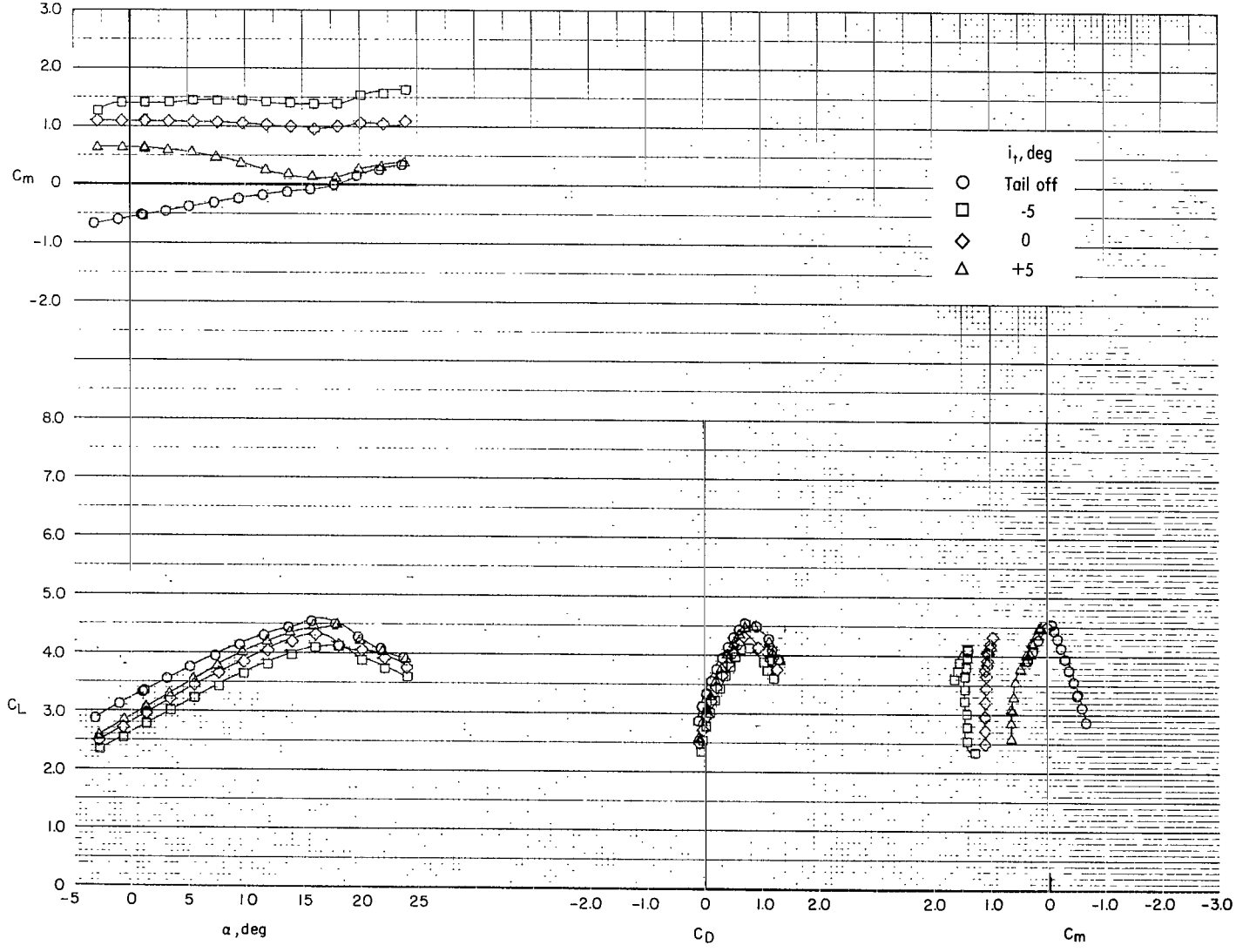


(b) $C_\mu = 1.0$.

Figure 20.- Continued.

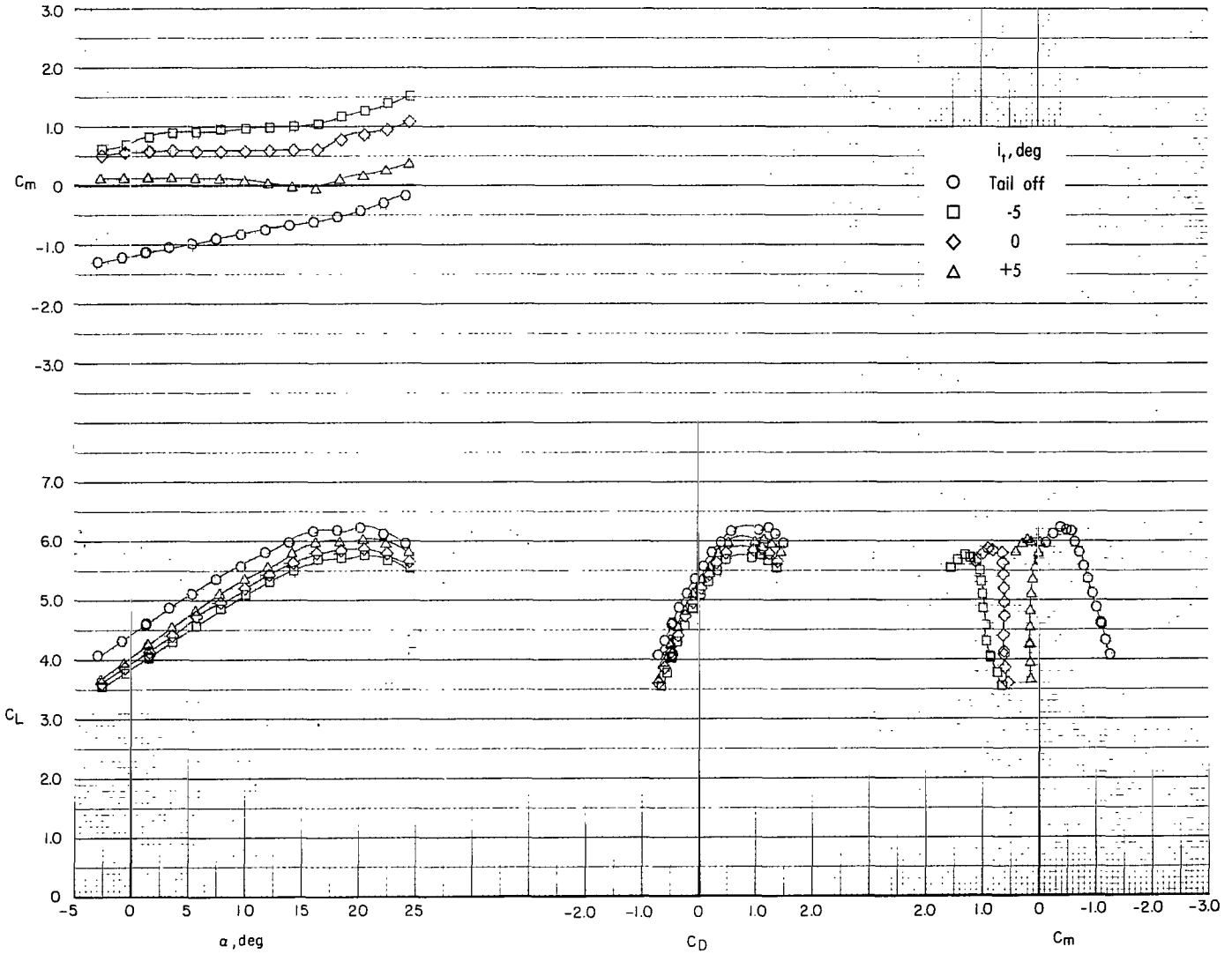


(c) $C_\mu = 2.0$.

Figure 20.- Continued.

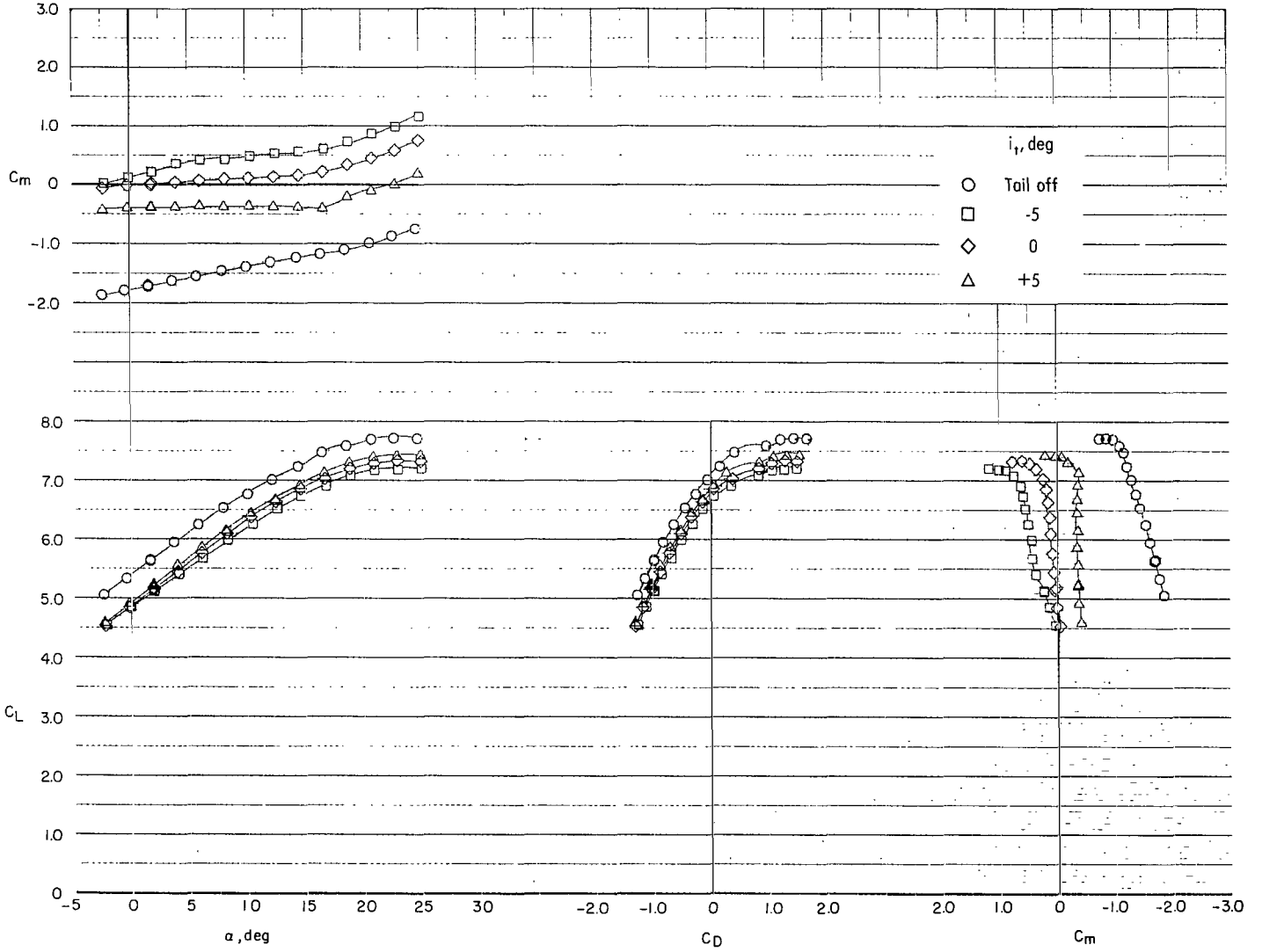


(d) $C_{\mu} = 3.0$.

Figure 20.- Continued.

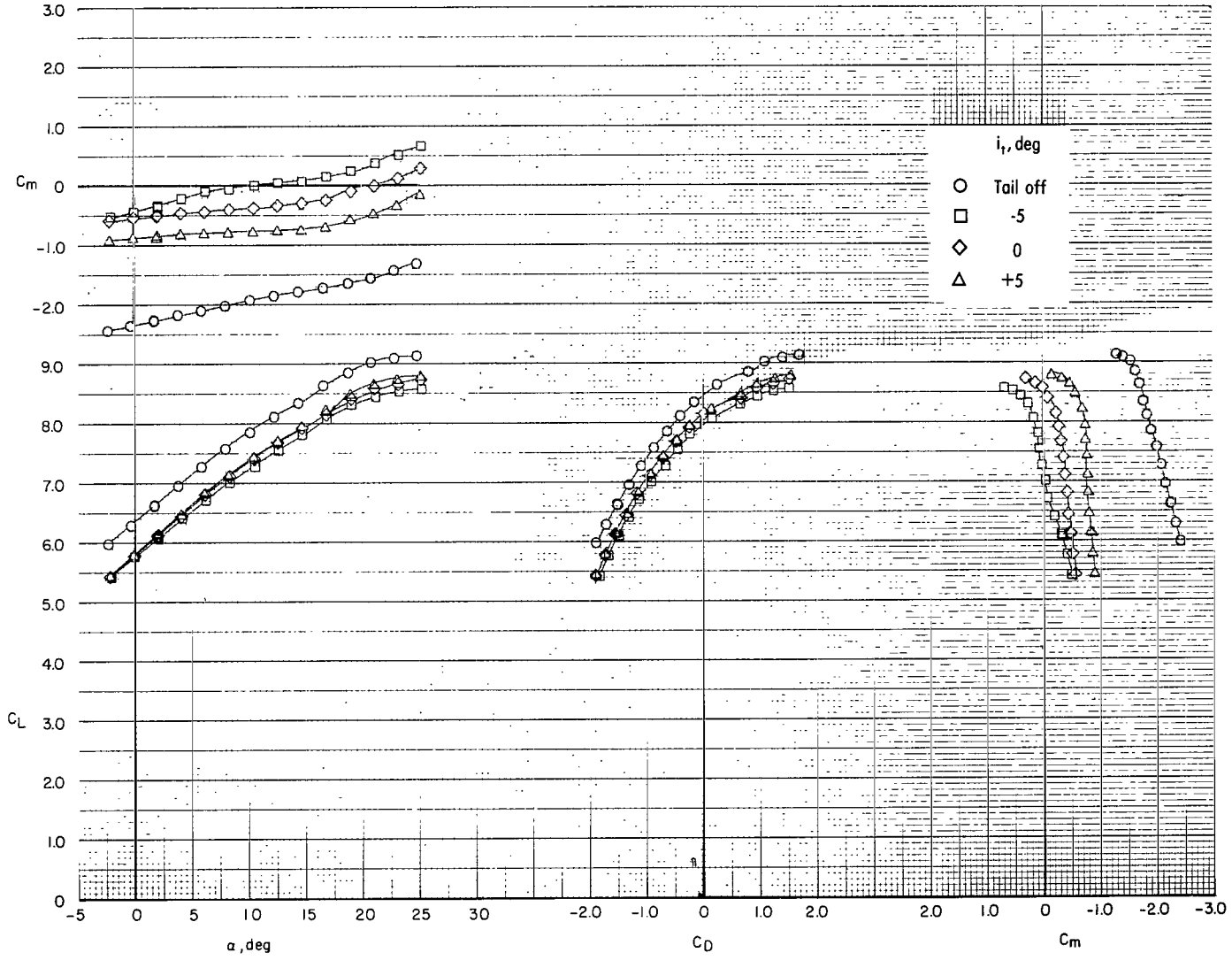


(e) $C_\mu = 4.0$.

Figure 20.- Concluded.

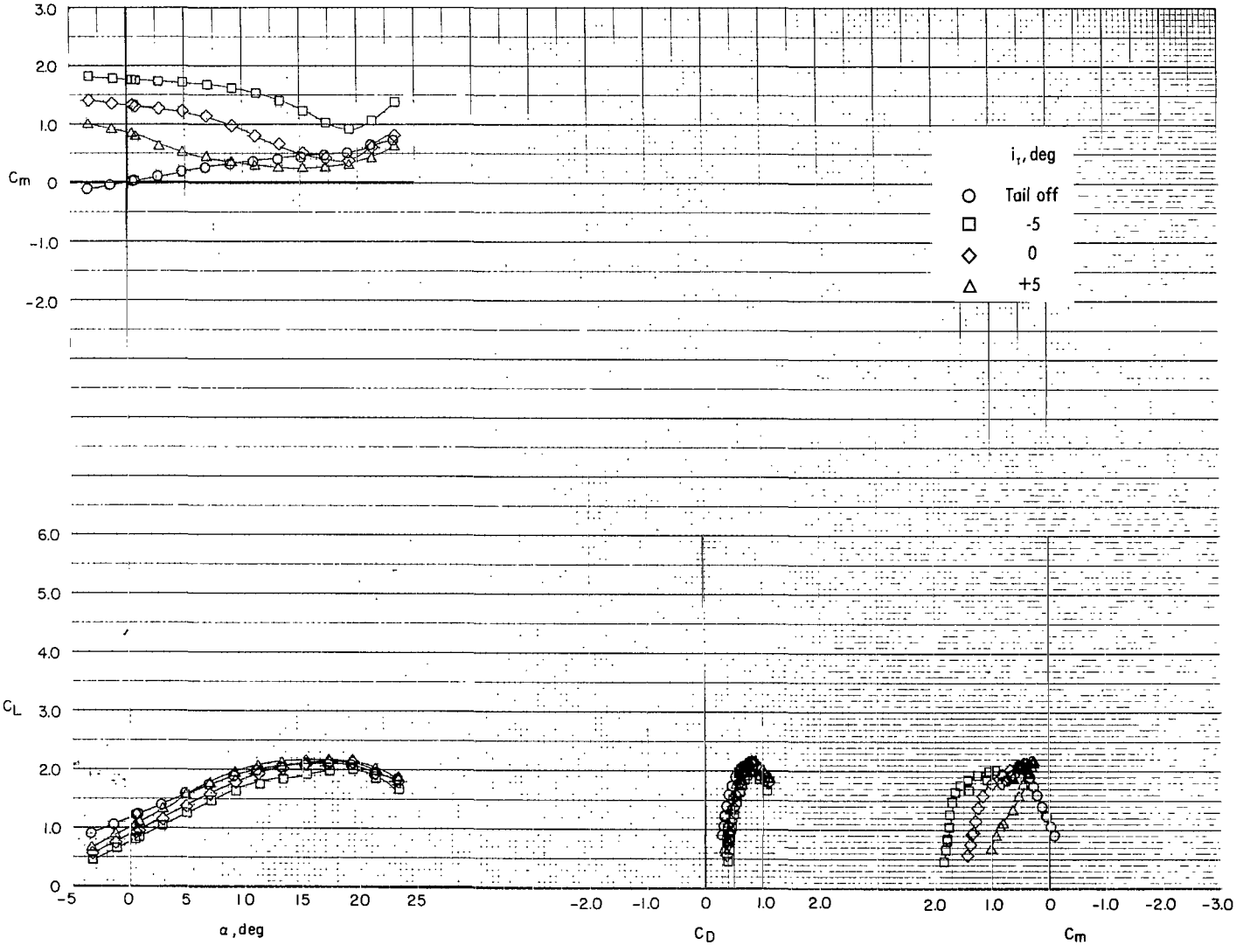


(a) $C_\mu = 0$.

Figure 21.- Effect of the horizontal-tail and stabilizer incidence on the longitudinal aerodynamic characteristics of the model with rectangular nozzles. Basic flap; $\delta_f = 65^o$; $\delta_s = 40^o$.

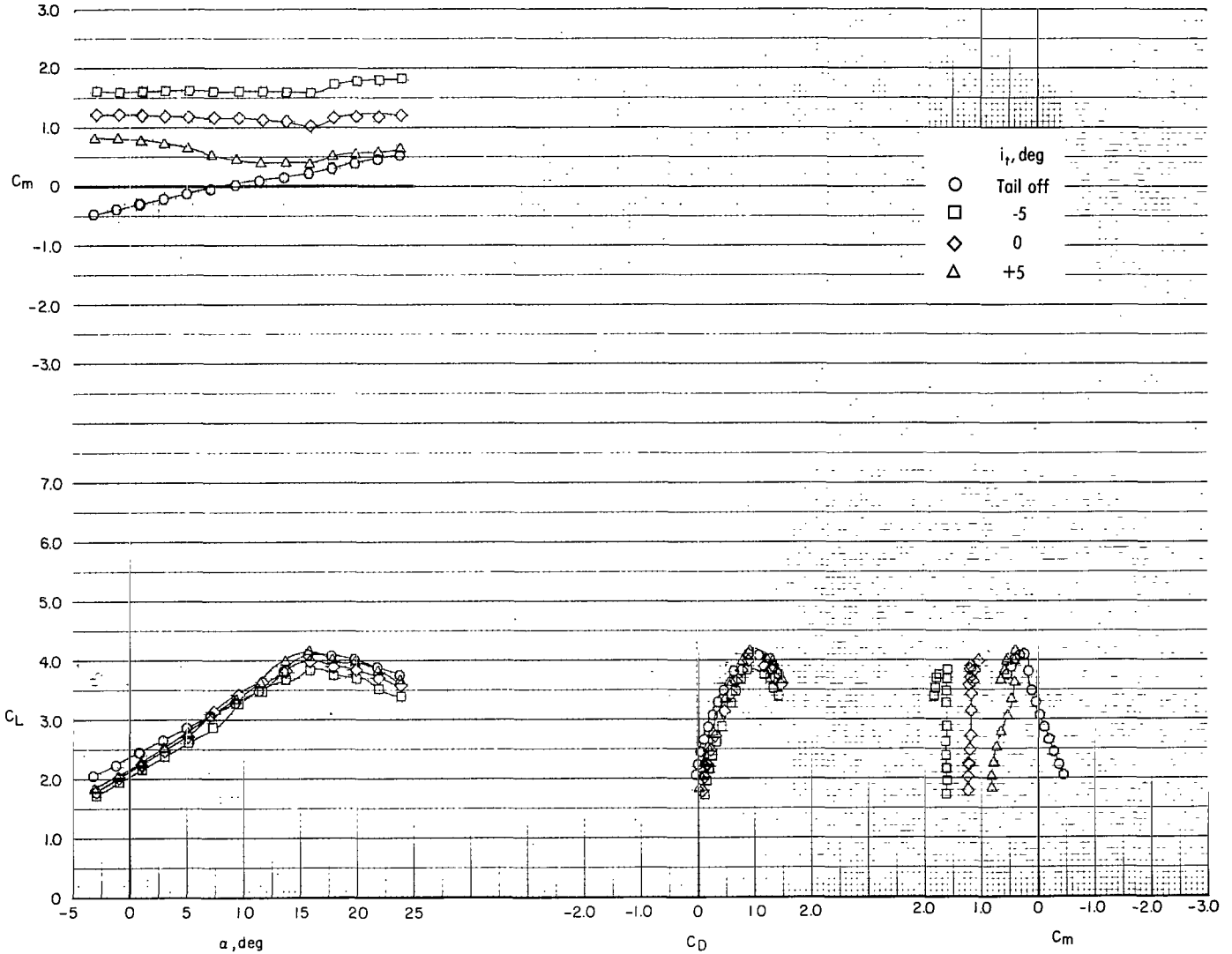


(b) $C_\mu = 1.0$.

Figure 21.- Continued.

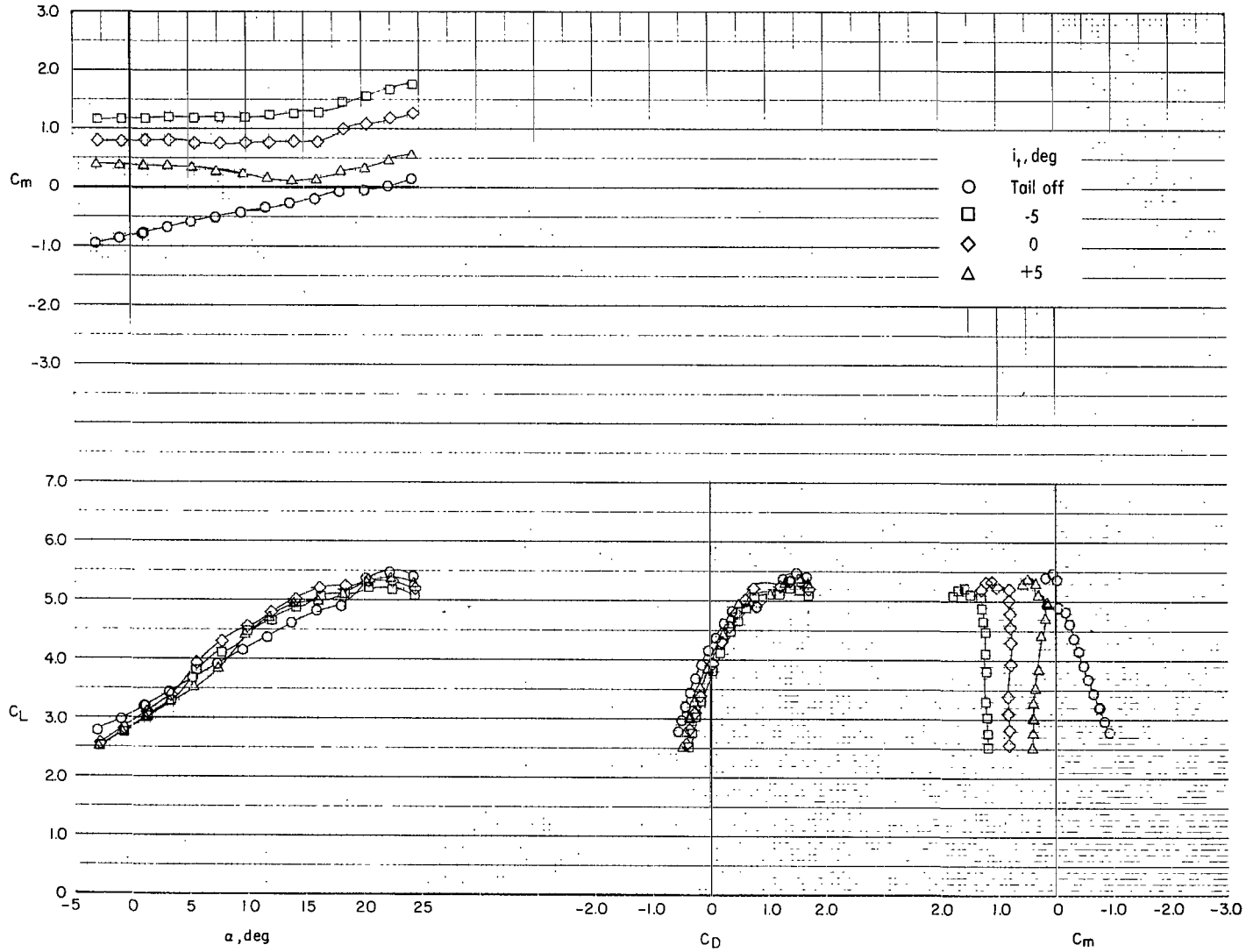


(c) $C_\mu = 2.0$.

Figure 21.- Continued.

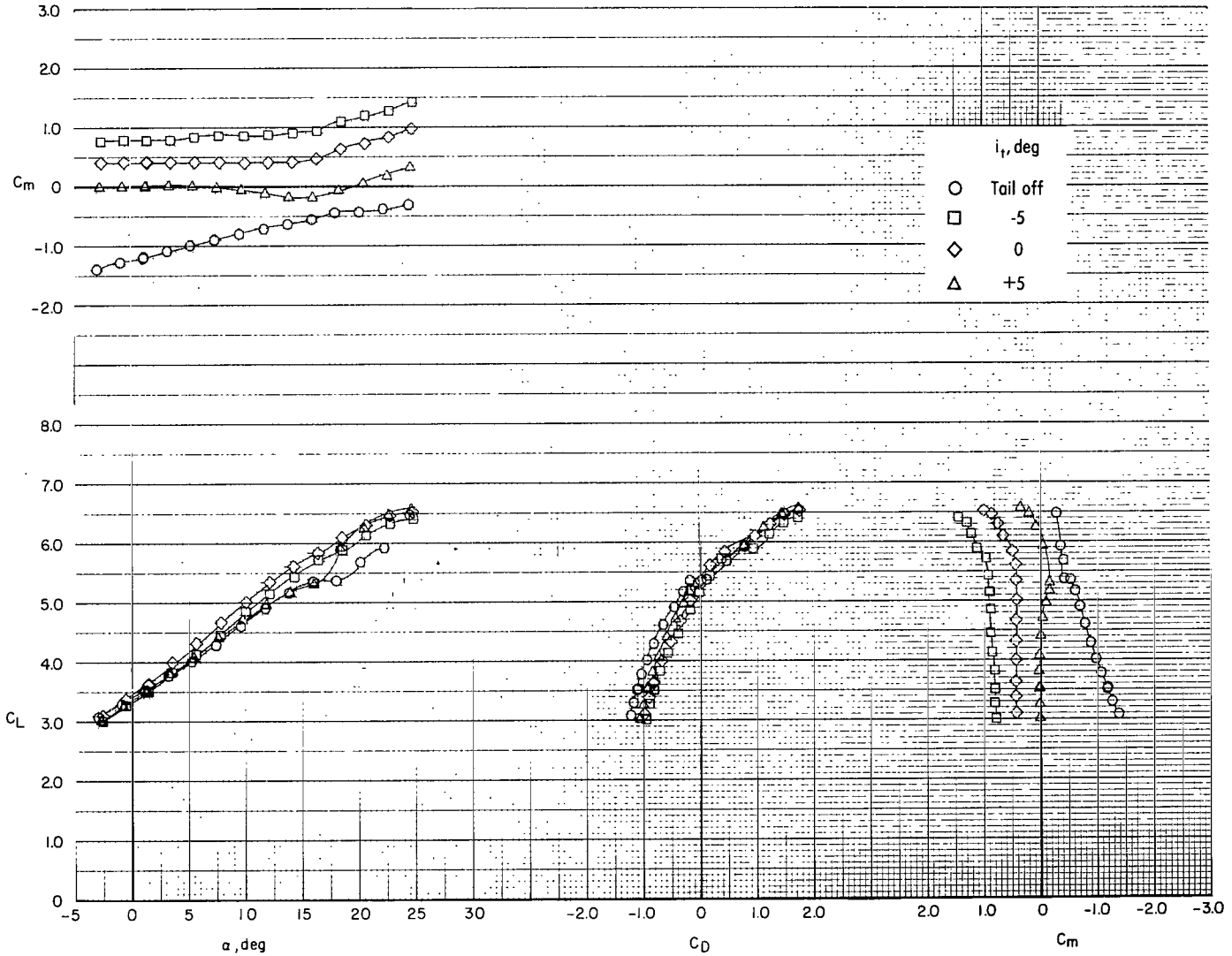


(d) $C_\mu = 3.0$.

Figure 21.- Continued.

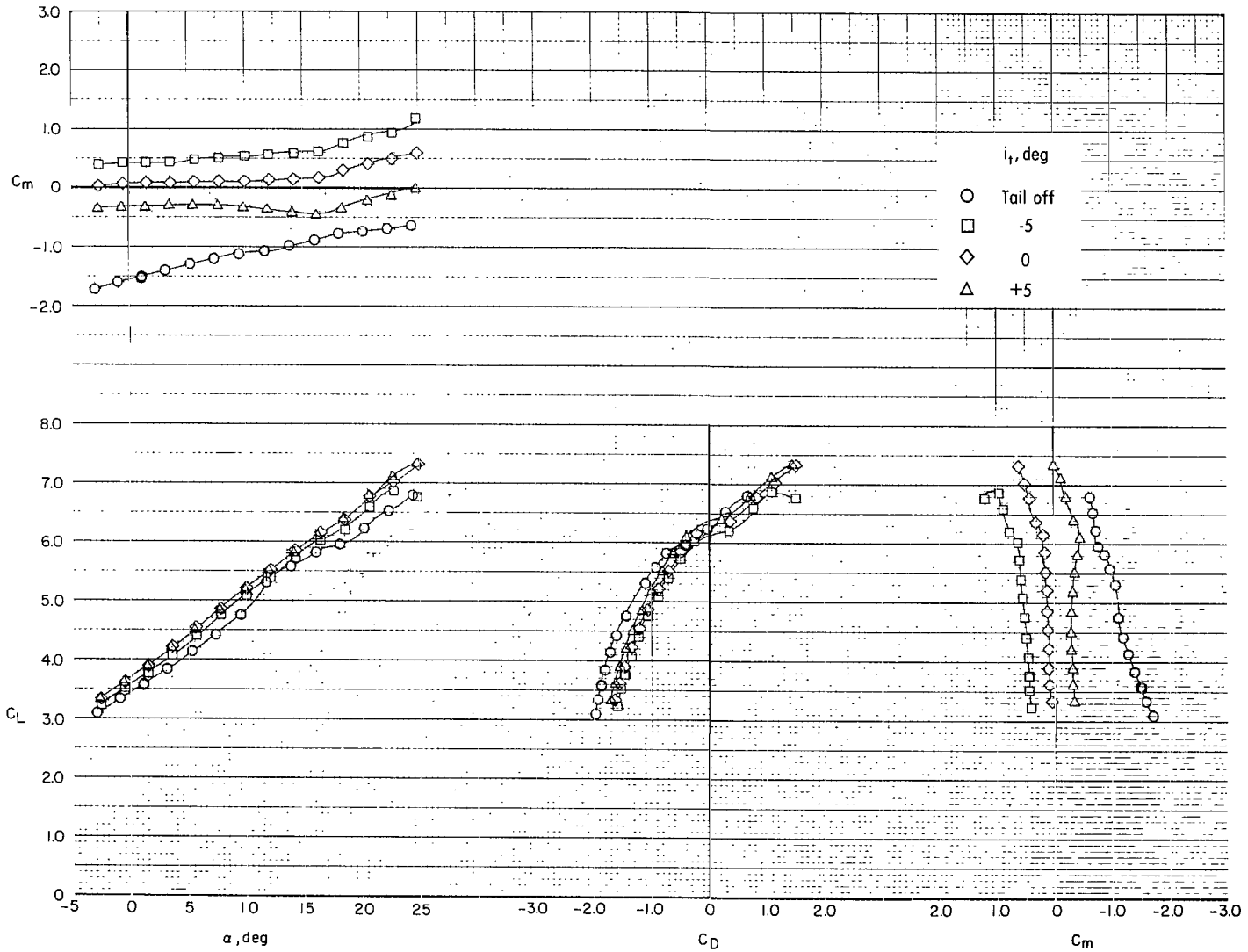


(e) $C_\mu = 4.0$.

Figure 21.- Concluded.

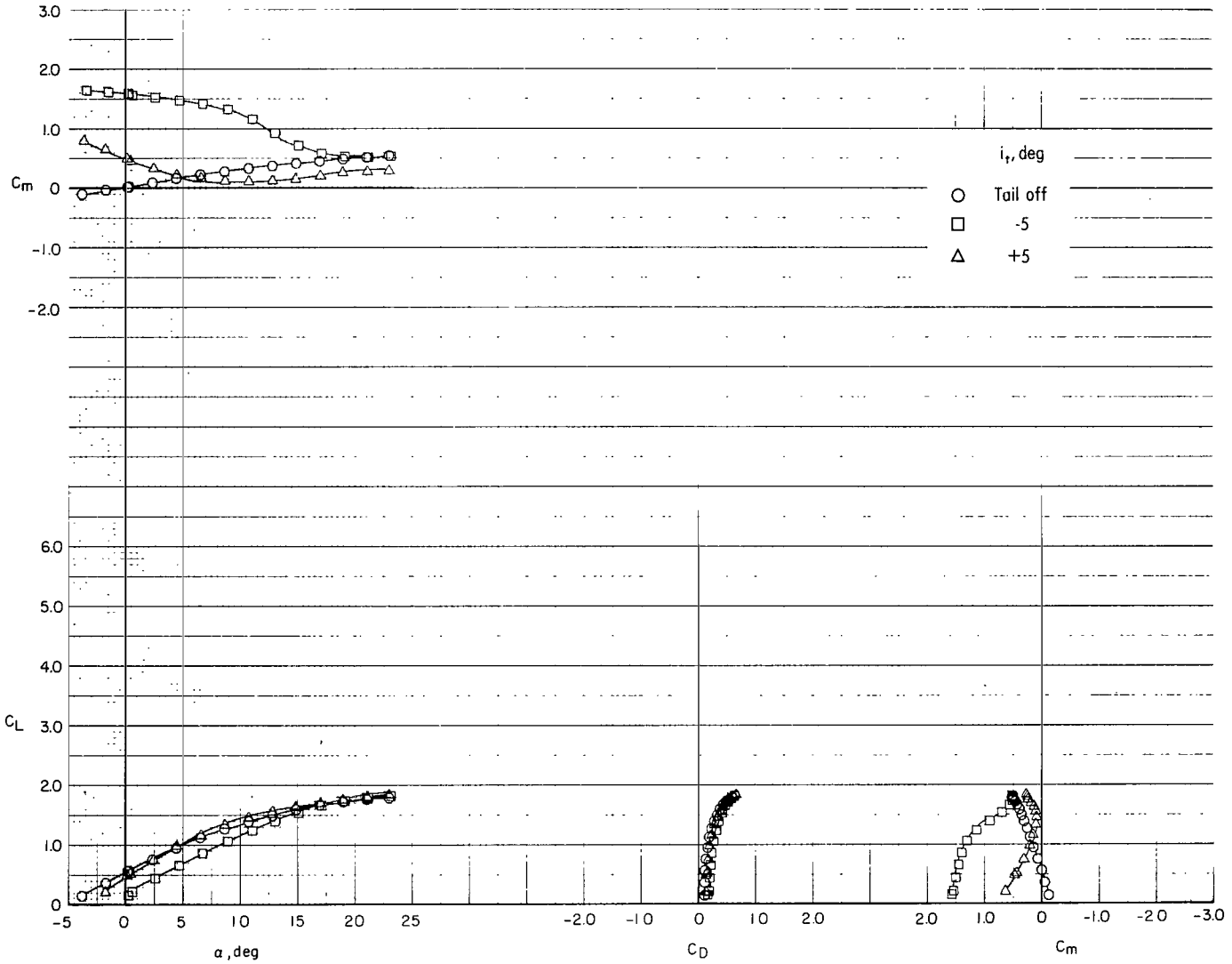


(a) $C_\mu = 0$.

Figure 22.- Effect of the horizontal-tail and stabilizer incidence on the longitudinal aerodynamic characteristics of the model with rectangular nozzles. Radius flap; $\delta_f = 45^o$; $\delta_s = 40^o$.

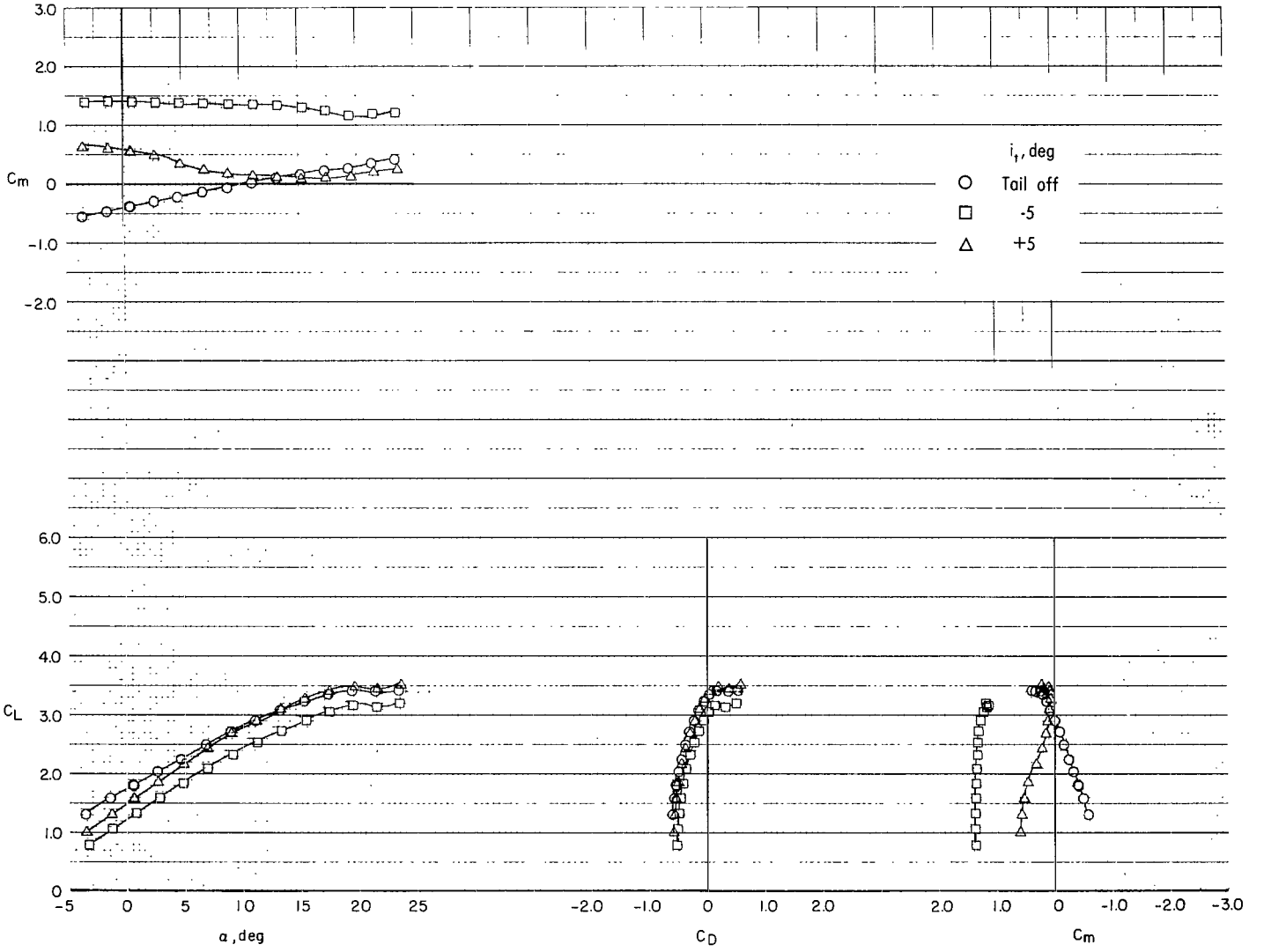


(b) $C_\mu = 1.0$.

Figure 22.- Continued.

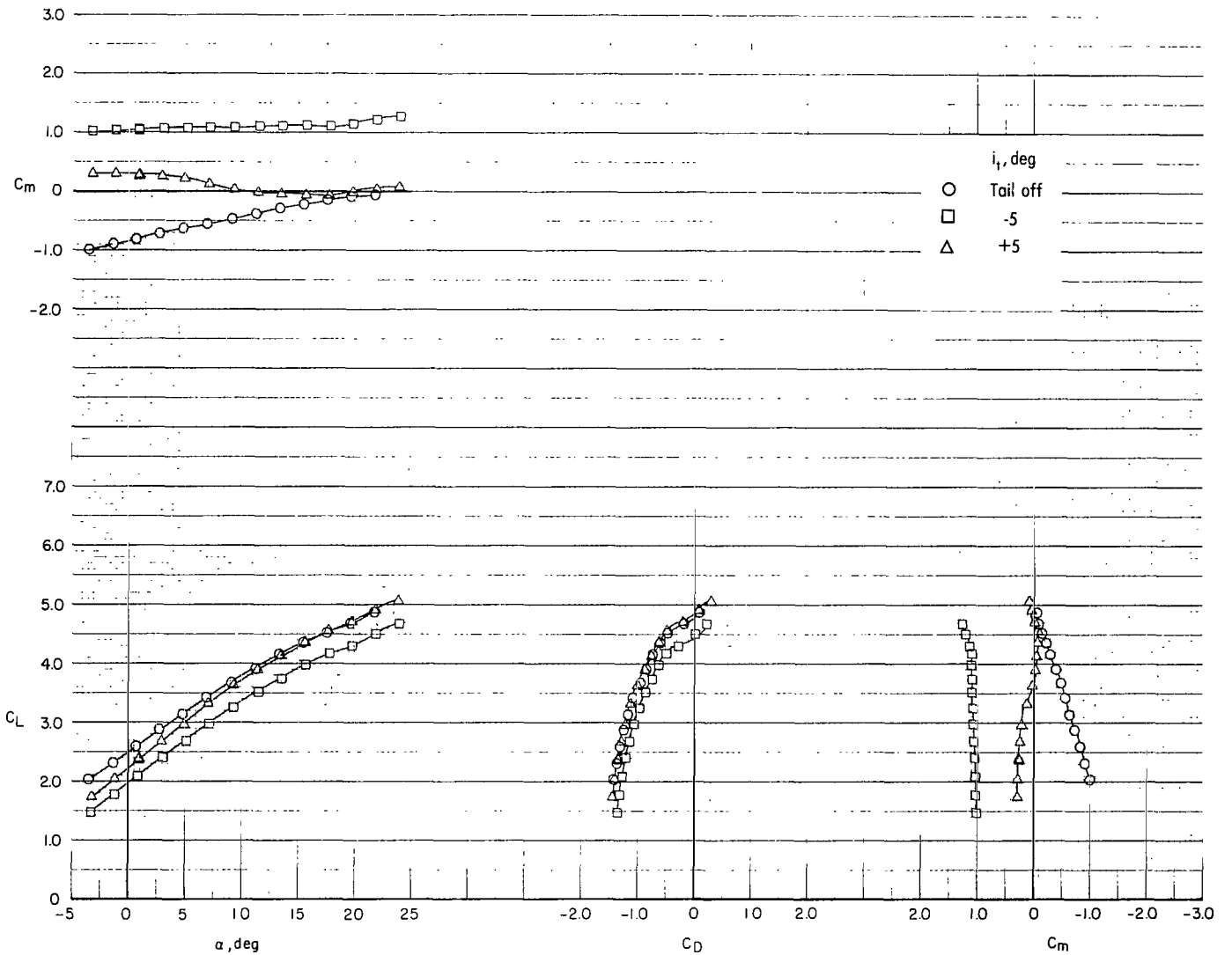


(c) $C_\mu = 2.0$.

Figure 22.- Continued.

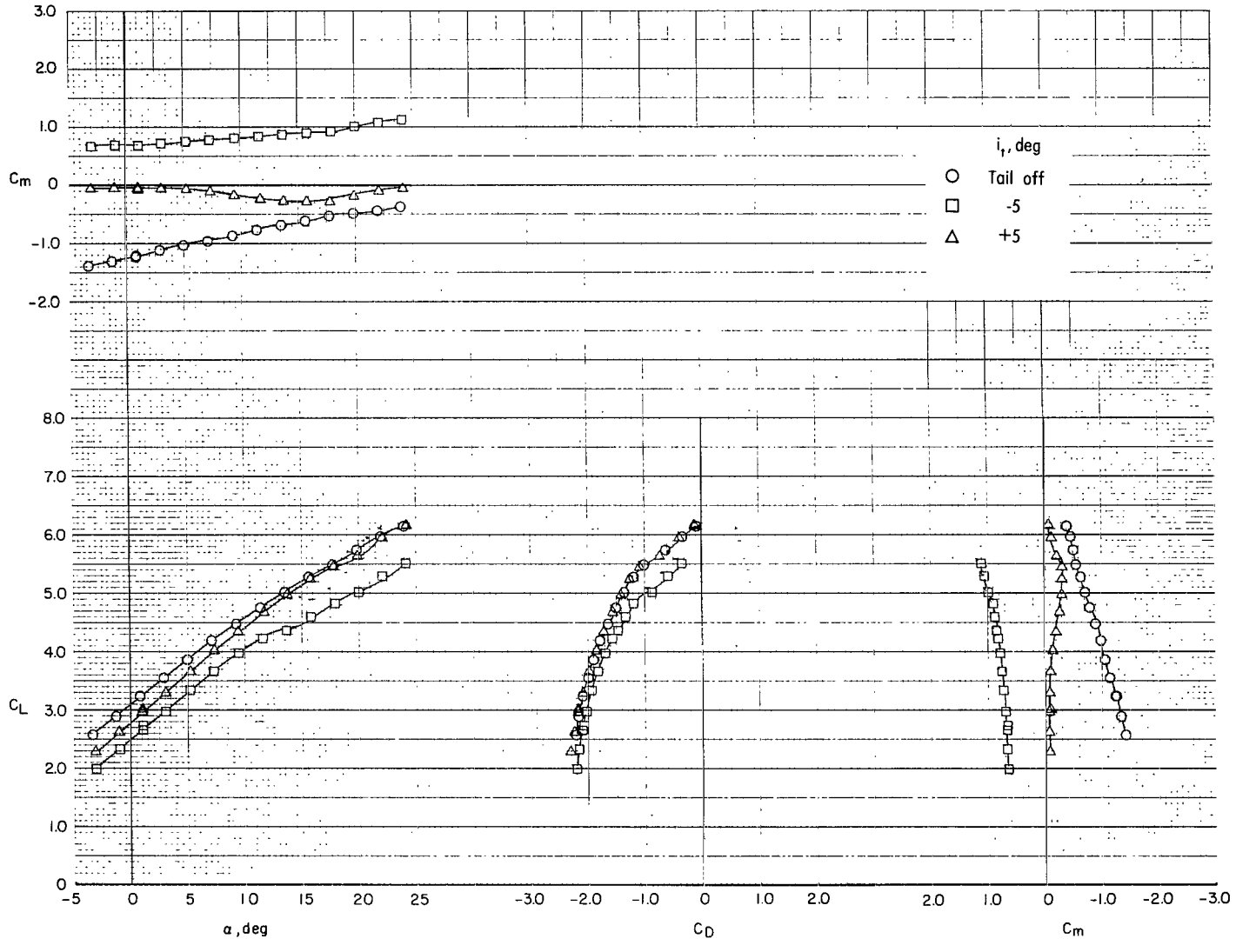


(d) $C_\mu = 3.0$.

Figure 22.- Continued.

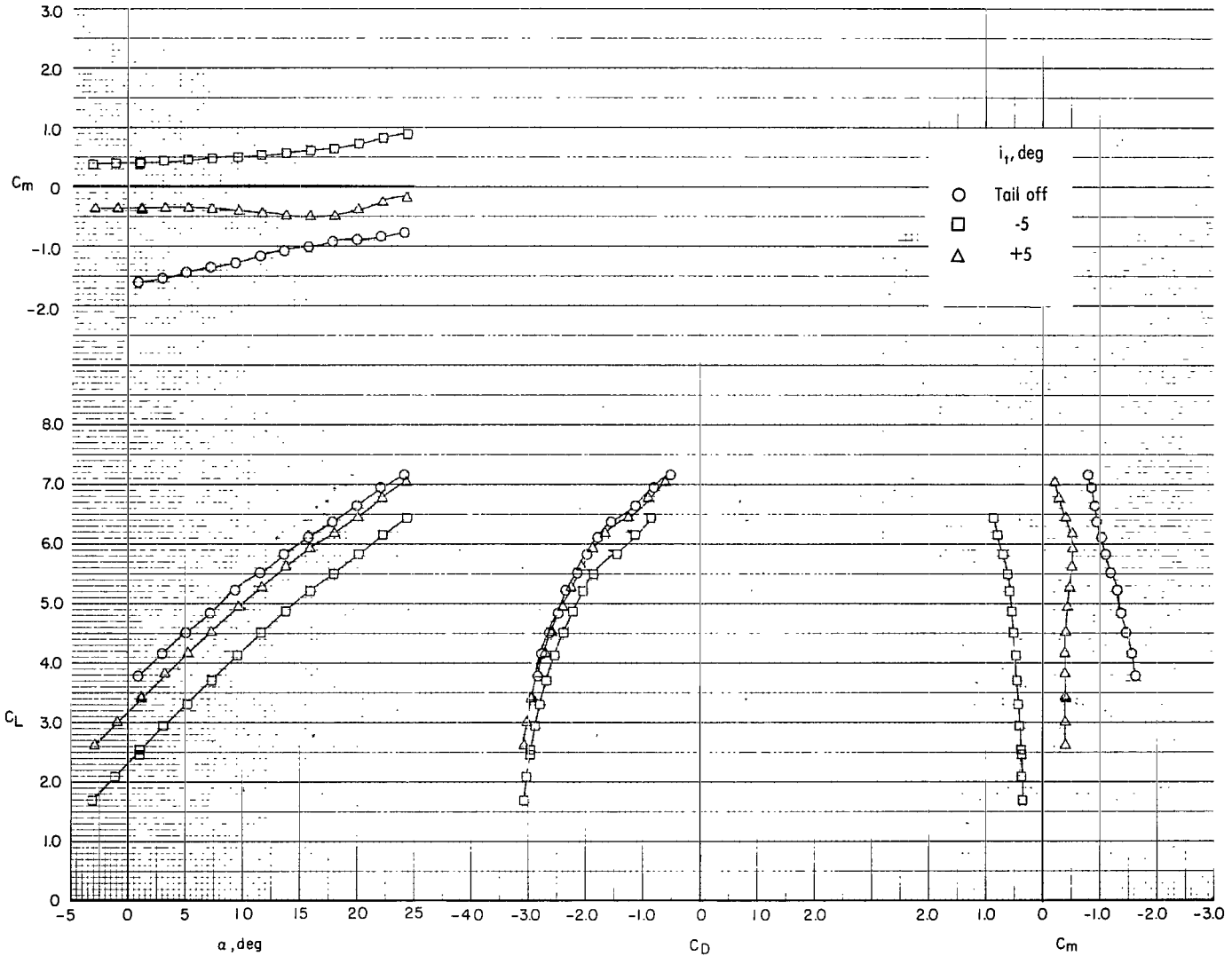


(e) $\dot{C}_{\mu} = 4.0$.

Figure 22.- Concluded.

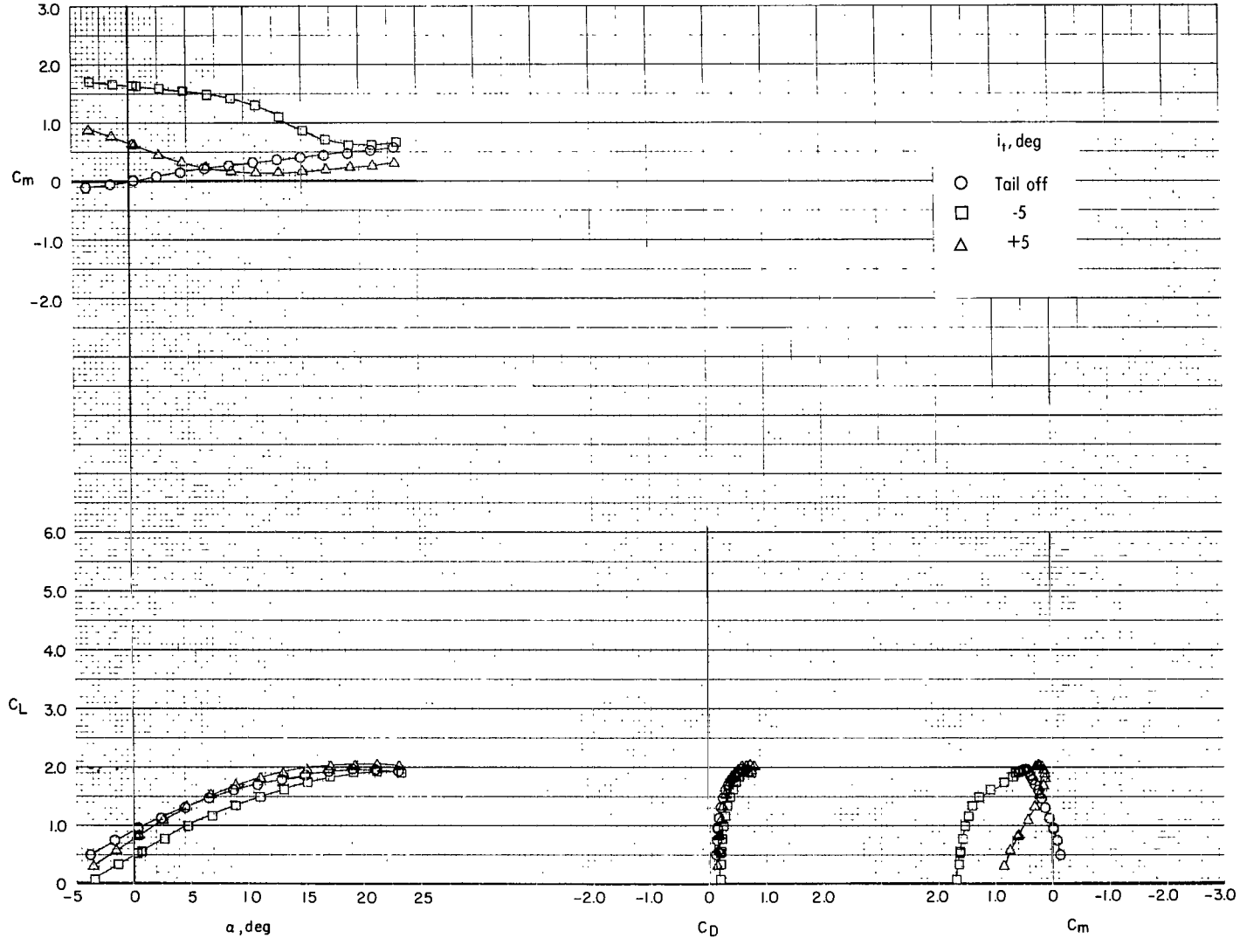


(a) $C_\mu = 0.$

Figure 23.- Effect of the horizontal-tail and stabilizer incidence on the longitudinal aerodynamic characteristics of the model with rectangular nozzles. Radius flap; $\delta_f = 60^o$; $\delta_s = 40^o$.

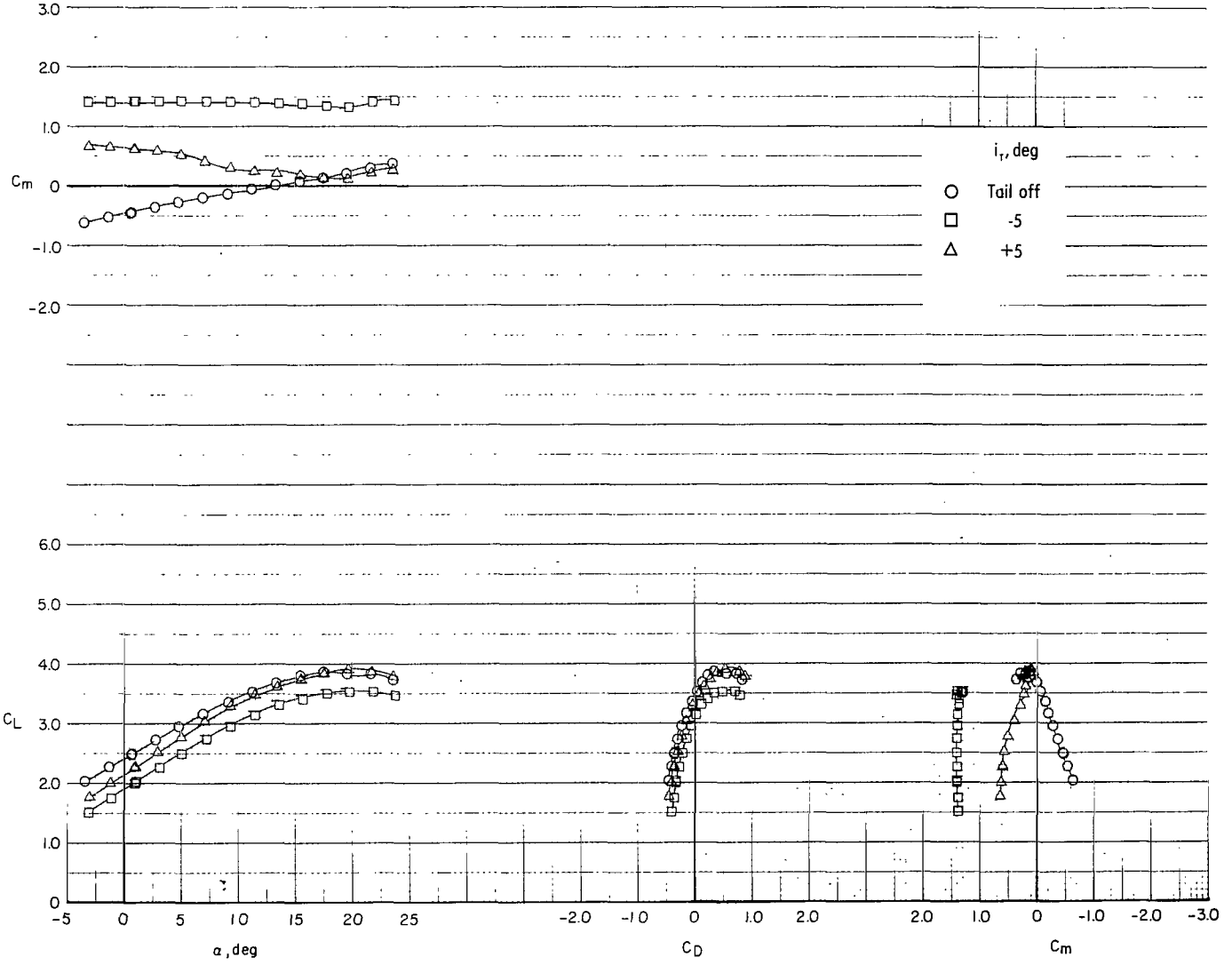


(b) $C_\mu = 1.0$.

Figure 23.- Continued.

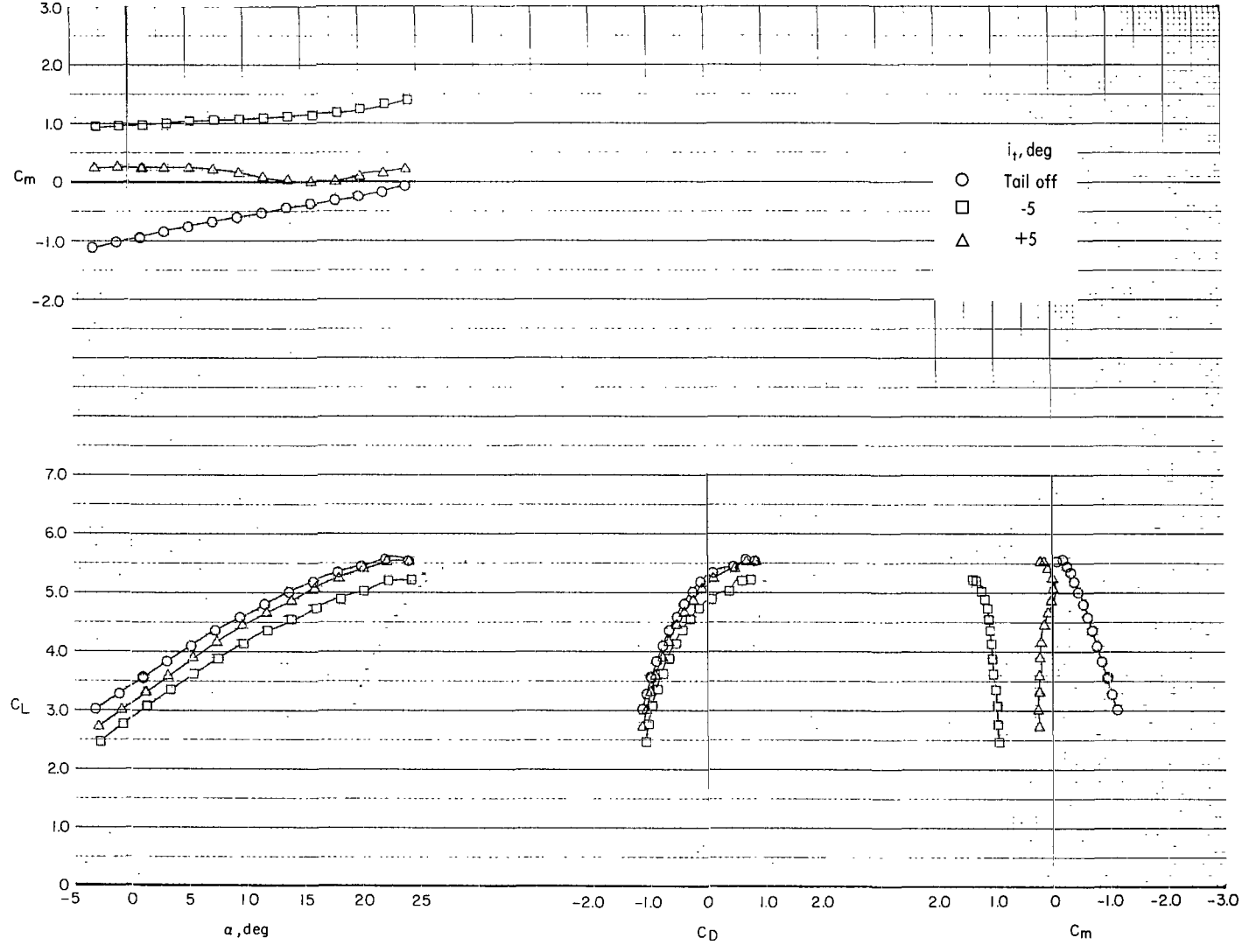


(c) $C_\mu = 2.0$.

Figure 23.- Continued.

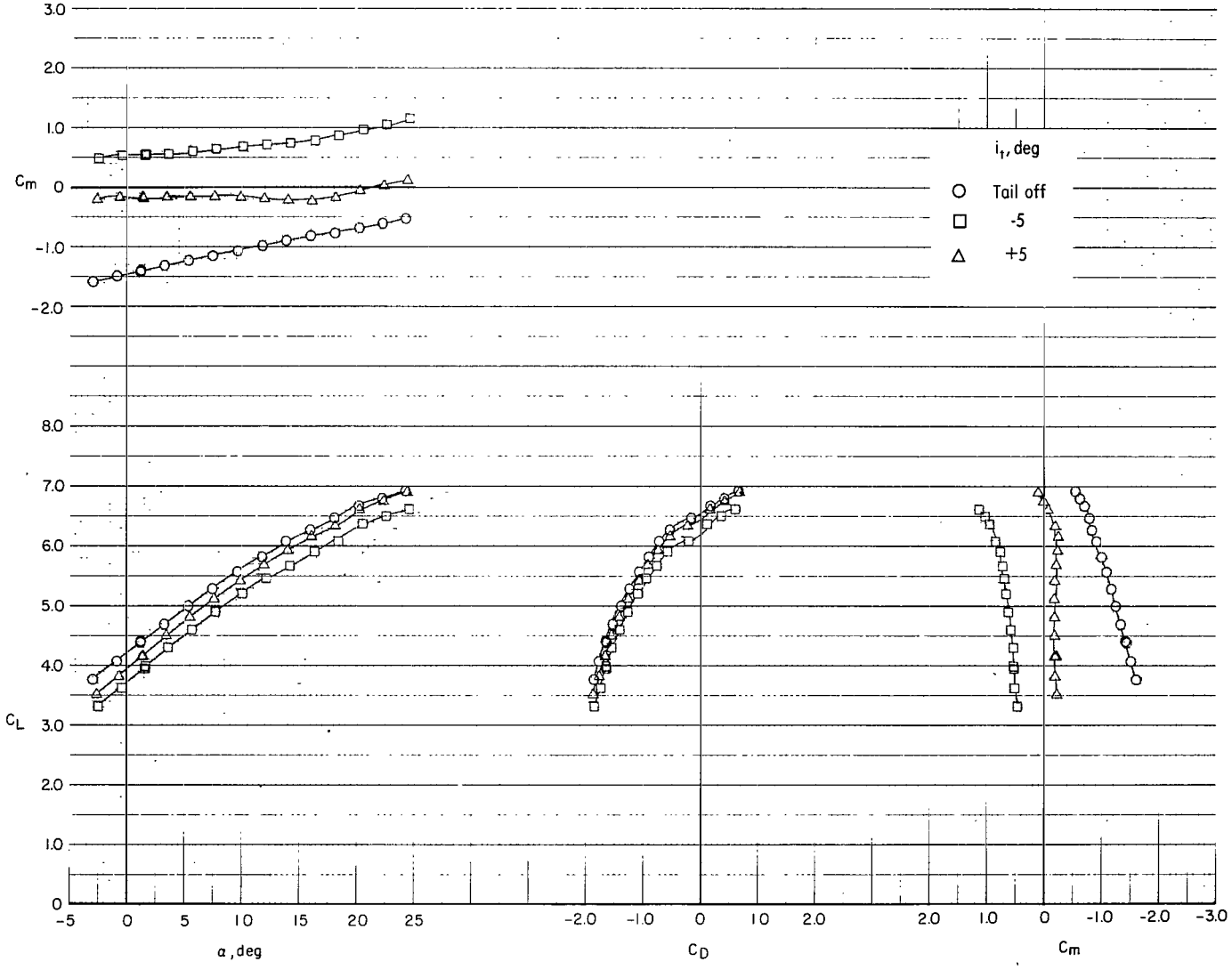


(d) $C_\mu = 3.0$.

Figure 23.- Continued.

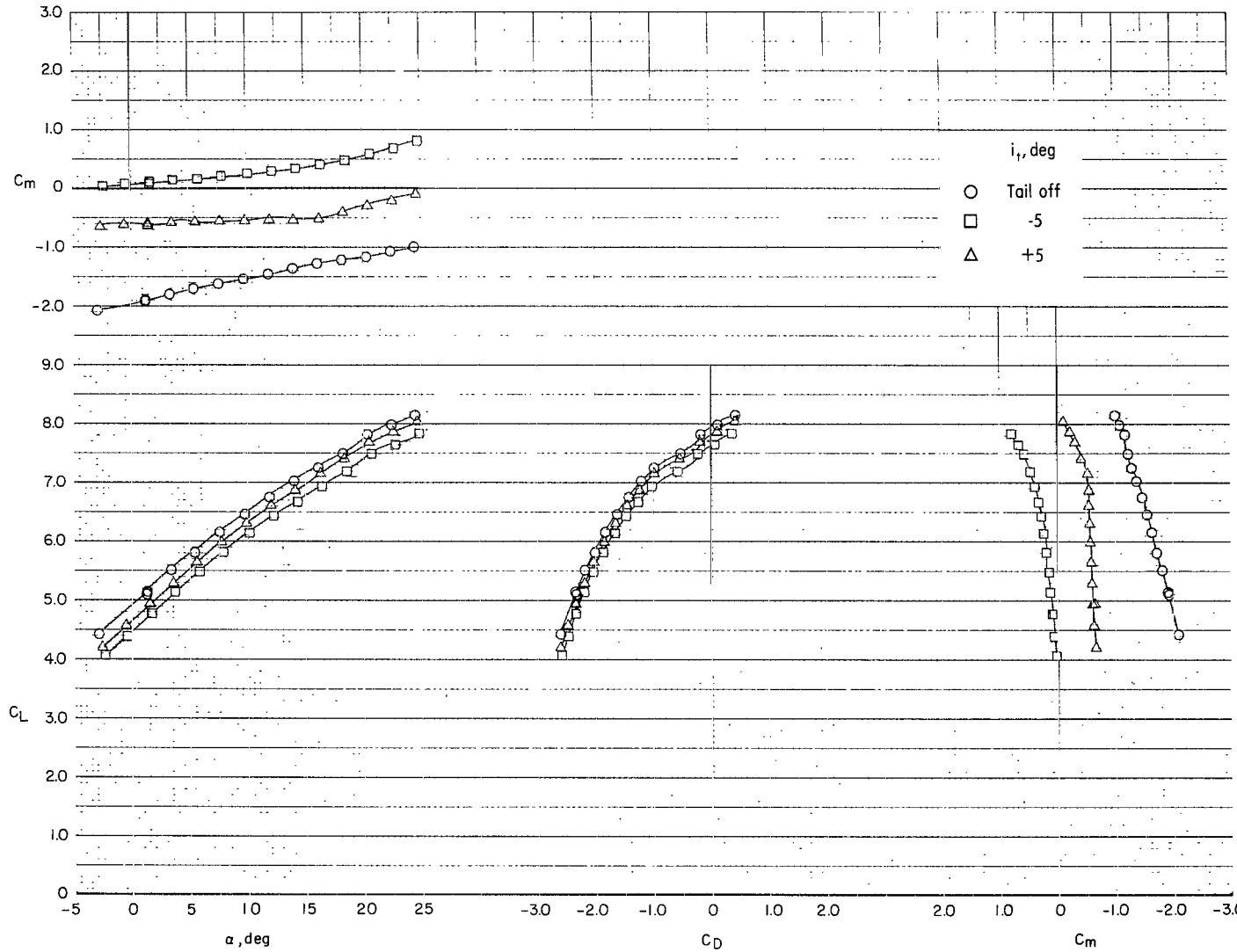


(e) $C_\mu = 4.0$.

Figure 23.- Concluded.

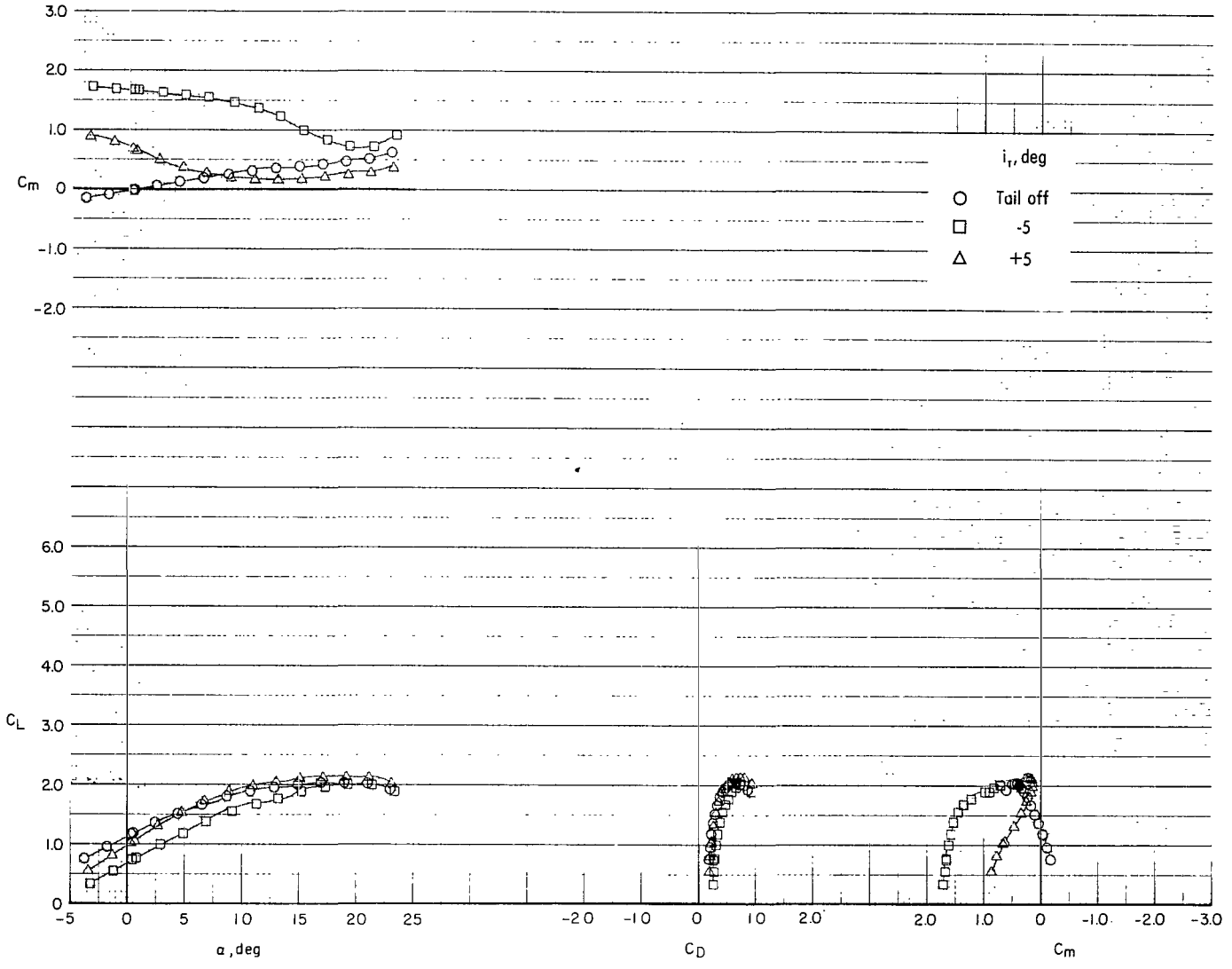


(a) $C_\mu = 0$.

Figure 24.- Effect of the horizontal-tail and stabilizer incidence on the longitudinal aerodynamic characteristics of the model with rectangular nozzles. Radius flap; $\delta_f = 75^o$; $\delta_s = 40^o$.

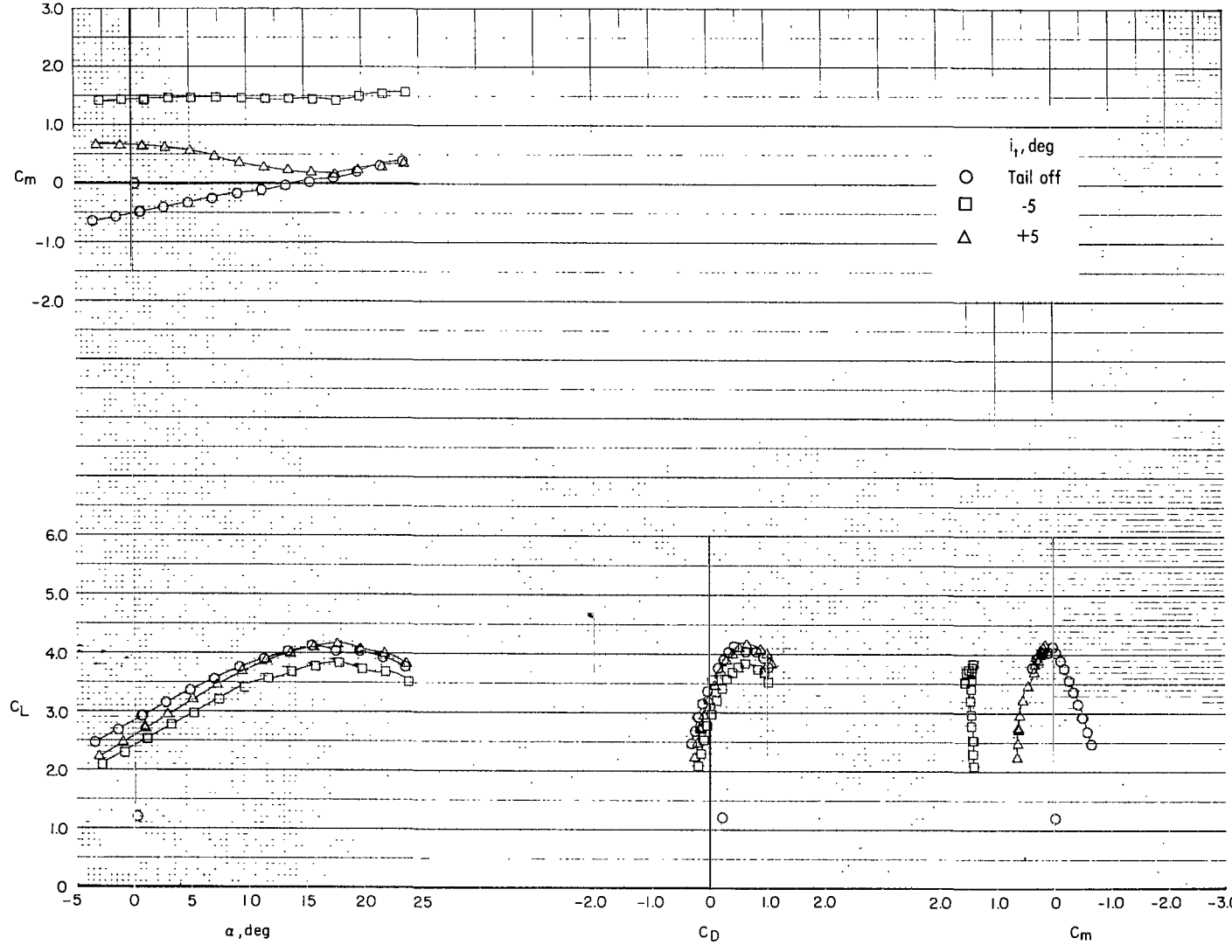


(b) $C_\mu = 1.0$.

Figure 24.- Continued.

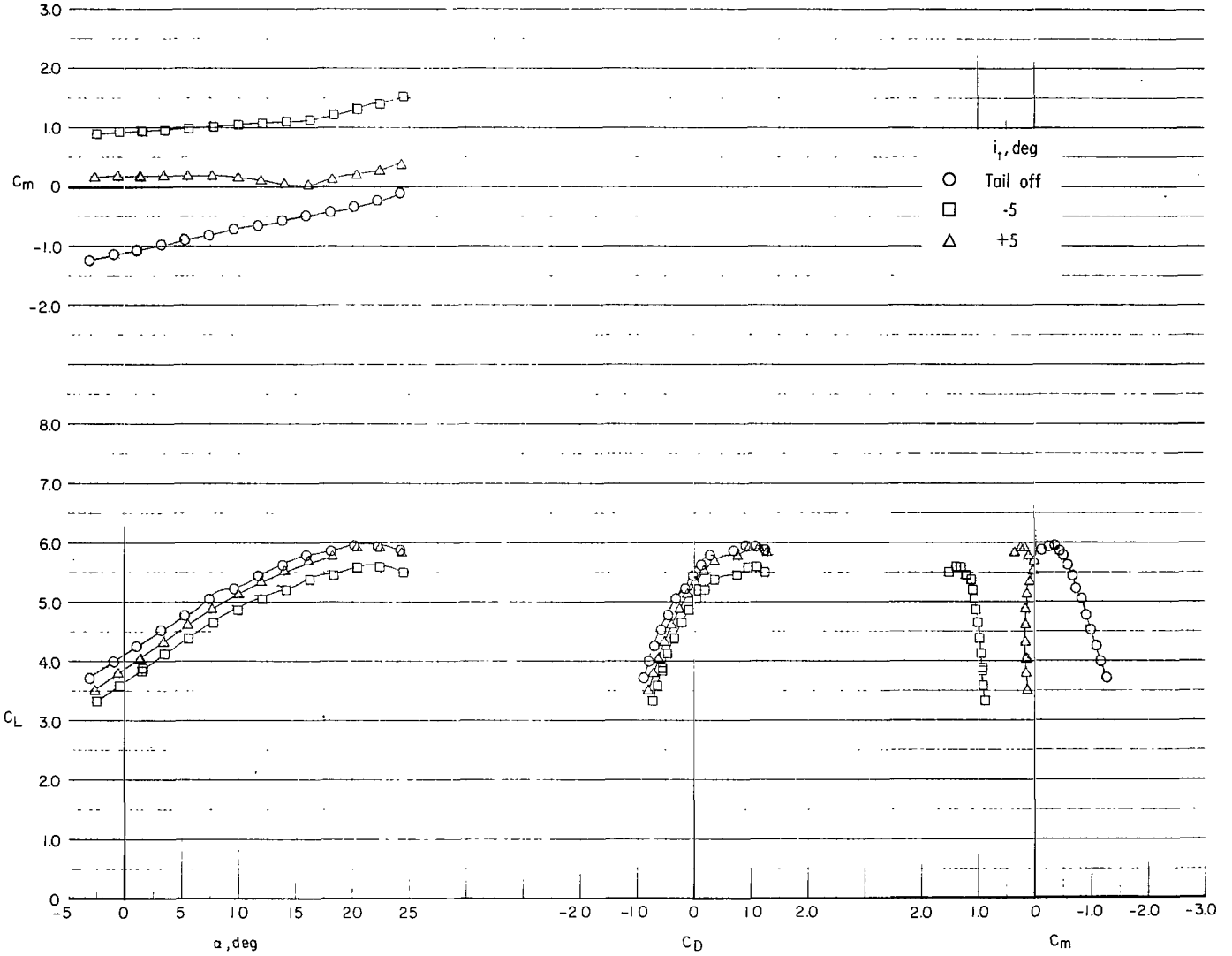


(c) $C_\mu = 2.0$.

Figure 24.- Continued.

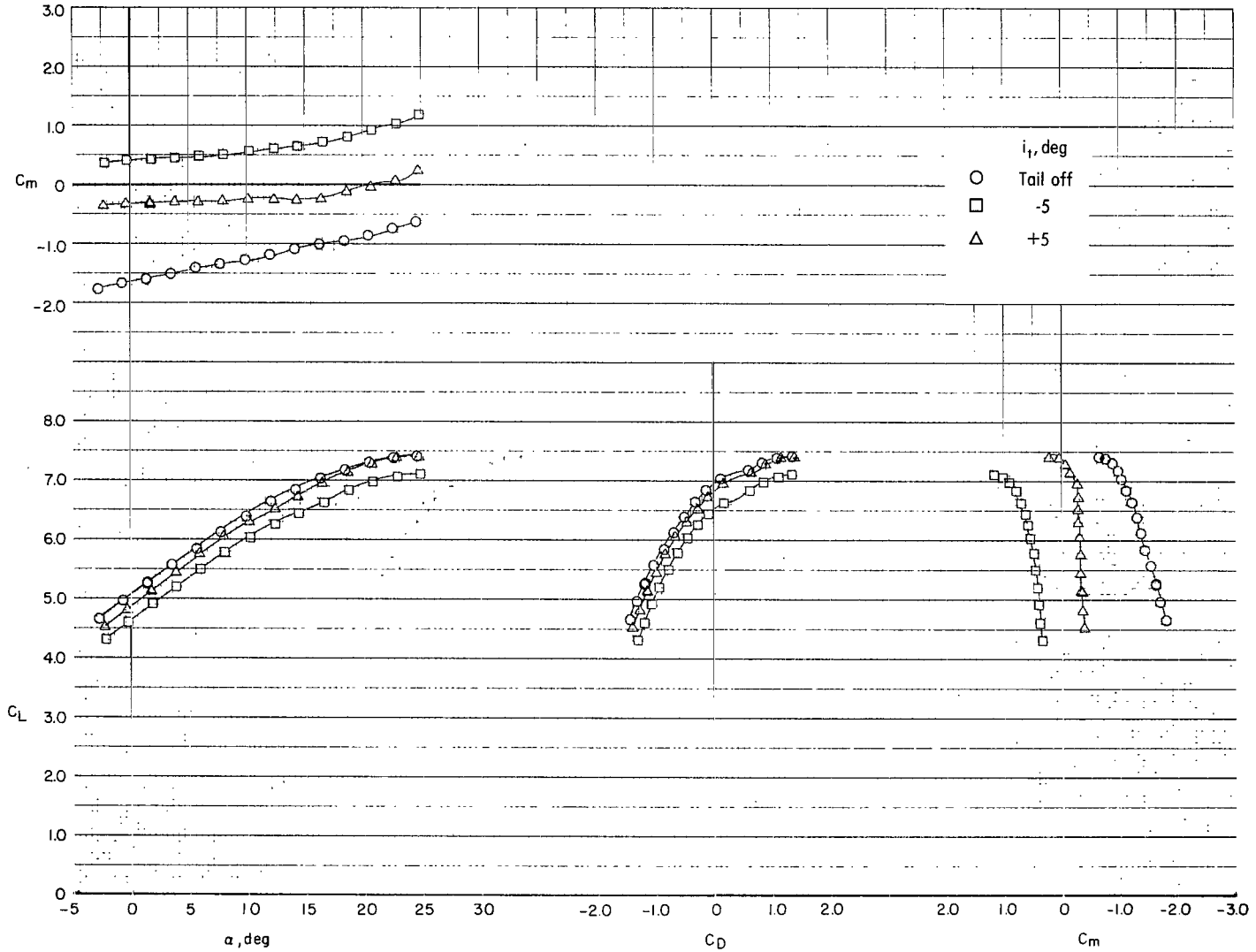


(d) $C_\mu = 3.0$.

Figure 24.- Continued.

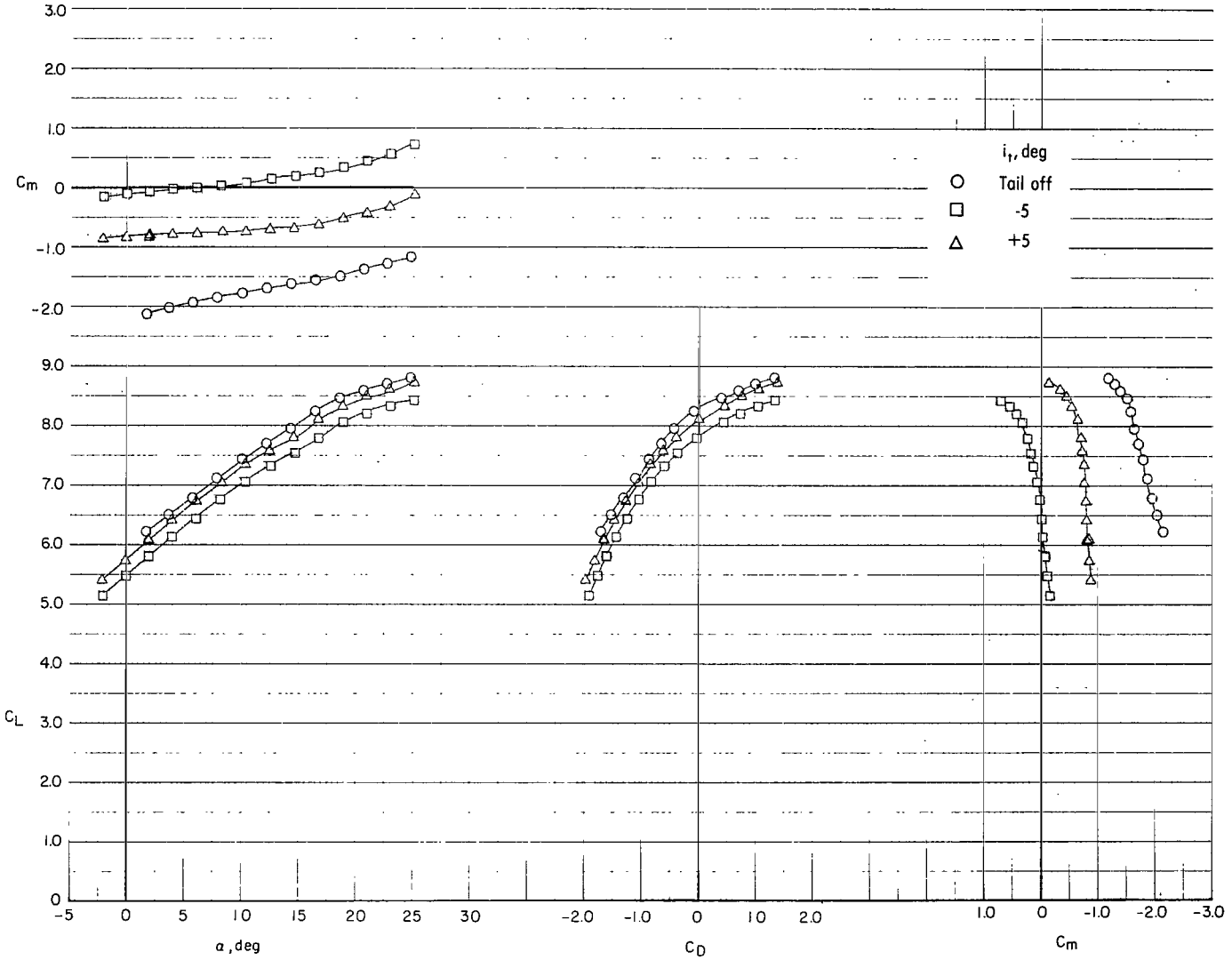


(e) $C_\mu = 4.0$.

Figure 24.- Concluded.

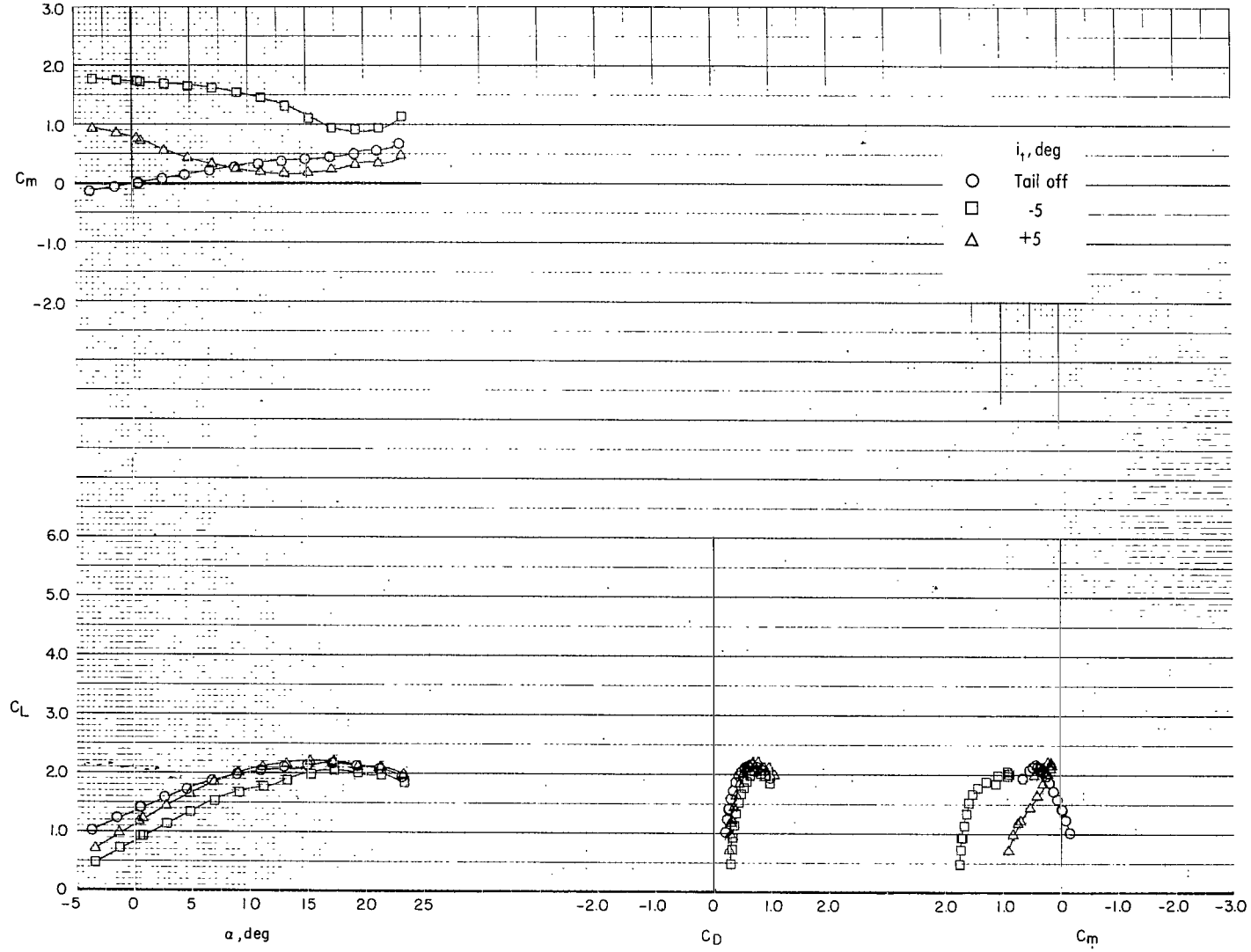


(a) $C_{\mu} = 0$.

Figure 25.- Effect of the horizontal-tail and stabilizer incidence on the longitudinal aerodynamic characteristics of the model with rectangular nozzles. Radius flap; $\delta_f = 90^o$; $\delta_s = 40^o$.

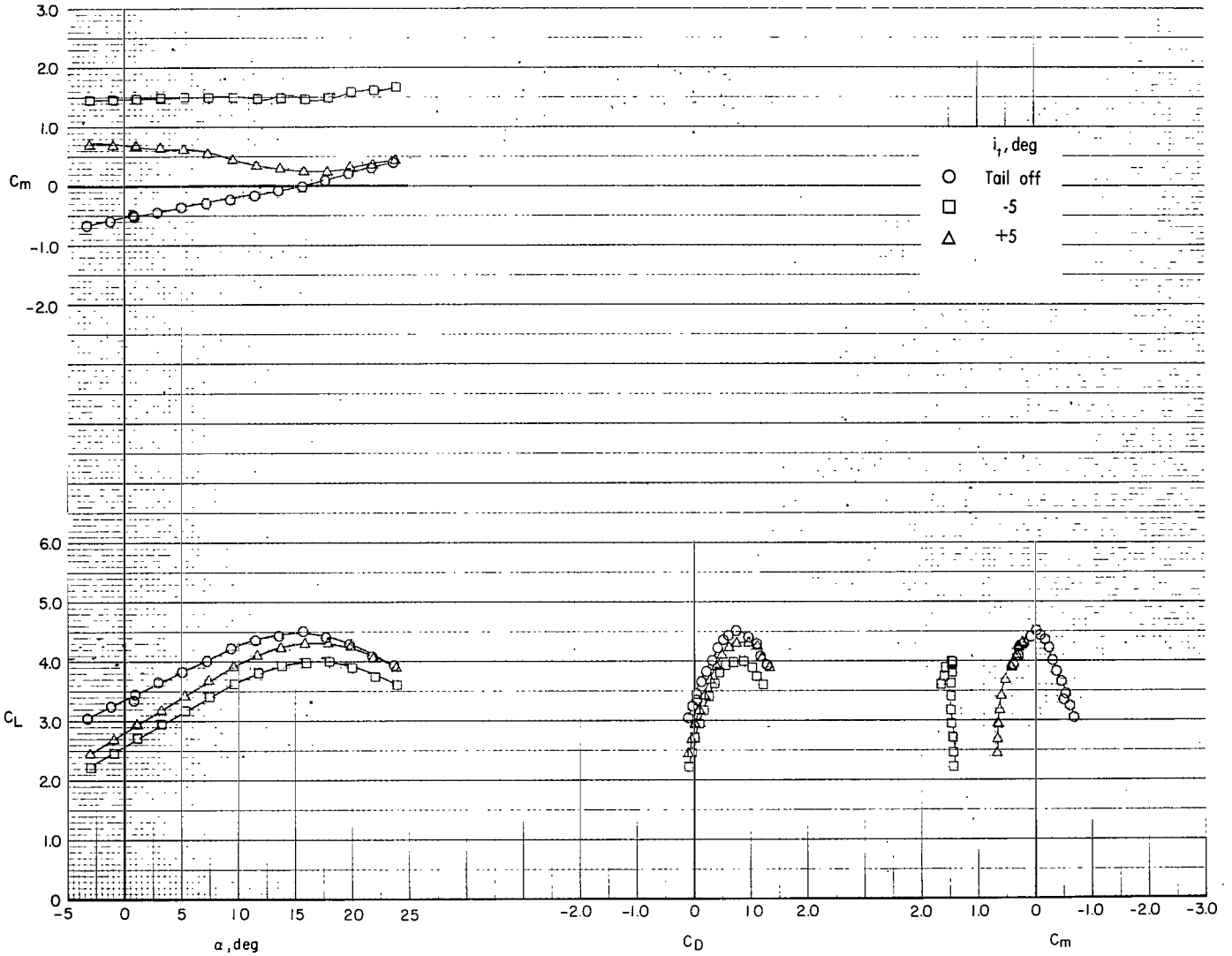


(b) $C_\mu = 1.0$.

Figure 25.- Continued.

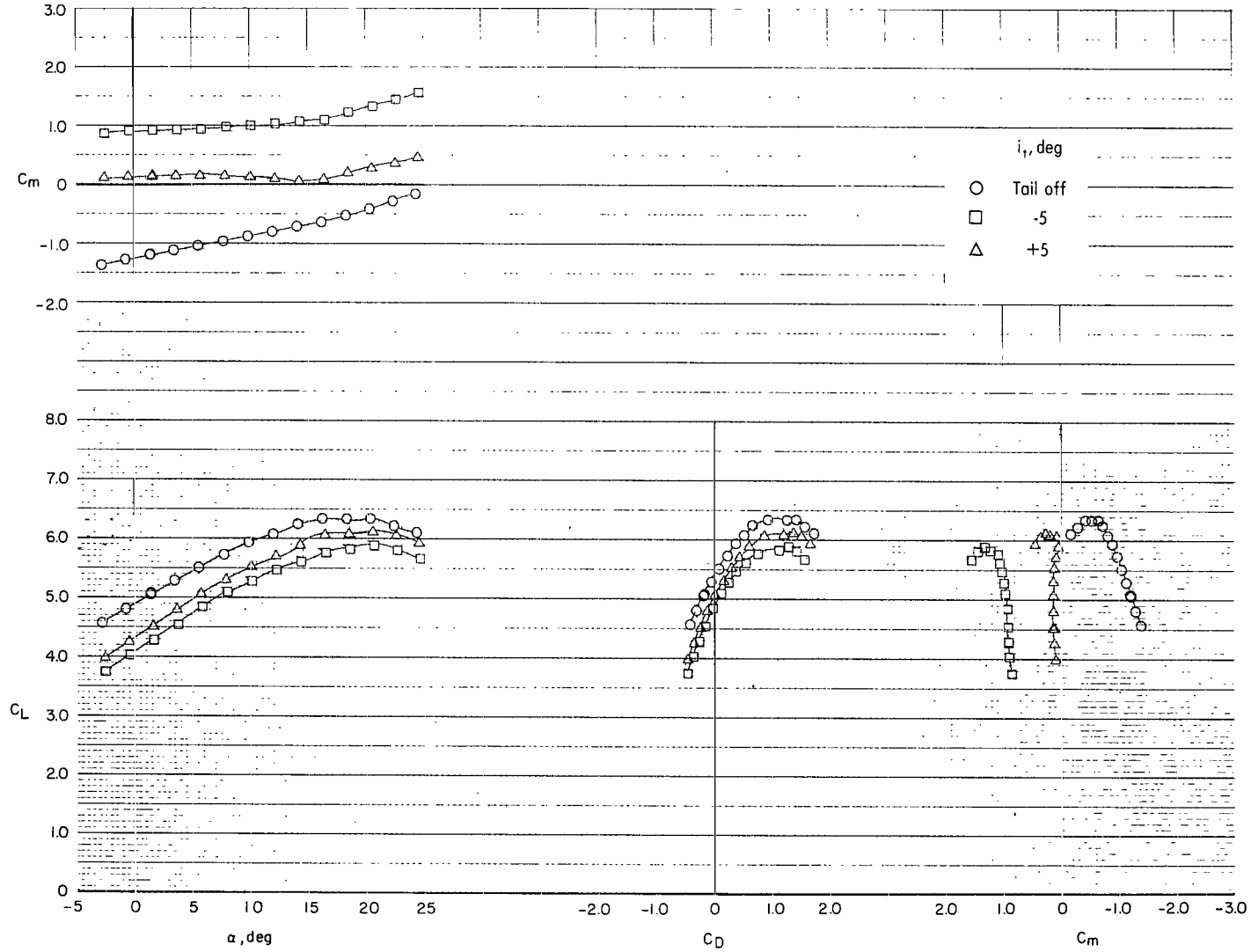


(c) $C_{\mu} = 2.0$.

Figure 25.- Continued.

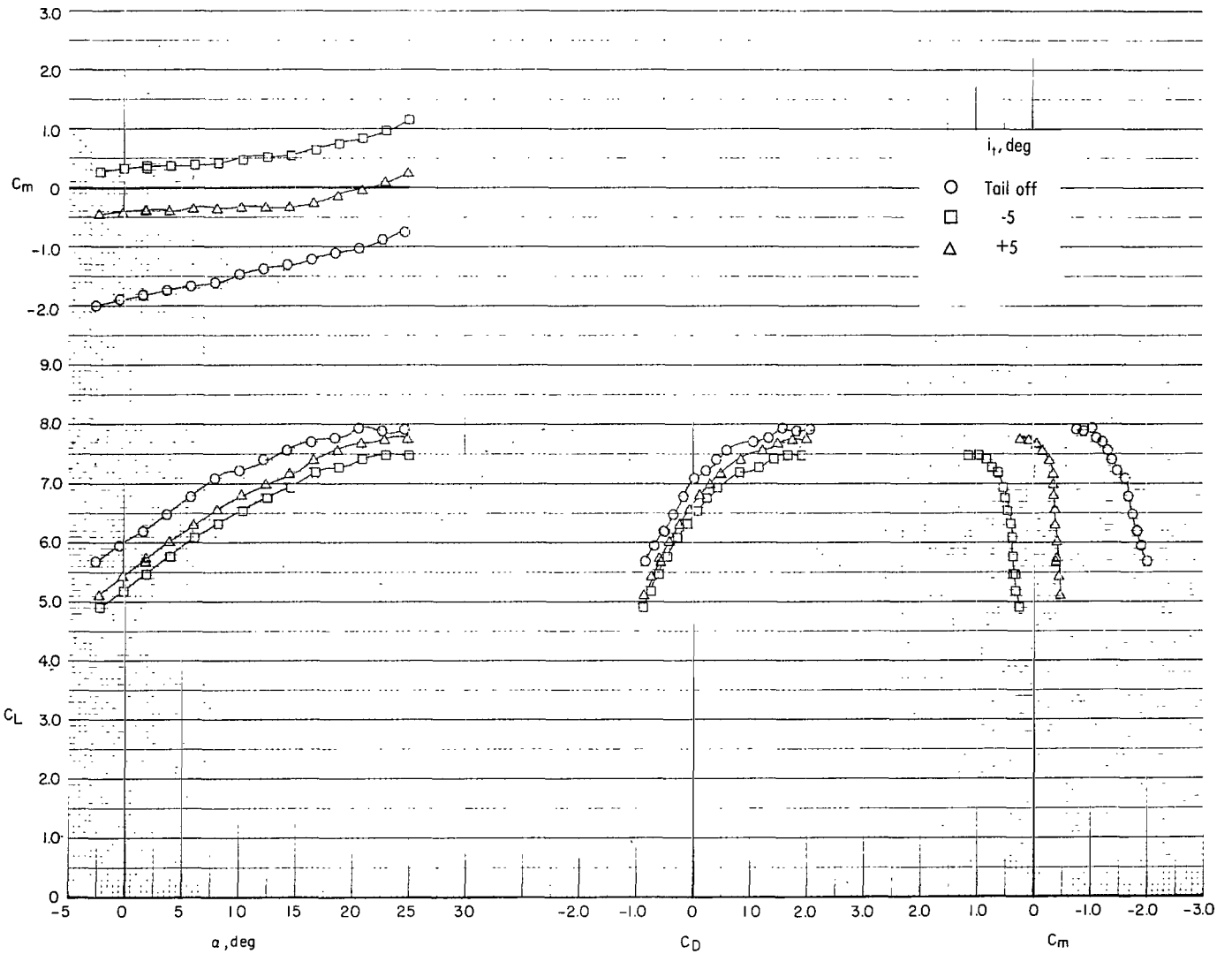


(d) $C_\mu = 3.0$.

Figure 25.- Continued.

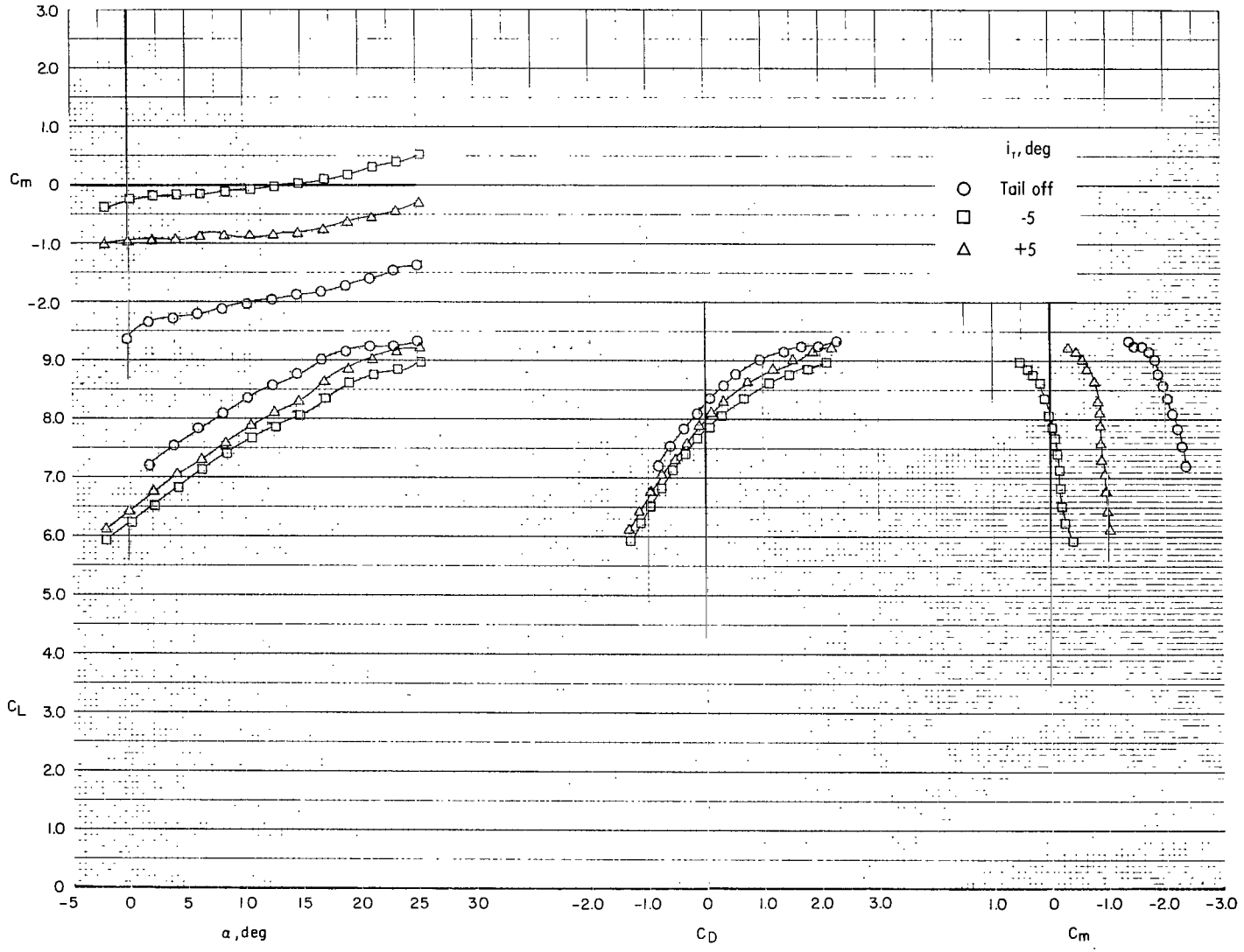


(e) $C_\mu = 4.0$.

Figure 25.- Concluded.

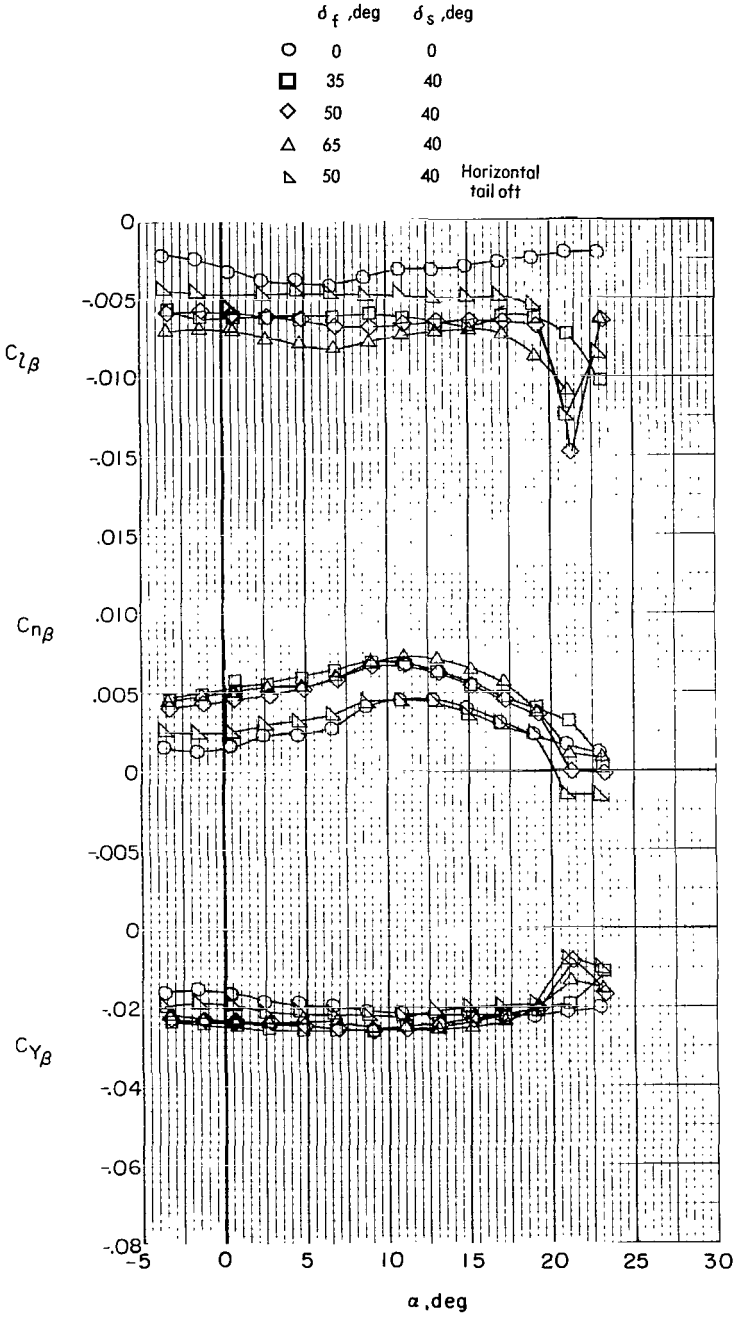


(a) $C_\mu = 0$.

Figure 26.- Effect of angle of attack on the static lateral stability derivatives of the model with rectangular nozzles. Basic flap; $i_t = -5^o$.

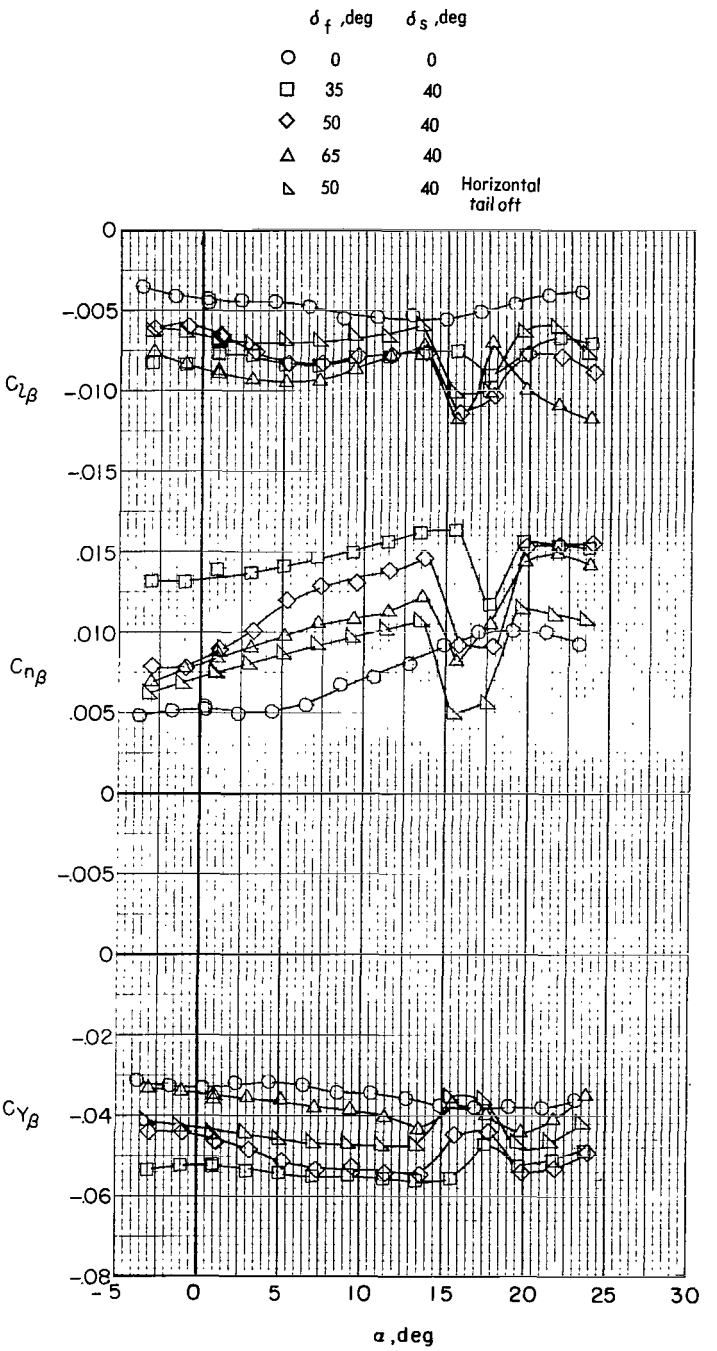


(b) $C_\mu = 2.0$.

Figure 26.- Continued.

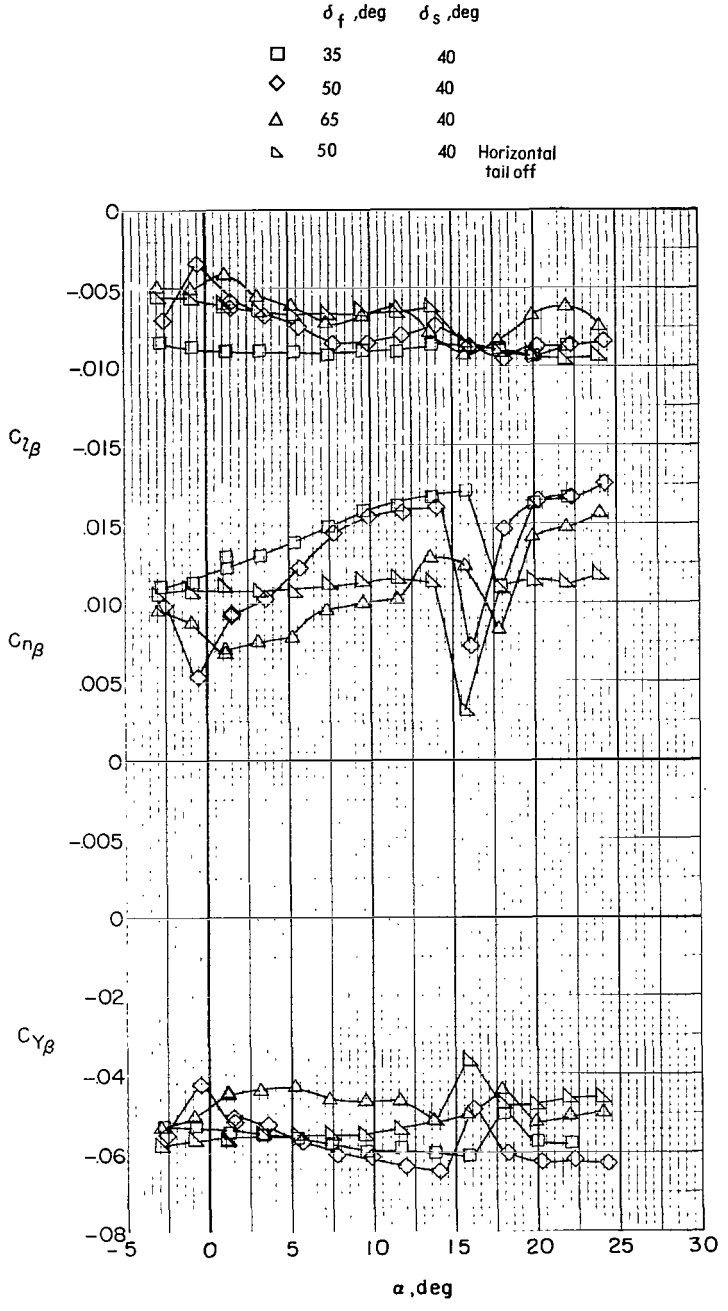


(c) $C_{\mu} = 4.0$.

Figure 26.- Continued.

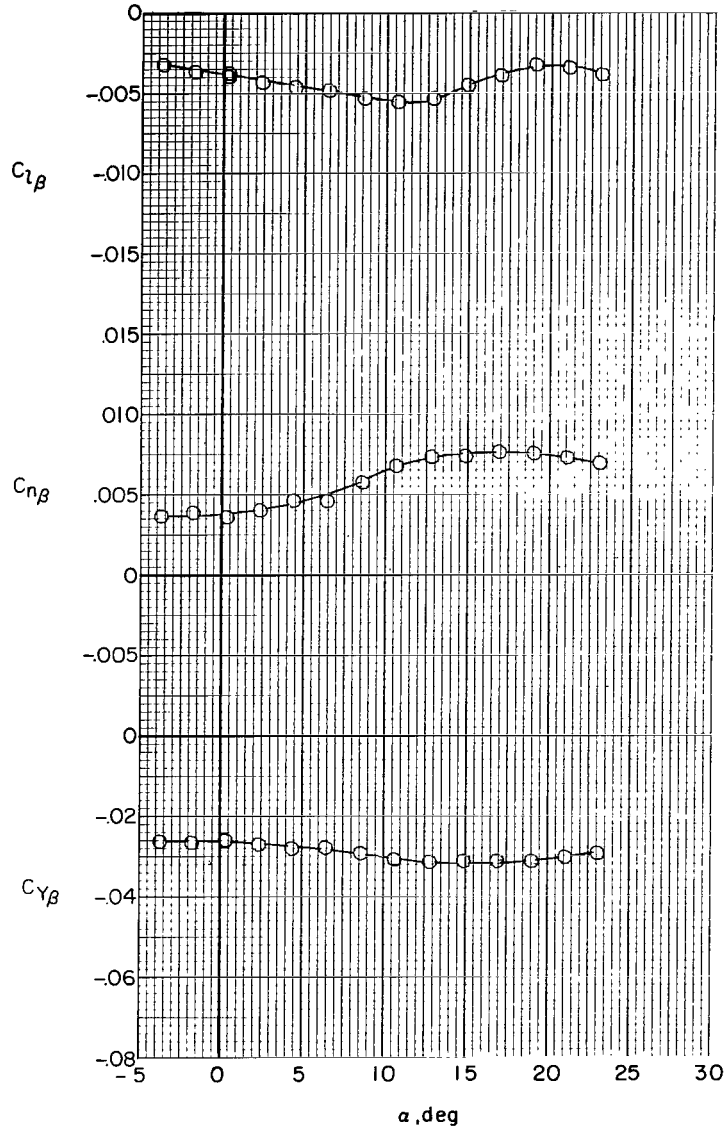


(d) $C_\mu = 1.0$; $\delta_s = 0^o$; $\delta_f = 0^o$.

Figure 26.- Concluded.

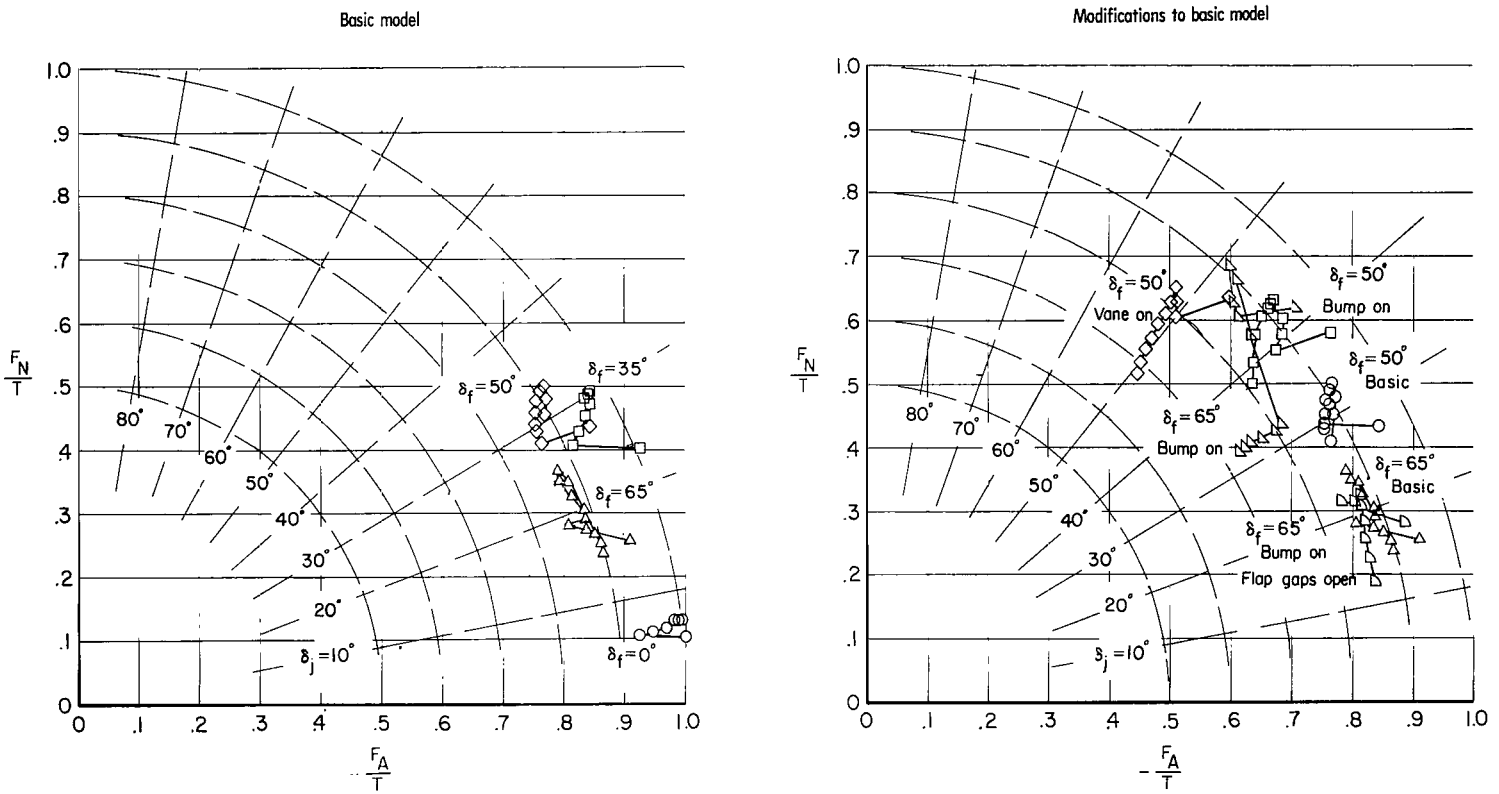


(a) Model with D-nozzles.

Figure 27.- Static thrust characteristics of upper surface blown model.

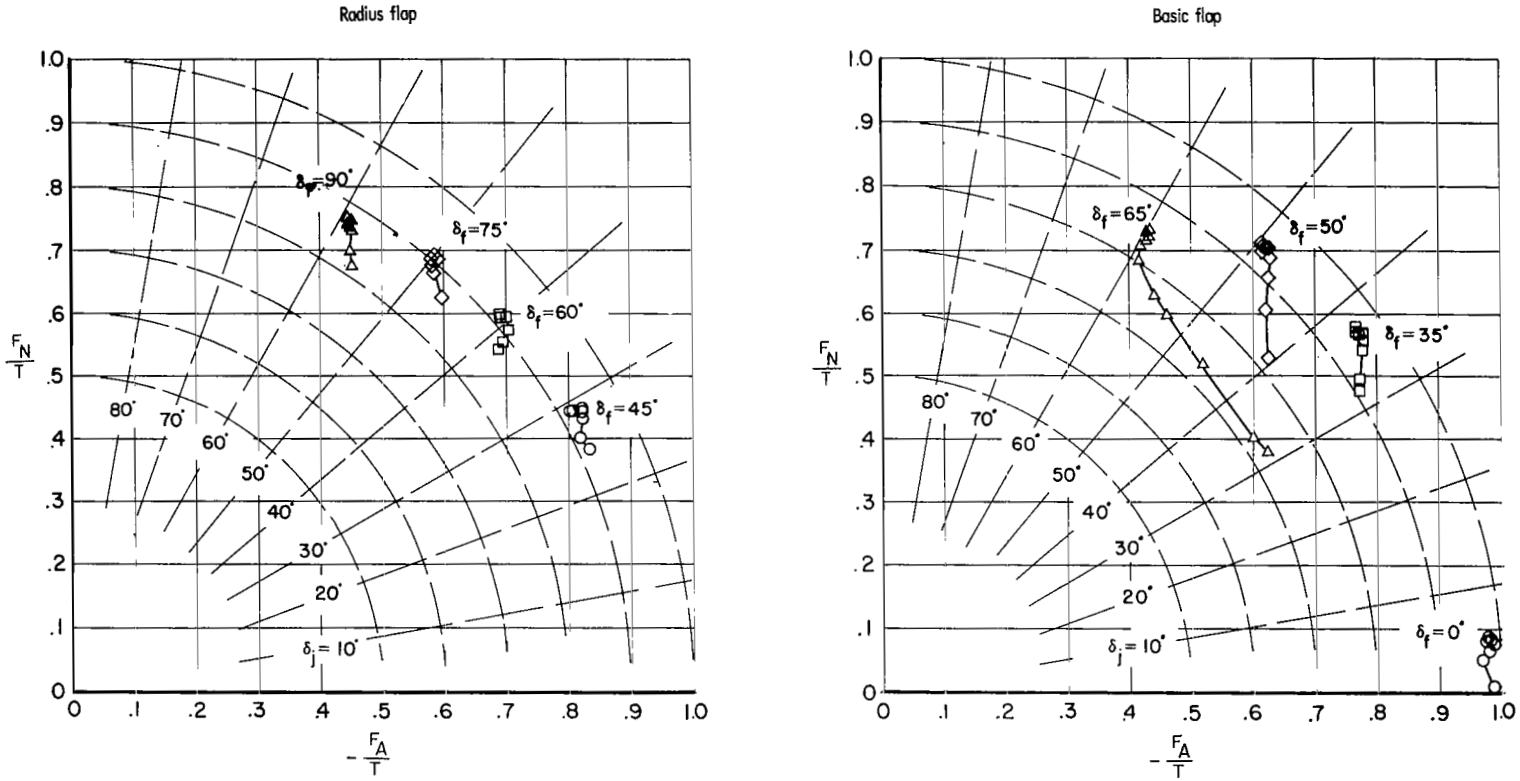


(b) Model with rectangular nozzles and four engines operating.

Figure 27.- Continued.

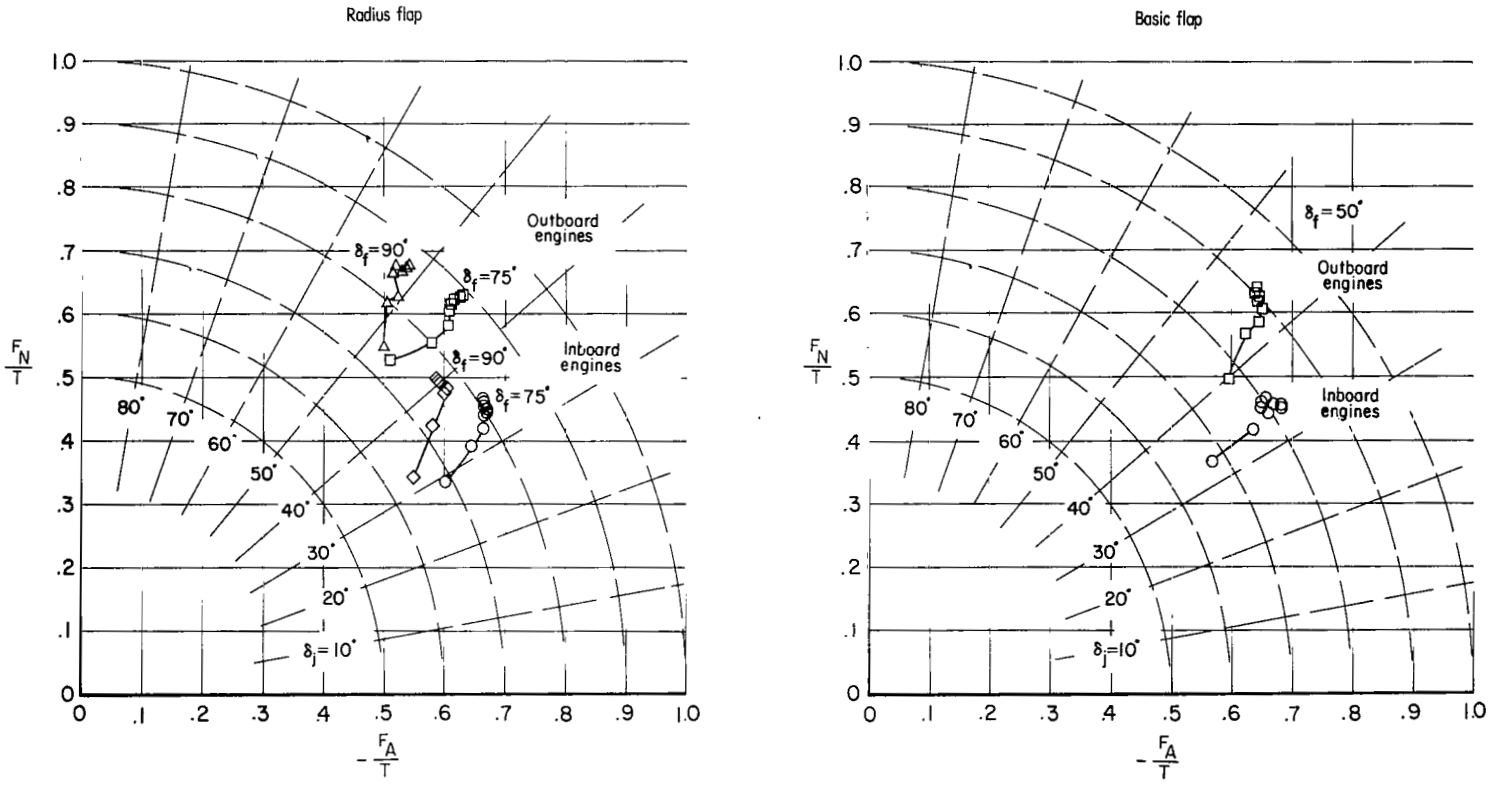


(c) Model with rectangular nozzles and two engines operating.

Figure 27.- Concluded.

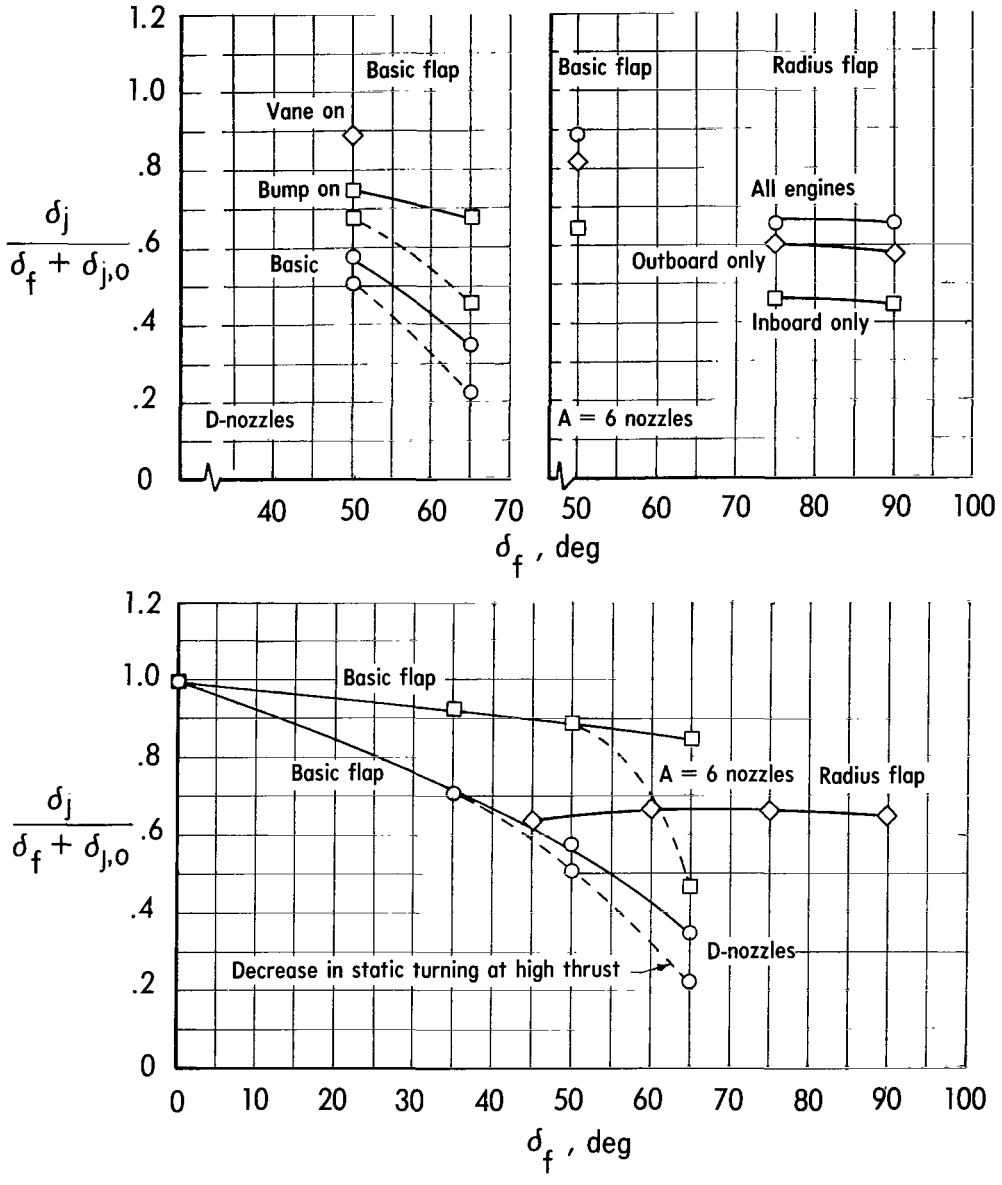


Figure 28.- Flap static-turning efficiency for upper surface blown model.

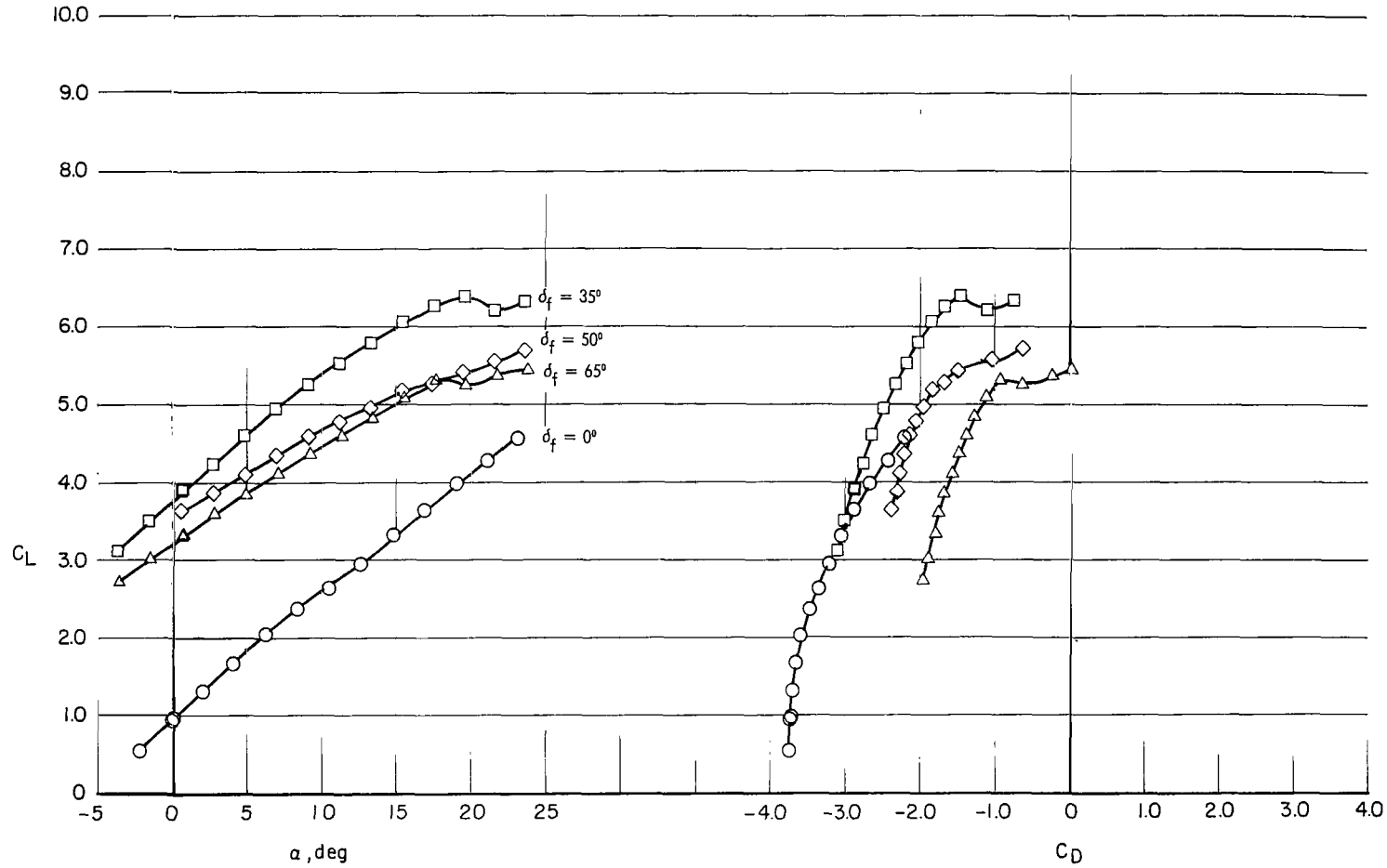


Figure 29.- Effect of flap deflection for basic model with D-nozzles.
Horizontal tail off; basic flap; $C_\mu = 4.0$.

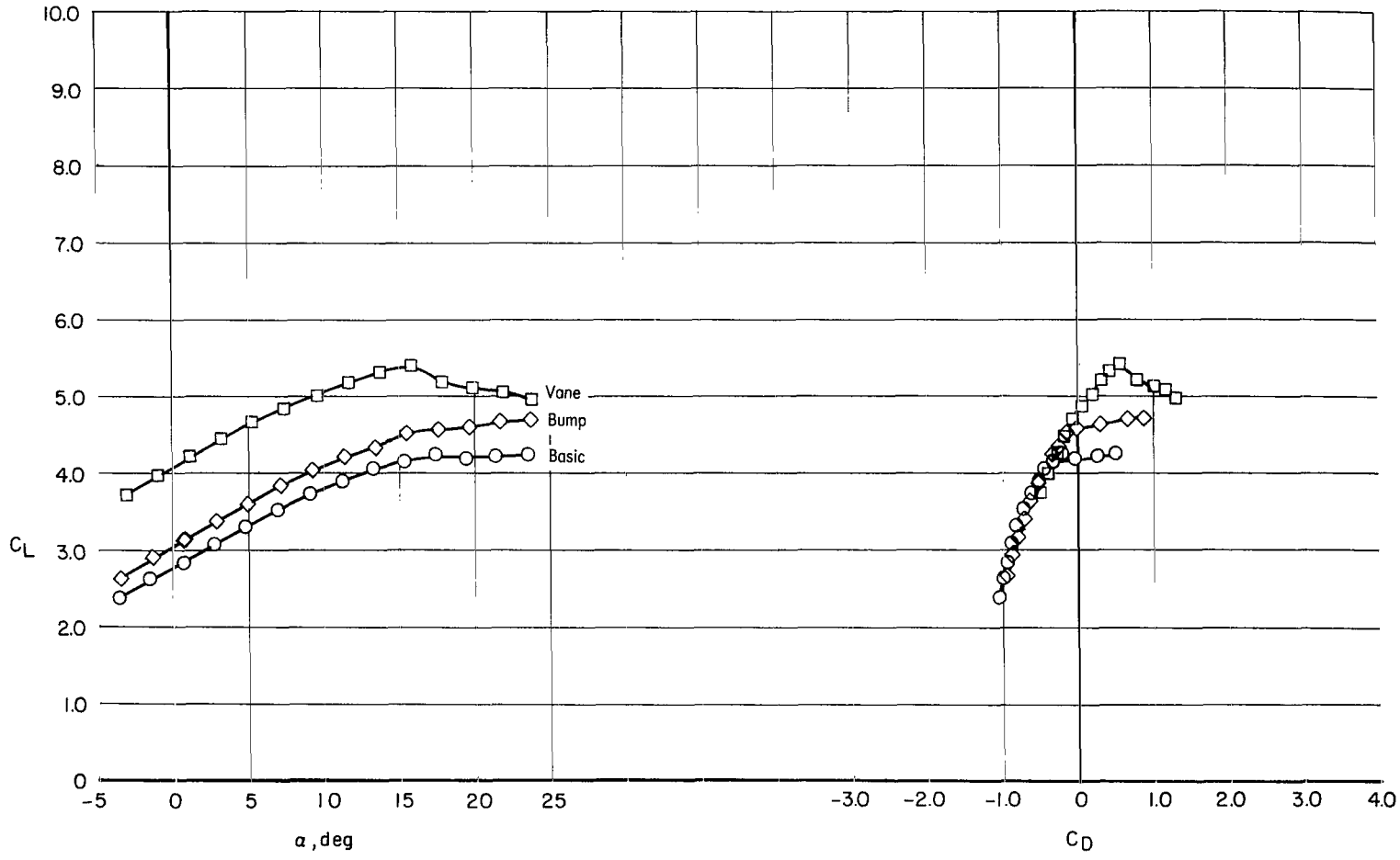


Figure 30.- Effect of modifications to the model with D-nozzles.
Horizontal tail off; $\delta_f = 50^o$; $\delta_s = 40^o$; $C_\mu = 2.0$.

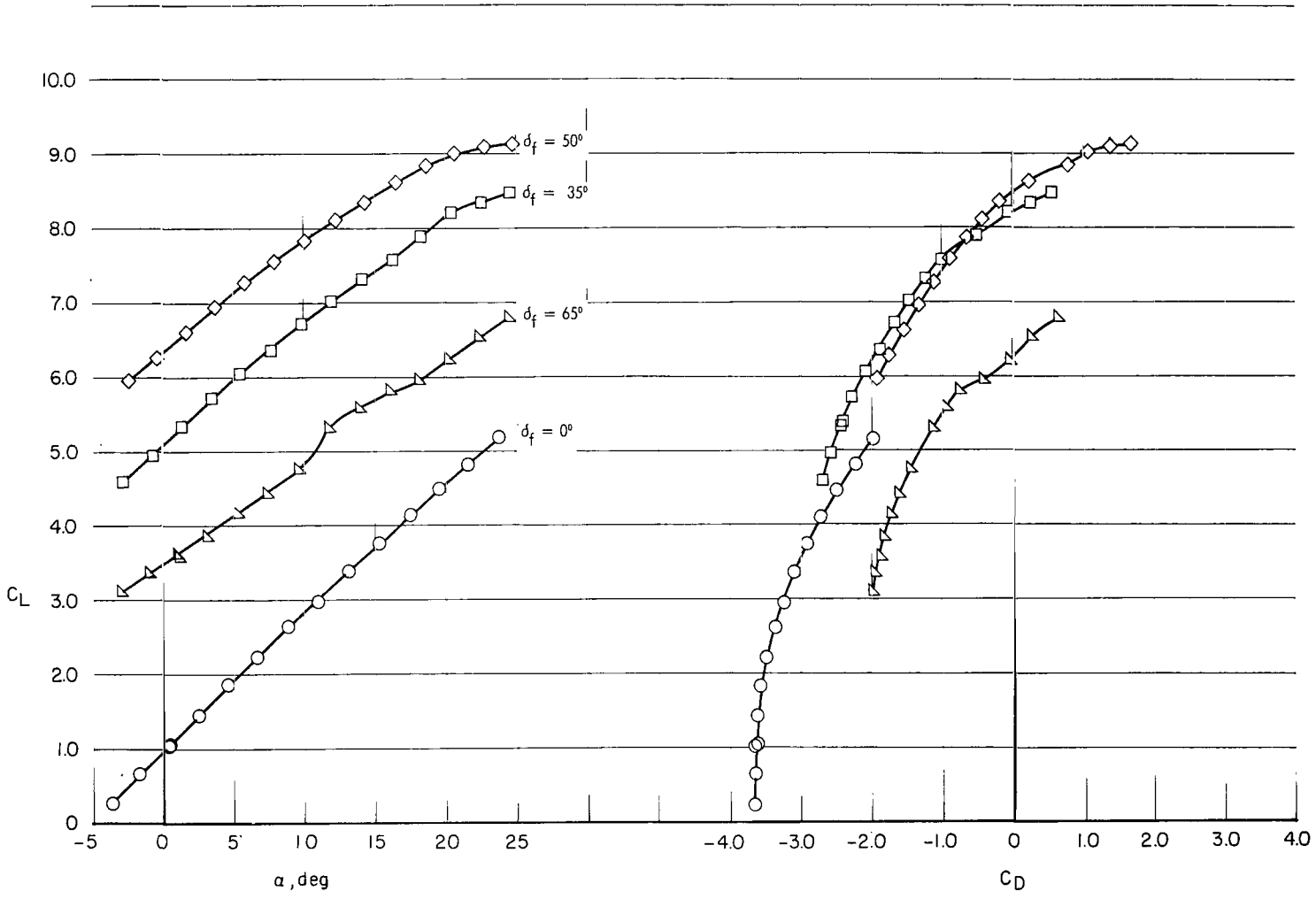


Figure 31.- Effect of flap deflection for the model with rectangular nozzles. Horizontal tail off; basic flap; $C_\mu = 4.0$.

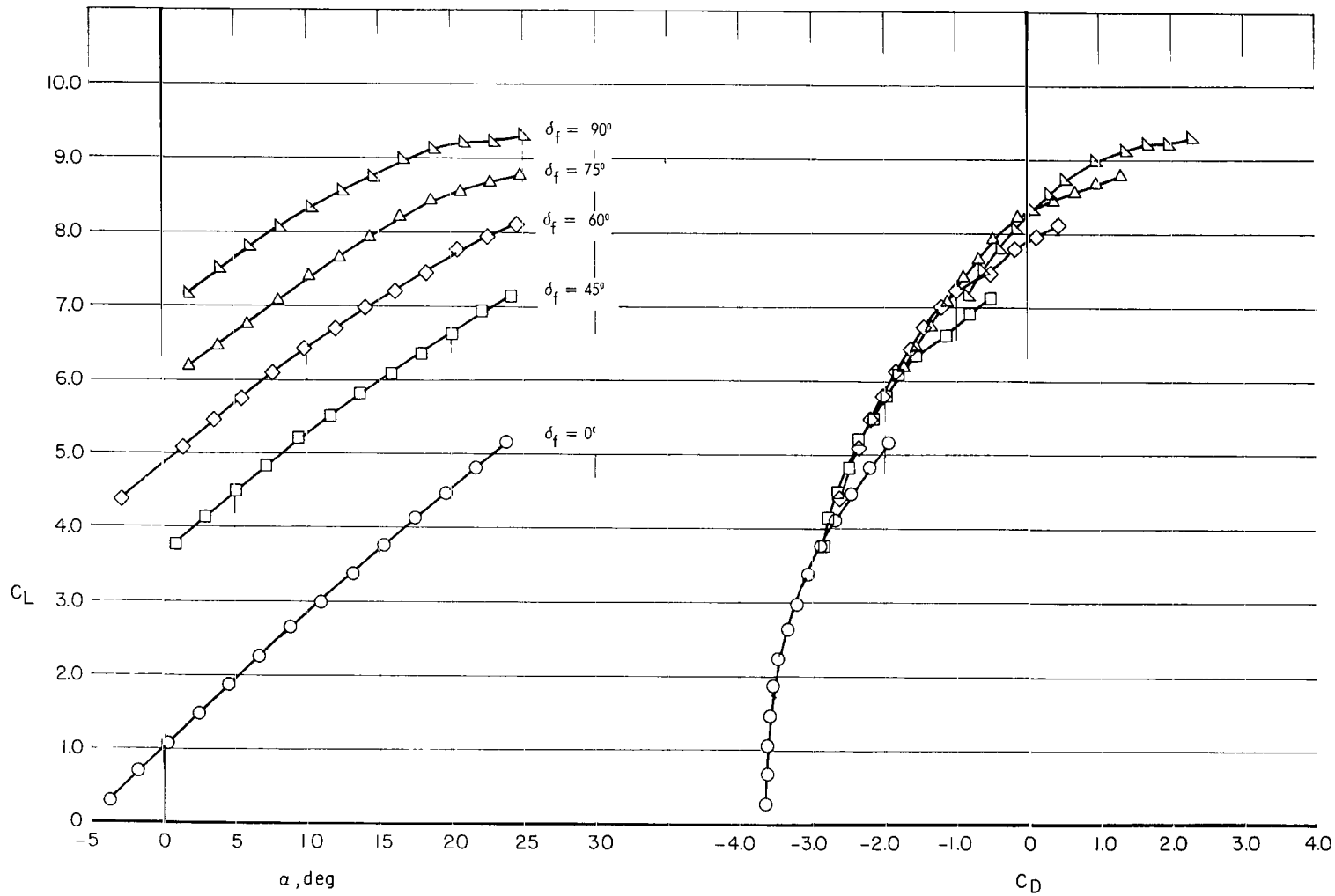


Figure 32.- Effect of flap deflection for the model with rectangular nozzles. Horizontal tail off; radius flap; $C_\mu$ = 4.0.

*"The aeronautical and space activities of the United States shall be conducted so as to contribute . . . to the expansion of human knowledge of phenomena in the atmosphere and space. The Administration shall provide for the widest practicable and appropriate dissemination of information concerning its activities and the results thereof."*

—NATIONAL AERONAUTICS AND SPACE ACT OF 1958

# NASA SCIENTIFIC AND TECHNICAL PUBLICATIONS

TECHNICAL REPORTS: Scientific and technical information considered important, complete, and a lasting contribution to existing knowledge.

TECHNICAL NOTES: Information less broad in scope but nevertheless of importance as a contribution to existing knowledge.

TECHNICAL MEMORANDUMS: Information receiving limited distribution because of preliminary data, security classification, or other reasons. Also includes conference proceedings with either limited or unlimited distribution.

CONTRACTOR REPORTS: Scientific and technical information generated under a NASA contract or grant and considered an important contribution to existing knowledge.

TECHNICAL TRANSLATIONS: Information published in a foreign language considered to merit NASA distribution in English.

SPECIAL PUBLICATIONS: Information derived from or of value to NASA activities. Publications include final reports of major projects, monographs, data compilations, handbooks, sourcebooks, and special bibliographies.

TECHNOLOGY UTILIZATION PUBLICATIONS: Information on technology used by NASA that may be of particular interest in commercial and other non-aerospace applications. Publications include Tech Briefs, Technology Utilization Reports and Technology Surveys.

***Details on the availability of these publications may be obtained from:***

**SCIENTIFIC AND TECHNICAL INFORMATION OFFICE**

**NATIONAL AERONAUTICS AND SPACE ADMINISTRATION**

**Washington, D.C. 20546**